

**UNIVERSITY OF SÃO PAULO**

**INSTITUTE OF CHEMISTRY**

**Graduate Program in Chemistry**

**DAIRON PÉREZ FUENTES**

**Development of methods for separation and determination of  
Pb, fractionation and speciation of As from waters using  
cellulose-based adsorbents**

Corrected version of defended Thesis

São Paulo

SPG filling date:

17/07/2023

**DAIRON PÉREZ FUENTES**

**Desenvolvimento de métodos para separação e  
determinação de Pb, fracionamento e especiação de As em  
amostras de águas usando adsorventes a base de celulose**

Tese apresentada ao Instituto de Química  
da Universidade de São Paulo para obtenção do  
Título de Doutor em Ciências (Química)

Orientador: Prof. Dr. Pedro Vitoriano de Oliveira

São Paulo

2023

Ficha Catalográfica elaborada eletronicamente pelo autor, utilizando o programa desenvolvido pela Seção Técnica de Informática do ICMC/USP e adaptado para a Divisão de Biblioteca e Documentação do Conjunto das Químicas da USP

Bibliotecária responsável pela orientação de catalogação da publicação:  
Marlene Aparecida Vieira - CRB - 8/5562

F 954d Fuentes, Dairon Pérez  
Desenvolvimento de métodos para separação e determinação de Pb, fracionamento e especiação de As em águas usando adsorventes a base de celulose / Dairon Pérez Fuentes. - São Paulo, 2023.  
148 p.

Tese (doutorado) - Instituto de Química da Universidade de São Paulo. Departamento de Química Fundamental.  
Orientador: Oliveira, Pedro Vitoriano

1. Arsênio. 2. Chumbo. 3. Especiação. 4. Extração em fase sólida . 5. Fracionamento. I. T. II.  
Oliveira, Pedro Vitoriano, orientador.

"Desenvolvimento de métodos para separação e determinação de Pb, fracionamento e especiação de As em águas usando adsorventes a base de celulose"

### **DAIRON PÉREZ FUENTES**

Tese de Doutorado submetida ao Instituto de Química da Universidade de São Paulo como parte dos requisitos necessários à obtenção do grau de Doutor em Ciências - no Programa de Química.

---

Prof. Dr. Pedro Vitoriano de Oliveira  
(Orientador e Presidente)

**APROVADO(A) POR:**

---

Prof. Dr. Jorge Cesar Masini  
IQ - USP

---

Prof. Dra. Márcia Andreia Mesquita Silva da Veiga *(por videoconferência)*  
FFCLRP - USP

---

Prof. Dr. César Ricardo Teixeira Tarley *(por videoconferência)*  
UEL

SÃO PAULO  
25 de agosto de 2023

*To my grandmother Ada  
for all the love and dedication.*

## Thanks

To Professor Pedro Vitoriano de Oliveira for the learning opportunity during the doctoral period under his guidance. Thanks for all the respect, support and friendship.

To my parents, Arleydis and Reinan, and grandmother Ada for all the love and affection, because without their support and encouragement I wouldn't have conquered everything I've achieved until today.

To my sister Daniela and my brother Damian for all their support and affection.

To my friend Lazara for always being by my side. Thank you for conversations and laughs, as well as for the support always I need it.

To Claudio my life partner for all the love and support during this last month.

To my best friends Massiel and Patricia for always be there for me, and all these years together as brothers, without you today I would not be who I am.

To friends who are or were part of GAPE (Group of Analyzes and Research in Spectrometry): Lucas, Gabriel, Jou, Giselaïne, Thais, Alê, Aline, Matheus, Sady and Aline Pereira for their company, collaboration, and friendship.

To the special friends Laïse. Thank you for all your collaboration and support during the realization of this work and for the friendship that goes beyond academic life.

To professor Cassiana Seimi Nomura for the conversations, exchange of knowledge and friendship.

To Professor Denise F. Petri for the collaboration for my training during the postgraduate period as a researcher and all the opportunities for collaboration.

To the IQ employees who in some way contributed to the realization this work. In particular, to the technicians Luciana for their help in the laboratory and for conversations and friendship.

To the Institute of Chemistry of the University of São Paulo for the opportunity and structure offered for the development of this work.

To CNPq for the scholarship granted.

To CAPES and FAPESP for financial support.

Thank you very much.

## Abstract

Fuentes, D.P. **Development of methods for separation and determination of Pb, fractionation and speciation of As from waters using cellulose-based adsorbents.** 2023. 148p. PhD Thesis – Chemistry Graduate Program. Chemistry Institute, São Paulo University.

The presence of potentially toxic elements, particularly lead and arsenic, in natural and drinking waters is of concern due to their widespread occurrence and harmful effects on human health. Therefore, developing materials and methods for removing, separating, and preconcentrating these elements is essential to mitigate contamination and for analytical purposes. Thus, the objective of the project was to develop methods for separation and determination of lead and fractionation and speciation of organic and inorganic species of arsenic in different water samples using cellulose-based adsorbent and detection by inductively coupled optical emission spectrometry (ICP OES) and graphite furnace atomic absorption spectroscopy (GF AAS). For the separation of lead from water, microcrystalline cellulose beads were prepared in 2 mol L<sup>-1</sup> HNO<sub>3</sub> as a coagulant medium, being named b-HNO<sub>3</sub>. The Pb(II) adsorption data fit to the Langmuir model, with a maximum adsorption capacity of 108 mg g<sup>-1</sup>. The b-HNO<sub>3</sub> were characterized by SEM, FTIR, XPS, and elemental analysis, and the adsorption performance was evaluated by different methods such as zero charge point and adsorption isotherm. The methodology developed for separating Pb(II) was made in columns packed with b-HNO<sub>3</sub>. The adsorption efficiency depended on the pH between 6-8 and flow rate of 0.5 mL min<sup>-1</sup> of solution flowing through the column, making it possible to reuse the column for several separation cycles, with effective Pb(II) desorption with 2 mol L<sup>-1</sup> of HCl. Applying the optimized conditions for separating Pb(II) from tap water, dam water, and high salinity water, recoveries ranging from 94% to 102% were obtained. Microcrystalline cellulose modified with glycidyl trimethylammonium chloride (MCC-GTA) was used as adsorbent for the fractionation and speciation of arsenic. Elemental analysis confirmed the incorporation of quaternary ammonium groups in the cellulose chain. Optimization studies demonstrated that MCC-GTA exhibited high affinity for As(V) at pH 6-7, with negligible adsorption of As(III), none of AsB, and moderate adsorption for MMAs and DMAs species, with percentages ranging from 30 to 50%, respectively. The adsorption process of As(V) was instantaneous and was not affected by the adsorbent mass. In this investigation, the studies were done in batch mode. The oxidation of As(III) to As(V) with sodium hypochlorite (NaClO) was one of the strategies for speciation, which did not affect the behavior of adsorption in MCC-GTA. Pre-concentration analysis and inorganic arsenic (iAs) speciation were performed in river water samples using batch MCC-GTA. The results showed that speciation of As(III) and As(V) was possible, with recoveries ranging from 93% to 109% for As(III) and 96% to 103% for As(V). Overall, the results demonstrated the efficiency of these materials, from natural sources, for separation of Pb(II) and speciation of As(III) from As(V) applied in natural water samples.

**Keywords: Arsenic, Lead, Speciation, Fractionation, Solid phase extraction**



## Resumo

Fuentes, D.P. **Desenvolvimento de métodos para separação e determinação de Pb, fracionamento e especiação de As em amostras de águas usando adsorventes a base de celulose.** 2023. 148p. Tese de Doutorado – Programa de Pós-Graduação em Química. Instituto de Química, Universidade de São Paulo.

A presença de elementos potencialmente tóxicos, particularmente chumbo e arsênio, em águas naturais e potáveis é preocupante devido à sua ocorrência generalizada e aos efeitos nocivos para a saúde humana. Portanto, o desenvolvimento de materiais e métodos para remoção, separação e pré-concentração desses elementos é essencial para mitigar a contaminação e para fins analíticos. Assim o objetivo do projeto foi desenvolver métodos de separação e determinação de chumbo e fracionamento e especiação de espécies orgânicas e inorgânicas de arsênio em diferentes amostras de água utilizando adsorvente à base de celulose e detecção por espectrometria de emissão óptica com plasma indutivamente acoplado (ICP OES) e espectrometria de absorção atômica com forno de grafite (GF AAS). Para a separação do chumbo da água foram utilizadas esferas de celulose microcristalina preparadas em 2 mol L<sup>-1</sup> de HNO<sub>3</sub> como meio coagulante, denominadas b-HNO<sub>3</sub>. Os dados de adsorção de Pb(II) ajustaram-se ao modelo de Langmuir, com capacidade máxima de adsorção de 108 mg g<sup>-1</sup>. Os b-HNO<sub>3</sub> foram caracterizados por MEV, FTIR, XPS e análise elementar, e o desempenho de adsorção foi avaliado por diferentes métodos como ponto de carga zero e isoterma de adsorção. A metodologia desenvolvida para separação do Pb(II) foi feita em colunas preenchidas com b-HNO<sub>3</sub>. A eficiência de adsorção dependeu do pH entre 6-8 e vazão de 0,5 mL min<sup>-1</sup> de solução passando pela coluna, possibilitando o reaproveitamento da coluna para vários ciclos de separação, com dessorção efetiva de Pb(II) com 2 mol L<sup>-1</sup> de HCl. Aplicando as condições otimizadas para separação de Pb(II) de água de torneira, água de represa e água de alta salinidade, foram obtidas recuperações variando de 94% a 102%. Celulose microcristalina modificada com cloreto de glicidil trimetilamônio (MCC-GTA) foi utilizada como adsorvente para fracionamento e especiação de arsênio. A análise elementar confirmou a incorporação de grupos quaternários de amônio na cadeia da celulose. Estudos de otimização demonstraram que o MCC-GTA exibiu alta afinidade por As(V) em pH 6-7, com adsorção desprezível de As(III), nenhuma de AsB, e adsorção moderada para espécies de MMAs e DMAs, com porcentagens variando de 30 a 50 %, respectivamente. O processo de adsorção foi instantâneo e não foi afetado pela massa do adsorvente. Nesta investigação, os estudos foram feitos em lote. A oxidação de As(III) a As(V) com hipoclorito de sódio (NaClO) foi uma das estratégias de especiação, o que não afetou o comportamento de adsorção no MCC-GTA. Análises de pré-concentração e especiação de arsênio inorgânico (iAs) foram realizadas em amostras de água de rio usando lote de MCC-TA. Os resultados mostraram que a especiação de As(III) e As(V) foi possível, com recuperações variando de 93% a 109% para As(III) e 96% a 103% para As(V). No geral, os resultados demonstraram a eficiência desses materiais, provenientes de fontes naturais, na separação de Pb(II) e especiação de As(III) de As(V) aplicados em amostras de águas naturais.

**Palavras-chave: Arsênio, Chumbo, Especiação, Fracionamento, Extração em fase sólida**

## LIST OF ABBREVIATIONS AND ACRONYMS

**AsB:** Arsenobetaine

**AsC:** Arsenocholine

**AsLp:** Arsenolipids

**ATSDR:** Agency for toxic substances and disease registry

**CID:** Charge Injection Device

**CONAMA:** From Portuguese “Conselho Nacional do Meio Ambiente”

**CV AAS:** Cold vapor atomic absorption spectrometry

**DMA:** Dimethyl arsenic acid

**GF AAS:** graphite furnace atomic absorption spectrometry

**FAAS:** Flame atomic absorption spectrometry

**FT-IR:** Fourier transform infrared

**GTAC:** Glycidyl trimethylammonium chloride

**HG AAS:** Hydride generation atomic absorption spectrometry

**iAs:** Inorganic arsenic

**ICP OES:** Inductively coupled plasma optical emission spectrometry

**ICP-MS:** Inductively coupled plasma mass spectrometry

**MCC:** Microcrystalline cellulose

**MCC-TA:** Modified MCC with glycidyl trimethylammonium chloride

**MMA:** Monomethyl arsenic acid

**SPE:** Solid-phase extraction

**SEM:** Scanning electron microscopy

**TETRA:** Tetramethylarsenic

**TMAO:** Trimethylarsine oxide

**WHO:** World Health Organization

**XPS:** X-ray photoelectron spectroscopy (XPS)

**XRF:** X-ray fluorescence

## List of Figures

Figure 1. Arsenic cycle in the environment. Reproduced from: <i>Arsenic removal from aqueous solution: A comprehensive synthesis with meta-data</i> . (Aktar et al., 2023). Copyright (2023) with permission of Elsevier.....	22
Figure 2. Chemical structure for most abundant arsenic species.....	24
Figure 3. Eh–pH diagram for the system As–O–H at 25°C and 1 bar. Source: Arsenic Eh–pH diagrams at 25°C and 1 bar. (Lu and Zhu, 2010). Copyright (2010) with permission of Springer Nature.....	25
Figure 4. The pathway of lead in the biogeochemical cycle. Source: A review on mechanism of biomineralization using microbial-induced precipitation for immobilizing lead ions. (Shan et al., 2021). Copyright (2021) with permission of Springer Nature.....	27
Figure 5. Chemical structure of cellulose. Source: Glucose, not cellobiose, is the repeating unit of cellulose and why that is important (French 2017). Copyright (2017) with permission of Springer Nature.....	34
Figure 6. Arsenic sorption mechanism on the biosorbent surface. Source : Remediation of arsenic-contaminated water using agricultural wastes as biosorbents. (Shakoor et al. 2016). Copyright (2016) with permission of Taylor & Francis. ....	39
Figure 7. (A) Schematic setting up for the bead preparation and (B) photography of bead formation.	56
Figure 8. Schematic setting up for the MCC-GTA preparation.....	66
Figure 9. Experimental set up used for arsenic fractionation and speciation: 1. Total determination of As by GF AAS; 2. Separation of arsenic species and determination by GFT AAS before addition of NaClO; and 3. Separation of arsenic species and determination by GF AAS after addition of NaClO.	69
Figure 10. Schematic setting up for preconcentration of inorganic As species in water .....	71
Figure 11. Photo of cellulose beads prepared in 1 mol L <sup>-1</sup> of HCl (a and b) and 2 mol L <sup>-1</sup> of HNO <sub>3</sub> (c and d) media, wet (a and d) and after drying in an oven (b and d) .....	73
Figure 12. Photography of beads prepared in different acid concentrations (a,d,g,i) and SEM images of dry microcrystalline cellulose beads prepared in 0.5 mol L <sup>-1</sup> of HNO <sub>3</sub> (a, b, c), in 1 mol L <sup>-1</sup> of HNO <sub>3</sub> (d, e, f), in 2 mol L <sup>-1</sup> of HNO <sub>3</sub> (g, h, i), and in 8 mol L <sup>-1</sup> .....	74
Figure 13. FTIR spectra of beads prepared in 2,0 mol L <sup>-1</sup> of HNO <sub>3</sub> (b-NHO <sub>3</sub> ) beads, beads loaded with Pb (b-HNO <sub>3</sub> +Pb) and pure MCC.....	76

Figure 14. XPS survey spectrum of the beads (a) before (black) and after (red) the lead adsorption (a). XPS high resolution spectra of Pb 4f (b) for beads after lead adsorption, O 1s (c) before lead adsorption and O 1s (d) after lead adsorption. ....	78
Figure 15. Experimental potentiometric titration curves with (a) 0.02 mol L <sup>-1</sup> NaOH and (b) with 0.02 mol L <sup>-1</sup> HCl, obtained for background electrolyte (KNO <sub>3</sub> 0.05 mol L <sup>-1</sup> ) (red) and for the b-HNO <sub>3</sub> sample (black).....	79
Figure 16. Isotherm of the number of protons released or adsorbed obtained for b-HNO <sub>3</sub> .....	80
Figure 17. Adsorption isotherms Langmuir nonlinear adjusted for b-HNO <sub>3</sub> , b-HCl, and pure MCC .....	82
Figure 18. Adsorption isotherms Langmuir linear adjusted for b-HNO <sub>3</sub> , b-HCl, and pure MCC ..	82
Figure 19. Effect of pH on adsorption of Pb(II) (1 mg L <sup>-1</sup> , 1 ml min <sup>-1</sup> ) onto 150 mg of b-HNO <sub>3</sub> column, at pH=6.....	85
Figure 20. Flow rate optimization of Pb(II) (1 mg L <sup>-1</sup> ) onto 150 mg of b-HNO <sub>3</sub> column, at pH=6.	86
Figure 21. Inter repeatability using 5 different columns and intra repeatability for adsorption-desorption (n=2): 1 mg L <sup>-1</sup> of Pb(II), mass 150 mg of b-HNO <sub>3</sub> , flow rate 0.5 mL L <sup>-1</sup> , and pH 6. ...	87
Figure 22. Reuse cycle of Pb(II) separation for nine adsorption-desorption cycle: 2 mL of eluent, 1 mg L <sup>-1</sup> of Pb(II), mass 150 mg of b-HNO <sub>3</sub> , flow rate 0.5 ml L <sup>-1</sup> , and pH 6. ....	89
Figure 23. Recoveries of Pb after adsorption/desorption using different type of eluent for Pb(II) desorption: 2 mL of eluent, 1 mg L <sup>-1</sup> of Pb(II), mass 150 mg of b-HNO <sub>3</sub> , flow rate 0.5 ml L <sup>-1</sup> , and pH 6. ....	89
Figure 24. The breakthrough curve for Pb(II) onto b-HNO <sub>3</sub> showing nonlinear fittings for the Thomas model: 5 mg L <sup>-1</sup> Pb(II) (C <sub>0</sub> ), mass 150 mg of b-HNO <sub>3</sub> , flow rate 0.5 ml L <sup>-1</sup> , and pH 6. ...	91
Figure 25. Calibration curves of Pb without (black) and with preconcentration step (red) for the ICP OES.....	92
Figure 26. Removal and recovery in water samples spiked with 1 mg L <sup>-1</sup> and Pb(II), using 0.150 g of b-HNO <sub>3</sub> column, pH 6, desorption with 1 mol L <sup>-1</sup> HCl: Drinking water, Dam water, and HS water 1 with flow rate 0.5 mL min <sup>-1</sup> and HS water 2 with flow rate 0. 25 mL min <sup>-1</sup> .....	94
Figure 27. Performance of Pb(II) removal and recovery in different dilutions of HS water samples using b-HNO <sub>3</sub> column: 0.150 g b-HNO <sub>3</sub> , samples spiked with 1 mg L <sup>-1</sup> Pb(II), ph 6 and flow rate 0.5 mL min <sup>-1</sup> .....	96
Figure 28. Influence of Cl <sup>-</sup> concentration on the removal of Pb(II) using b-HNO <sub>3</sub> column, solutions with 1 mg L <sup>-1</sup> Pb(II) and different Cl <sup>-</sup> (1-20 mg L <sup>-1</sup> ) with flow rate 0,5 mL min <sup>-1</sup> .....	97

Figure 29. FTIR spectra of pure MCC and after functionalization with different amounts of glycidyl trimethylammonium chloride (9%, 18% and 36%). ..... 100

Figure 30. Arsenic species adsorption as a function of pH using 10 mg of MCC-GTA at pH 2-10. .... 103

Figure 31. . Arsenic species adsorption as a function of pH using pure MCC, mass 10 mg and at pH 6-7..... 104

Figure 32. Arsenic species adsorption as a function of pH using activated MCC with NaOH (10 mol L<sup>-1</sup>), without modification with GTA, mass 10 mg and at pH 6-7. .... 105

Figure 33. Contact time for arsenic species adsorption using 10 mg MCC-GTA, initial concentration 100 µg L<sup>-1</sup> of As species, at pH 6-7. .... 106

Figure 34. Adsorbent dose for arsenic species adsorption using MCC-GTA, initial concentration 0,1 mg/L and pH 6-7. .... 107

Figure 35. Anion exchange chromatogram of As species by LC-ICP OES: dimethyl arsenic (DMA), monomethyl arsenic (MMA), arsenobetaine AsB), As(V) and As(III). .... 109

Figure 36. Anion exchange chromatogram of As species mixture by LC-ICP OES: Mix (without oxidant), Mix R<sub>NaClO/As</sub>=1 (after oxidation with same molar ratio between NaClO and As species) and Mix R<sub>NaClO/As</sub>=2 (after oxidation with twice molar ratio between NaClO and As species). ... 110

Figure 37. Arsenic species adsorption using MCC-GTA at pH 6-7: 0 (without oxidant) and 1, 2 and 3 (after oxidation with NaClO). .... 111

Figure 38. GF AAS standard calibration of As (blue) without preconcentration, with preconcentration of As(V) (black) and with preconcentration of As(III) and As(V) after oxidation of As(III) with NaClO (red). .... 114

## List of Tables

Table 1. Instrumental set up of ICP OES for As and Pb detection. ....	50
Table 2. Heating program for the transversally heated graphite atomizer for As determination. .	52
Table 3. Adsorption isotherms Langmuir nonlinear adjust parameters.....	82
Table 4. Adsorption isotherms Langmuir linear adjust parameters. ....	83
Table 5. CNH elemental analysis of MCC and MCC-GTA with different % of GTAC.....	101
Table 6. Concentrations of As after fractionation in aqueous solution and water samples. ....	118
Table 7. iAs preconcentration and speciation analysis in water samples.....	121

## Summary

1. Introduction .....	19
1.1. Arsenic occurrence and health effects.....	20
1.2. Lead occurrence and health effects.....	26
1.3. Methods for remediation, recovering and monitoring ptentially toxic elements	30
1.4. Cellulose.....	33
1.4.1. Adsorption methods using cellulose-base adsorbent for fractionation and speciation of As.....	36
1.4.2. Adsorption methods using cellulose-base adsorbents for remediation and recovery of Pb.....	42
2. Objective .....	49
2.1. Specific Objective .....	49
3. Experimental Section .....	50
3.1. Instrumental.....	50
3.2. Material and reagents.....	53
3.3. Samples .....	54
3.4. Cellulose beads preparation.....	55
3.5. Cellulose beads characterization.....	57
3.5.1. Point of zero charge determination for b-HNO <sub>3</sub> .....	57
3.5.2. Adsorption isotherm of Pb(II) onto b-HNO <sub>3</sub> in batch .....	58
3.6. Optimization of Pb(II) adsorption onto b-HNO <sub>3</sub> in a fixed-bed column.....	60
3.6.1. Adsorption rate as function of pH.....	60
3.6.2. Flow-rate optimization.....	61
3.6.3. Intra e inter column repeatability and type of eluent for desorption.....	62
3.6.4. Breakthrough curve for Pb(II) adsorption onto b-HNO <sub>3</sub> column .....	63
3.7. Separation-removal of Pb(II) from water samples using b-HNO <sub>3</sub> column.....	64



3.8. Microcrystalline cellulose with glycidyl trimethylammonium chloride (MCC-GTA) preparation for As fractionation and speciation .....	65
3.9. Macrocrystalline cellulose with glycidyl trimethylammonium chloride (MCC-GTA) characterization .....	66
3.10. Optimization of As species adsorption onto MCC-GTA in batch .....	67
3.10.1. Adsorption rate as function of pH .....	67
3.10.2. Contact time and adsorbent mass .....	67
3.10.3. Oxidation of arsenic species and monitoring by LC-ICP-OES .....	68
3.11. Arsenic speciation and fractioning using MCC-GTA in batch .....	69
3.12. Preconcentration and speciation of inorganic arsenic in water samples using MCC-GTA .....	70
4. Results and Discussion.....	72
4.1. Preparation and characterization of microcrystalline cellulose beads .....	72
4.1.1. Characterization using SEM .....	73
4.1.2. Characterization using FTIR .....	75
4.1.3. Characterization using XPS .....	76
4.1.4. Characterization using PZC .....	79
4.1.5. Adsorption isotherm of Pb(II) .....	80
4.2. Optimization of Pb(II) adsorption onto b-HNO <sub>3</sub> in a fixed-bed column.....	84
4.2.1. Effect of pH on the Pb(II) adsorption.....	84
4.2.2. Effect of flow rate through the column on the Pb(II) adsorption .....	85
4.2.3. Intra and inter column repeatability and type of eluent for desorption .....	86
4.2.4. Breakthrough curve for Pb(II) on b-HNO <sub>3</sub> .....	90
4.3. Analytical characteristics for the detection of Pb using ICP OES .....	92
4.4. Separation-removal of Pb(II) from water using b-HNO <sub>3</sub> column .....	93

4.5.	Preparation of modified MCC with Glycidyl trimethylammonium chloride (MCC-GTA)	98
4.6.	Arsenic species adsorption optimization.....	101
4.6.1.	Arsenic species removal as a function of pH onto MCC-GTA.....	101
4.6.2.	Contact time and adsorbent mass for arsenic species adsorption onto MCC-GTA	105
4.6.3.	LC-ICP OES arsenic species monitoring and oxidation process.....	107
4.6.4.	Influence of sodium hypochlorite as oxidant agent on the adsorption of As species on MCC-GTA .....	111
4.7.	Analytical characteristics for the detection of As using GF AAS.....	112
4.8.	Fractionation of arsenic species in water samples using MCC-GTA as adsorbent	115
4.9.	Preconcentration and speciation of iAs from water samples using MCC-TA..	119
5.	Conclusions .....	122
6.	Bibliography .....	124

## 1. Introduction

With the rise of the industrial age, environmental issues have become more pressing. The global concern for the environment impacts due to urban, industrial, and population expansion, which can negatively affect air, water and soil quality is a discussion in the agenda for sustainable development (Spano et al. 2020). Water pollution is a particularly widespread problem, with causes ranging from agricultural runoff to sewage, wastewater, oil pollution up to radioactive substances. In general, industrial wastewater can contain a variety of potentially toxic elements (Ali Redha, 2020).

Potentially toxic elements comprise a class of metallic or metalloid elements that can exert toxic effects at low concentrations. In addition to their toxicity, occur in the earth's crust with a lower extent over the ecosystems, but become hazardous due to their widespread and rapid environmental cycling and higher potential toxicity and bioaccumulation in living beings, therefore, this behavior is highly influenced by anthropic intense competition activities to exploit natural resources (Machate, 2023). Potentially toxic elements, such as As, Cd, Cr, Cu, Ni, Pb, and Zn, are among the most hazardous chemicals present in industrial environments. Due to their high solubility, aquatic organisms can easily absorb them, eventually entering the food chain. If ingested in excessive amounts, these metals can accumulate in the human body and cause severe health disorders (Barakat, 2011). The 2022 Substance Priority List, provided by Agency for Toxic Substances and Disease Registry (ATSDR) listed arsenic and lead, as first and second hazardous substances based on a combination of their frequency, toxicity, and potential for human exposure (ATSDR, 2022).

The World Health Organization (WHO) has established limits for potentially toxic elements and the potential impacts on human health when those limits are exceeded in drinking and industrial wastewater (WHO, 2017). To reduce potentially toxic elements concentrations in wastewater to levels that are below the established limits, it must be subjected to a treatment process prior to being discharged into the environment or reused in industry. Not only must these levels not exceed the permissible limits for humans and animals, but they also need to be kept below the limits for plants (Shrestha et al., 2021).

Considering the toxicity of arsenic and lead for the environment and for living beings, finding ways to prevent these elements from being increasingly dispersed into the environment is a task for specialists and scientists. Therefore, one of the most recognized ways of removing or separating these elements, or detecting them at trace levels, as established by regulators organization, is through inorganic, organic or mixed adsorbents, seeking whenever possible separation efficiency, selectivity, and lower production cost, as was the aim of this research.

### **1.1. Arsenic occurrence and health effects**

Arsenic is an abundantly available element ( $1.8 \text{ mg kg}^{-1}$ ) at earth crust ranging from trace levels to hundreds of milligrams per kilogram widely distributed in the environment (Anand et al., 2022). The contamination of soil and groundwater occurs due to its discharge from natural and anthropogenic sources. Natural processes such as weathering of rocks, volcanic emissions, and various anthropogenic activities such as industrial activities, excess utilization of agrochemicals, improper disposal of waste,

application of wood preservatives, and mining operations are among some of the main sources of environmental contamination (Yuan et al. 2022). In the past 20 years, there has been a significant amount of attention given to the presence, spread, source, and movement of arsenic in the environment. In order to have a better understanding of the contamination caused by As, it is important to have knowledge about the natural geochemical and biological processes that influence its transport and transformation (Asere et al., 2019). At the Figure 1, as presented by Aktar et al. (2023), is illustrated the arsenic cycle in the environment. As it is possible to observe, arsenic is naturally occurring element present in all environmental media (air, soil, and water). It can enter to the food chain through plants and animals, leading to human exposure through various pathways such as ingestion of contaminated food and water, inhalation of arsenical dust, and dermal uptake from contaminated soil. The use of arsenic-containing pesticides, herbicides, and insecticides can also lead to the accumulation of arsenic in crops. Groundwater contaminated with elevated levels of naturally occurring inorganic arsenic is a direct exposure pathway and can result in mass poisoning. Organic arsenic accumulation in organisms, can also contribute to arsenic exposure (Aktar et al., 2023). Constant use of arsenic-contaminated groundwater for irrigation of crops is one of the most hazardous situations for humans (Chakrabarti et al., 2019).

According to a Scientific Report published by the European Food Safety Authority (EFSA), the foods that mostly contributing to As exposure are cereal grains and cereal-based products, followed by foods for special dietary uses, bottled water, coffee and beer, rice grains and rice-based products, fish and vegetables (Baer et al., 2011). Water contamination by arsenic is a concern worldwide. The WHO recommends that the arsenic

content in drinking water should be below  $10 \mu\text{g L}^{-1}$  (WHO 2017), meanwhile high arsenic concentrations in groundwater have been recorded in many parts of the world (Morales-Simfors and Bundschuh, 2022; Matos et al., 2022; Viana et al., 2022; Adeloju et al., 2021). Arsenic contamination of water resources and other environments at toxic levels has been reported in 20 Latin American countries (Bundschuh et al., 2021).

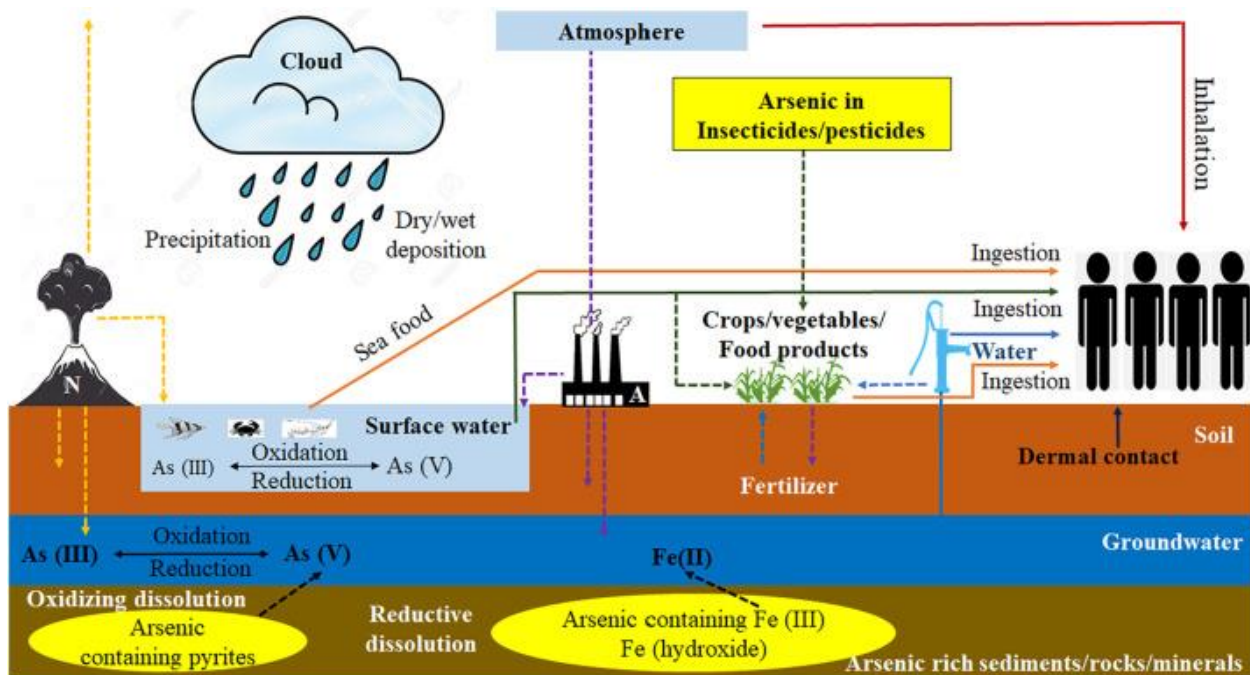


Figure 1. Arsenic cycle in the environment. Reproduced from: *Arsenic removal from aqueous solution: A comprehensive synthesis with meta-data*. (Aktar et al., 2023). Copyright (2023) with permission of Elsevier.

Podgorski and Berg (2020), constructed a global prediction map of areas with arsenic concentrations above  $10 \mu\text{g L}^{-1}$ , using global arsenic prediction model with household groundwater usage statistics. They estimated that 94 million to 220 million people are potentially exposed to high arsenic concentrations in groundwater, the vast majority (94%) being in Asia (Podgorski and Berg, 2020). Shaji et al. present an overview

of the current scenario of arsenic contamination of groundwater in various countries across the globe with an emphasis on the Indian Peninsula. It was estimated that nearly 108 countries are affected by arsenic contamination in groundwater (with concentration beyond maximum permissible limit of  $10 \mu\text{g L}^{-1}$ , recommended by the World Health Organization. The highest among these are from Asia (32) and Europe (31), followed by regions like Africa (20), North America (11), South America (9) and Australia (4) (Shaji et al. 2021).

There are four main species of As in groundwater, including two inorganic species – arsenate “As(V)” and arsenite “As(III)”, and two organic species – monomethyl arsenic acid (MMA) and dimethyl arsenic acid (DMA) (Tao et al., 2022). The toxicity of arsenic depends very much on its chemical forms, inorganic oxyanions are predominant forms, which exhibit higher toxicity over other forms:  $\text{As(III)} > \text{As(V)} > \text{MMA} > \text{DMA}$  (Hughes 2002; Tao et al., 2022). The arsenic species are causes of diseases such as skin, lung, bladder, liver, kidney, and prostate cancers, cardiovascular diseases, abnormal glucose metabolism, type II diabetes and neurotoxicity (Matos et al., 2022). Other organics species as arsenobetaine (AsB), the main As compound in most marine organisms is not metabolized in the human body and, therefore, no toxic effect is associated with AsB exposure (Popowich et al., 2016).

The main arsenic species and their structures are shown in Figure 2. As stated by Altowayti et al. (2022), certain key organic and inorganic compounds in living organisms can undergo biochemical changes due to the highly reactive nature of arsenic. The existence of inorganic arsenic in a solution is primarily governed by two key factors: the pH and the potential for oxidation or reduction (Altowayti et al., 2022).

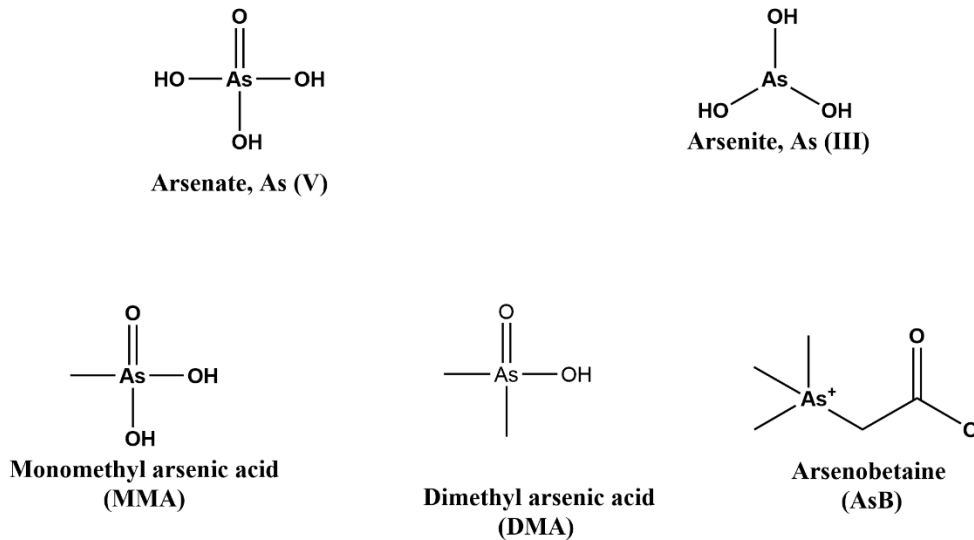


Figure 2. Chemical structure for most abundant arsenic species.

The predominance of arsenic species in the system As–O–H, at different pH, 25°C and 1 bar, is showed in Figure 3. Arsenite species, including  $\text{H}_3\text{AsO}_3$ ,  $\text{H}_2\text{AsO}_3^-$ , and  $\text{HAsO}_3^{2-}$ , are present in anoxic reduction conditions such as groundwater. The uncharged form of  $\text{H}_3\text{AsO}_3$  dominates the pH 9.2 environment. On the other hand, arsenate species such as  $\text{H}_3\text{AsO}_4$ ,  $\text{H}_2\text{AsO}_4^-$ ,  $\text{HAsO}_4^{2-}$ , and  $\text{AsO}_4^{3-}$  are stable in aerobic oxidation environments and have a higher oxidation potential than arsenite species. While  $\text{H}_3\text{AsO}_4$  and  $\text{AsO}_4^{3-}$  are found, respectively, in highly acidic and alkaline environments,  $\text{H}_2\text{AsO}_4^-$  is predominant in the low to middle pH range (2–6.9) and  $\text{HAsO}_4^{2-}$  in the middle to high pH range (6.9–11.8) (Najib and Christodoulatos, 2019).



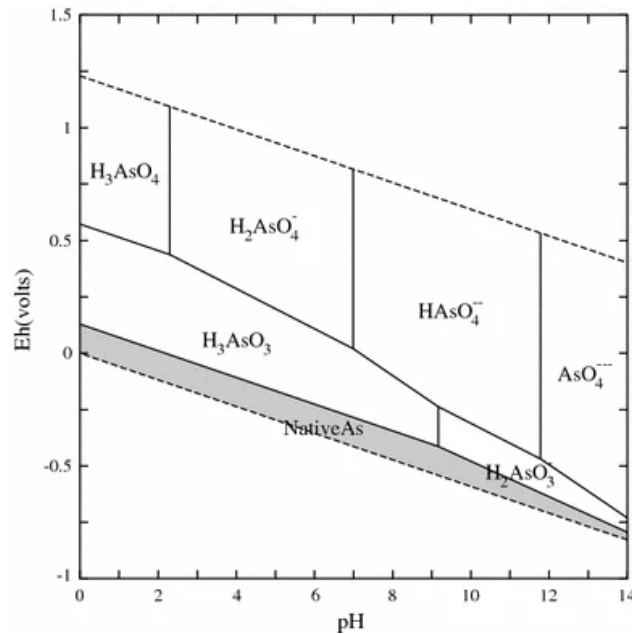


Figure 3. Eh–pH diagram for the system As–O–H at 25°C and 1 bar. *Source: Arsenic Eh–pH diagrams at 25°C and 1 bar.* (Lu and Zhu, 2010). Copyright (2010) with permission of Springer Nature.

Precise determination of amounts of different arsenic species in real samples is necessary to estimate the environmental impact and potential health risks. In view of the above facts, fast, sensitive, accurate and simple analytical methods for the speciation of inorganic arsenic is necessary (Montoro et al., 2018). So far, most of the methods reported for arsenic speciation analysis are chromatographic methods, which are very precise. However, consume substantial amounts of reagents and time, not well recommended for many samples. In this way, non-chromatographic methods for arsenic speciation can be attractive due to some characteristics, such as are faster, low cost and can be used for screening analysis for many samples.

## 1.2. Lead occurrence and health effects

Lead is a potentially toxic elements that could exist in both organic and inorganic states. Inorganic lead (Pb) is primarily present in dust, soil, aged paint, and various consumer goods, while organic lead was found in gasoline, especially tetraethyl and tetramethyl lead. Both of these Pb forms are toxic, however, organic Pb complexes pose an excessive level of toxicity to biological systems compared to inorganic Pb (Kumar et al., 2020). Lead is being the second most hazardous substances (ATSDR, 2022). Naturally occurring lead ores comprise 0.002% of the Earth's crust. Furthermore, its natural concentration remains below  $50 \text{ mg kg}^{-1}$  (Tarragó and Brown, 2017).

The Pb cycle in the environment at the different pathways for human exposure are represented in Figure 4. In general, human exposure to Pb occurs through various pathways, including atmospheric dust, automobile exhaust, paint, polluted food, and water (Kumar et al., 2020; Shan et al., 2021). Precipitation removes lead from the atmosphere, transferring it to soil or surface water. In addition, lead was used as a pesticide in vegetable and fruit cultivation (Gall et al., 2015). Rainwater carries these soil particles, leading to the introduction of lead into water bodies and lakes. Consequently, the cycle continues as lead is transferred to animals and plants from air, water, and soil (ATSDR, 2002). Despite the pervasive presence of Pb in aqueous ecosystems, elevated concentrations can arise due to human-induced actions such as the production of batteries, paint, and cement, as well as mining and smelting operations (Lee et al., 2019). Currently, human exposure to Pb is mainly through the ingestion of dust particles from soil in homes , drinking water and contaminated food (Shan et al., 2021).

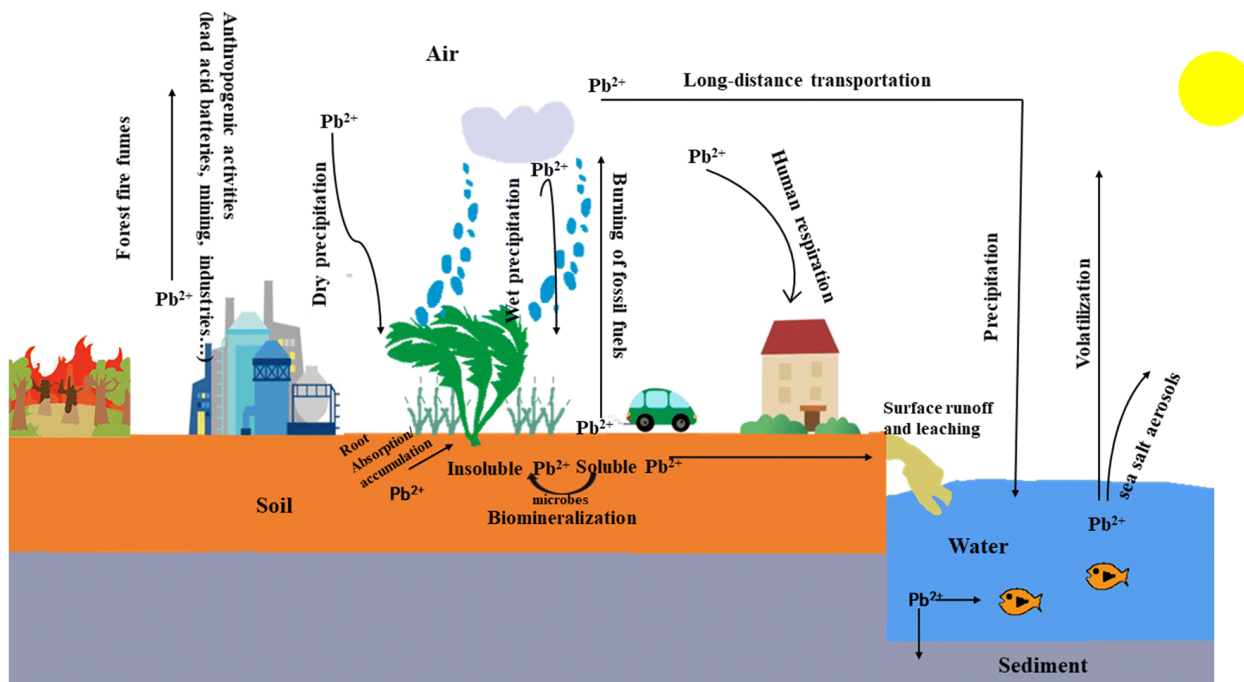


Figure 4. The pathway of lead in the biogeochemical cycle. *Source: A review on mechanism of biomineralization using microbial-induced precipitation for immobilizing lead ions.* (Shan et al., 2021). Copyright (2021) with permission of Springer Nature.

In Brazil, lead has not been used in automotive gasoline since 1993, and in 1996, primary lead smelting facilities ceased operations. The main causes of known poisoning in Brazil are lead-acid battery production, recycling plants and mining areas (Ferron et al., 2012). Although not considered an important source of lead contamination, the gasoline used in airplanes in Brazil, until 2009, had lead as an additive (Resolução ANP Nº 5 DE 03/02/2009 - Federal - LegisWeb, 2009).

Some investigations have examined the occurrence of lead poisoning in Brazilian children, with two studies specifically focusing on children residing in areas without prior reports of environmental lead contamination. In a study conducted by Carvalho et al. (2000), in Salvador, the authors observed the prevalence of 33% of Pb in children aged from two to 39 months, with blood lead levels exceeding  $10 \mu\text{g dL}^{-1}$ . In this work, no

specific sources of lead contamination were identified (Carvalho et al., 2000). Furthermore, a study from Oliveira et al. (2009) conducted in a community in Rio de Janeiro assessed the blood lead levels of 64 children and teenagers. The study revealed a lead poisoning prevalence of 5% of the population studied. The sources of lead exposure within this population were associated with local traffic, industrial plants, and household dust (Oliveira et al., 2009). Ferron et al. (2012) investigated lead poisoning in children in Porto Alegre state, the results show that the 16.5% of the children studied present blood lead levels exceeding  $10 \mu\text{g dL}^{-1}$ . The study also analyzed soil contamination on the studied area, the plausible causes of soil contamination can be related to the process of land use and previous informal garbage dump. Some environmental contaminations resulting from this garbage dump could be responsible for the elevated level of lead found in the soil. Also the area was located close to a region of industrial plants, including some secondary metal processing industries; they might have contributed to previous deposition of lead in the soil (Ferron et al., 2012). It is also important to manage and control lead contamination levels in food and waters to avoid human poisoning. Recent research from Cabral et al. (2019) reported lead levels in different food produced and consumed in Brazil, higher levels of Pb were observed in infant food, vegetables, meat, and meat products. Lead levels obtained in this study for most of the food categories are: beverages ( $0.0483 \text{ mg kg}^{-1}$ ), fruits and fruit products ( $0.0472 \text{ mg kg}^{-1}$ ), vegetables and vegetable products ( $0.1671 \text{ mg kg}^{-1}$ ), and meat and meat products ( $0.1248 \text{ mg kg}^{-1}$ ) (Cabral et al., 2019).

According to International Agency for Research on Cancer (IARC), Pb is classified as carcinogenic (Group 2B) to humans (IARC, 2023). The human body absorbs a

considerable amount of ingested Pb, ranging from 20% to 70%, and this values are known to be higher in children, and can suffer profound and permanent adverse health impacts, particularly on the development of the brain and nervous system (WHO, 2022). Lead can accumulate in the human body and distributed in the brain, kidney, liver, and bones. Lead primarily impacts the nervous system, leading to disruptions in its normal functioning when individuals are exposed to it over extended periods. Furthermore, prolonged exposure to lead also results in significant adverse effects on both the kidneys and the brain (ATSDR, 2002). Lead poisoning also can damage reproductive system. It is well reported by Wu et al. (2012), that high level of lead in semen reduce the sperm count and contributed to infertility, also was affected the motility and the morphology of the sperm (Wu et al., 2012). A review by Bellinger (2005) demonstrated the impact of lead exposure on the reproductive system, elevated paternal lead exposure exceeding  $40 \mu\text{g dL}^{-1}$  or a cumulative exposure of over  $25 \mu\text{g dL}^{-1}$  for several years has been associated with diminished fertility, heightened chances of spontaneous abortion, and impaired fetal growth, including preterm delivery and low birth weight. Maternal blood lead levels around  $10 \mu\text{g dL}^{-1}$  have been correlated with elevated risks of pregnancy-induced hypertension, spontaneous abortion, and compromised neurobehavioral development in offspring (Bellinger, 2005). Lead contamination affects children more severely than adults, children have higher absorption rates of lead compared to adults, particularly those aged 6 and younger, as their developing bodies and organs are more vulnerable to the harmful effects of lead (Levin et al., 2008). The developing nervous system in children is highly susceptible to the detrimental effects of lead. Lead interferes with the formation of myelin, a substance that protects nerve fibers, and disrupts the transmission of signals between

brain cells, impairing neurodevelopment. This can lead to cognitive and behavioral problems, including learning difficulties, decreased attention span, and behavioral issues such as hyperactivity and aggression (Olympio et al. 2010; Grandjean and Landrigan 2014).

Analytical methods are of utmost importance in monitoring and remediating lead contamination in environmental samples. Among the various environmental matrices, water is one of the primary sources of lead exposure in humans. Therefore, it is crucial to implement robust techniques for remediation lead levels in water sources. Accurate and sensitive analysis allows for the identification of lead-contaminated water bodies, assessment of the extent of contamination, and implementation of appropriate remediation measures. By regularly monitoring water sources for lead, we can effectively safeguard human health and reduce the risk of lead exposure-related health problems.

### **1.3. Methods for remediation, recovering and monitoring potentially toxic elements**

Potentially toxic elements have been removed from industrial effluents by conventional treatment methods such as reverse osmosis (Zhang et al., 2021), electrodialysis (Juve et al., 2022), ultrafiltration (Ren et al., 2021), ion exchange (Korak et al., 2023), chemical precipitation (Wu, 2019), and adsorption (Arora, 2019). Some of these methodologies have some disadvantages for removing potentially toxic elements such as high cost, high energy needs, ineffectiveness at removing metals at low concentrations (1-50 mg L<sup>-1</sup>), large amounts of reagents required, and potential for

secondary pollution through the creation of chemical sludge and disposal of floc residues (Ali Redha 2020).

Adsorption can be advantageous in terms of cost, adaptability, and environmental impact when compared to other remediation methods. There are some recent review articles that demonstrate the efficiency, capacity of a wide variety of adsorbent materials used for the remediation and monitoring of potentially toxic elements (Arora, 2019; Gupta et al., 2021; Llompарт et al., 2019; Redha, 2020). Over the past few decades, the use of environmentally friendly and cost-effective materials such as agricultural, industrial, or urban residues for the adsorption of potentially toxic elements has emerged as a promising technique for the elimination of pollutants from wastewater.

Potentially toxic elements can be adsorbed onto solid surfaces and this process is called adsorption. Adsorption is a process in which a particular compound attaches to the solid surface by physical forces or by chemical bonds (Shrestha et al., 2021). There are mainly three steps involved in potentially toxic elements adsorption: (I) the transport of potentially toxic elements from the bulk solution to the adsorbent surface; (II) frontier diffusion, layer of stagnant solution adjacent to the surface of the particle; (III) adsorption on particle surface; and (IV) finally the transport within the adsorbent particle. There are some factors affecting the adsorption such as temperature, nature of the adsorbate and adsorbent, presence of other species, and experimental conditions (pH, the concentration of metal species, contact time, and particle size of the adsorbent) (Pandey, 2021).

For many years, adsorption has been utilized for metal separations on a small scale to yield a product of extremely high purity or to achieve exceptionally challenging separations. This technique is based on the concept of using a reactive material to

selectively take in the desired metals from an aqueous solution, such as a mineral or leachate derived from waste. The solid utilized will usually have a strong attraction to the adsorption of a particular metal or set of metals when compared with any other co-existing species (Brewer et al., 2022). The materials used in adsorption systems are often inexpensive to acquire or produce and can be reused, increasing the cost-effectiveness of the process. Additionally, the technique is highly adjustable to meet the needs of a variety of inputs, making it a viable choice for metal purification and recovery. The utilization of adsorption for metal recovery boasts a great deal of variety, as the functional groups present on the material's surface can be naturally occurring or artificially modified, this promotes good selectivity for the recovery of a wide variety of metals from wide variety of matrices (Brewer et al., 2019). However, the use of adsorbents for wastewater treatment is limited due to various drawbacks, including the long time required to reach equilibrium, unsatisfactory removal efficiency, and unsuitability for low-concentration applications (Garba et al., 2020). To be effective, an adsorbent must have some characteristics such as cellular structure, abundant functional groups, and high mechanical and chemical stability, which allow for a large contact area, adsorption selectivity, and structural stability (Gupta et al., 2021; Cao et al., 2017).

Microcrystalline cellulose (MCC) has a highly crystalline structure, unique mechanical and chemical properties and is a suitable candidate as a framework for synthesizing adsorbents. However, the adsorption capacity of MCC may not be optimal without modification, as it lacks strong binding sites for potentially toxic elements (Garba et al., 2020).



## 1.4. Cellulose

Cellulose is the most abundant renewable biopolymer in nature with an annual production estimated above  $7.5 \times 10^{10}$  tons. Obtaining of cellulose and cellulose derivatives for use in different fields from alternative sources of raw materials have gained importance. Currently, cellulose has been used in industry as both raw material and product for thousands of years (Başaran et al., 2020). Due to the strong intermolecular and hydrogen bonds between the hydroxyl groups, cellulose tends to aggregate into bundles and form highly crystalline structure, which limits its elemental ions removal performance. On the other hand, the large number of hydroxyl groups endow chemical modification characteristics of cellulose to obtain better adsorption performance and provide the possibility of large-scale application (Fakhre and Ibrahim, 2018).

Cellulose as natural polymer is highly attractive owing to its unique properties and characteristics, such as excellent thermal stability, chemical resistance, and biodegradability. Cellulose has been used as an emerging adsorbents, alternative to synthetic polymers to solve important environmental issues such as removal of dyes and potentially toxic elements (Garba et al., 2020). Cellulose consists of glucose repeating units, as represented in Figure 5, with abundant hydroxyl groups, which not only enable extensive hydrogen bonding, but also provides excellent reactive sites to incorporate a range of chemical functionalities to achieve desirable properties (Choi et al., 2020; Wang et al., 2017).

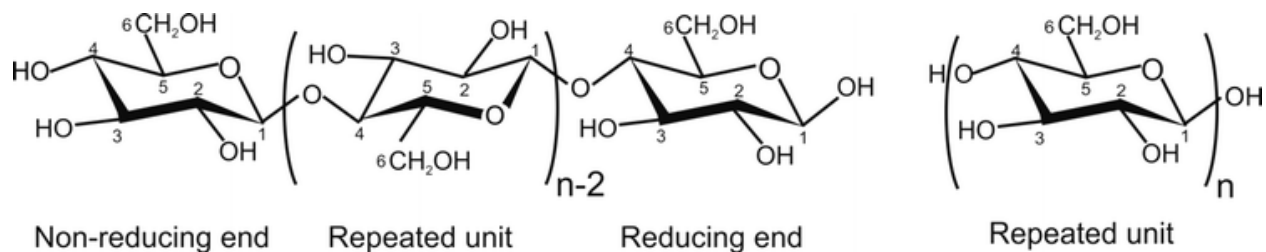


Figure 5. Chemical structure of cellulose. Source: Glucose, not cellobiose, is the repeating unit of cellulose and why that is important (French 2017). Copyright (2017) with permission of Springer Nature.

Since the mid-19th century, the properties of cellulose have been changed by chemical modification for commercial and scientific purposes, and their substituted polymers have found a wide range of applications. However, the inherent polydispersity and supramolecular organization of starch and cellulose cause the products resulting from their modification to display high complexity (Mischnick and Momcilovic, 2010).

Cellulose is often functionalized through various methods to improve the adsorption capacity and effectiveness to make it a better adsorbent. Various chemical modifications of its surface have been reported in the literature (Hokkanen et al., 2016). For instance, esterification (Choi et al., 2020), etherification (Oyewo et al., 2019), sulfonation (Suopajärvi et al., 2015), and oxidation (Sharma et al., 2018), which resulted in improved physical and chemical properties are usually the most used. Several studies indicate that specific functional groups such as amino (-NH<sub>2</sub>), carboxyl (-COOH), hydroxyl (-OH), and/or thiol (-SH) can provide adsorption sites for potentially toxic elements ions. Modified cellulose containing carboxyl and amino groups has been found to exhibit greater capacity for adsorbing potentially toxic elements ions and organic pollutants than

unmodified cellulose, after undergoing chemical treatment (Wu et al., 2020; Fakhre and Ibrahim, 2018; Alila and Boufi, 2009).

As discussed earlier, cellulose, whether chemically modified or in its natural form, has reached a considerable field of application in environmental and analytical chemistry as an adsorbent material, in the stage of pre-concentration and separation of chemical elements and organic compounds. The most used forms for analytical purposes are the following:

- ❖ **Beads:** Were simply prepared by hand-dropping a viscose solution into an aqueous coagulation bath. Since that report, various procedures for obtaining cellulose beads with diameters ranging from about 10  $\mu\text{m}$  to 1-3 mm have been developed using different solvents and techniques to obtain spherical particles (Gericke et al., 2013; Nie et al., 2021). Cellulose beads are excellent filling materials for chromatographic applications (Du et al., 2010). They have also been used as metal ion exchange and water treatment (Wang et al., 2019; Luo et al., 2016).

- ❖ **Membrane/Filter:** Cellulose is modified chemically, generally to obtain cellulose esters, providing greater mechanical strength (Qiu and Hu, 2013), and are subsequently used as drug delivery (Reid et al., 2008), separation (Güell et al., 2011), water treatment (Choi et al., 2020), bio-membrane (Perendija et al., 2021), and adsorption (Pei et al., 2021).

- ❖ **Aerogel:** Functional cellulose aerogels are the next generation of eco-friendly porous materials (after silica aerogels and organic polymer aerogels) with some extraordinary physicochemical properties such as low density, high surface area, and tunable surface chemistry. Drying methods, such as freeze and supercritical drying are

routinely used to remove the liquid phase of hydrogels, while maintaining a highly porous solid structure (Li et al., 2019). They have been widely used as catalyst supports (Li et al., 2018, Li et al., 2017), thermal insulator (Han et al., 2015), energy storage materials (Yang et al., 2015) and environmental remediation materials (Syeda and Yap, 2022).

#### **1.4.1. Adsorption methods using cellulose-base adsorbent for fractionation and speciation of As**

Besides the total concentration of some elements for quantitative analysis in a sample, the qualitative analysis to know the species related to these elements has been quite common to answer several questions about the toxicity, mobility, bioavailability, essentiality, etc. The term speciation has often been used to indicate the analytical activity of identifying chemical species and measuring their distribution. Sometimes, it is used to indicate that a method gives more information on the form in which the element is present than other more commonly applied techniques. In some cases, some species are stable and differentiable enough to allow direct determination. This does not mean that speciation was determined only by the concentration of one or a few species was found. In many cases, many individual species will make it impossible to determine speciation. In practice, it is possible to identify several classes of species of the same element and determine the sum of their concentrations in each class. Such subdivisions can be based on many different properties of the chemical species, such as size, solubility, affinity, charge, and hydrophobicity. Fractionation may involve a physical separation (e.g., filtering, size exclusion chromatography). In some cases, the fractionation can be refined

by supplementary speciation analysis in each of the separate fractions (Templeton et al., 2000; Templeton and Fujishiro, 2017).

Speciation analysis of trace elements has become increasingly important due to the impact of a given element in an environmental or biological system depends critically on its chemical form. Arsenic is an omnipresent toxic trace element and is mainly found in environmental water with its inorganic species, As(III) and As(V). It is well known that As(III) is the most toxic form of the water-soluble species while As(V) is also relatively toxic. Thus, separation of As(III) and As(V) for speciation analysis of arsenic is very necessary (Li et al., 2014).

Organic arsenic compounds such as monomethyl arsenic acid (MMA), dimethyl arsenic acid (DMA), arsenocholine (AsC), arsenobetaine (AsB), trimethyl arsine oxide (TMAO), tetramethylarsenic (TETRA), arsenosugars and arsenolipids (AsLp), are common forms detected in marine organisms, terrestrial plants, and mushroom. Methylated arsenic species, such as MMA and DMA, have been confirmed to be much less toxic (Li et al., 2017). The toxicity of arsenic not only depends on their chemical forms but also their bioavailability. The toxicity of As(III) and As(V) was reported to be related to their high bioavailability, as their absorption rate in the human gastrointestinal tract was over 80% (Zou et al., 2019).

Thus, it is important to the development of new methods that can be used quickly, efficiently and at low cost for the monitoring of inorganic arsenic species since this can be a routine analysis in many water and food quality control laboratories. So far, most of the methods reported for this analysis are chromatographic methods (B'Hymer and Caruso, 2004; Reid et al., 2020; Virk et al., 2023), which are very precise. However,

because the consume of substantial amounts of reagents and time, it is not well recommended for many samples analysis. In this way, non-chromatographic methods can be attractive due to some characteristics, such as are faster, low cost and can be used for a screening analysis for a large number of samples (Ferreira et al., 2020).

In recent years, there has been a growing interest in developing "green" methods that promote a cleaner and more sustainable environment. The use of natural adsorbents (biosorbents) has been a clear alternative in the development of analytical methods. Biosorbents of vegetable origin (lignocellulosic) are abundant in nature and can be modified chemically or physically to improve their adsorptive capacity while meeting most of the criteria established for an analytical method to be considered sustainable. Studies have shown that biosorbents can be used to remove or determine toxic metals in effluents. The biosorbents commonly exhibit various functional groups such as hydroxyl, carboxyl, phenolic, amino, sulfhydryl, alcoholic and ester groups. These functional groups possess a considerable potential for removing As species from water by means of sorption, complexation, ion exchange, diffusion, or co-precipitation reactions (Asere et al., 2019), as illustrated in Figure 6.

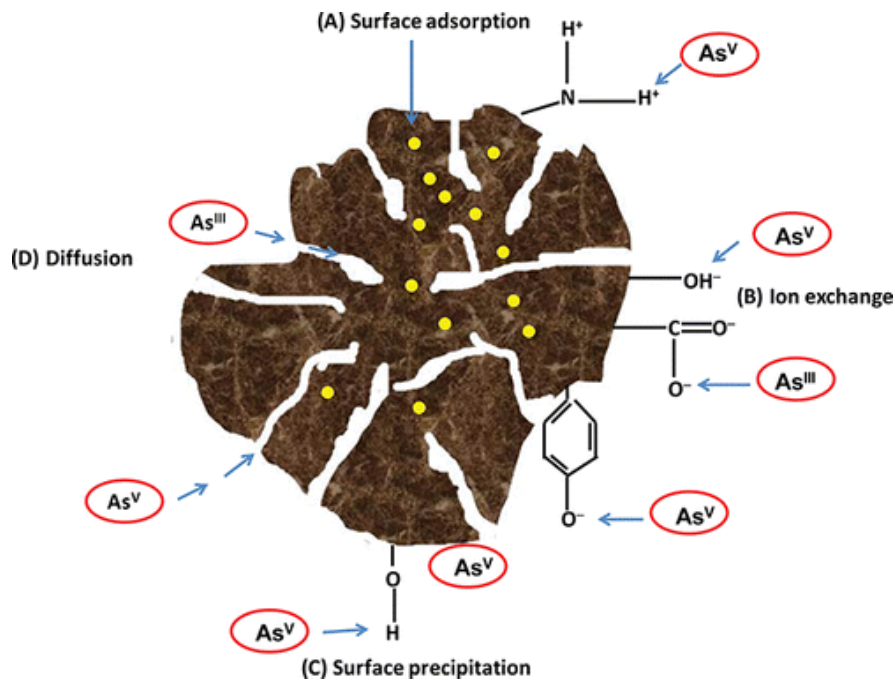


Figure 6. Arsenic sorption mechanism on the biosorbent surface. *Source : Remediation of arsenic-contaminated water using agricultural wastes as biosorbents.* (Shakoor et al. 2016). Copyright (2016) with permission of Taylor & Francis.

Several techniques, including flame atomic absorption spectrometry (FAAS), cold vapor atomic absorption spectrometry (CV AAS), hydride generation atomic absorption spectrometry (HG AAS), graphite furnace atomic absorption spectrometry (GF AAS), inductively coupled plasma optical emission spectrometry (ICP-OES), inductively coupled plasma mass spectrometry (ICP-MS), and X-ray fluorescence (XRF), can be employed in association with preconcentration strategies, using lignocellulosic adsorbents, for the determination of metals and metalloids in food, water, and environmental samples (Dias et al., 2023).

The adsorption capacity of cellulosic materials is improved through pretreatment and chemical modification. Adsorbents are prepared through various methods including

acidic and/or basic reactions, impregnation with metal ions or oxides, and reactions with organic compounds (Maia et al, 2021; Guisela et al., 2022; Asere et al., 2019).

Deng et al. (2016) reported the preparation of hyperbranched polyethylenimine modified cellulose fiber as an effective biosorbent for the removal of inorganic arsenic from aqueous solution. The adsorption mechanism for arsenic adsorption occurred through to electrostatic attraction and surface complexation with the amine groups on the modified surface of the fiber. The experimental data fit the Langmuir model and the maximum adsorption capacity for As(III) and As(V) were 54.13 mg g<sup>-1</sup> and 99.35 mg g<sup>-1</sup>, respectively (Deng et al. 2016). However, the authors did not explore the modified cellulose for application in water samples. Hokkanen et al. (2015) prepared a microfibrillated cellulose with magnetic iron nanoparticles for As(V) removal from waters. The uptake properties of the modified fiber show an improvement respect to the original Fe nanoparticles, the adsorption take place at lower pH values, with maximum adsorption capacity of 2.460 mmol g<sup>-1</sup> of As(V), at pH 2, and best adjust the Langmuir model (Hokkanen et al., 2015). Santra and Sarkar (2016) synthesize a cellulose nanocomposite by a sol gel technique, using cellulose powder and cerium ammonium nitrate for As(V) removal from water. The adsorption mechanism of As(V) adsorption is assessed to be electrostatic rather than ion exchange, and pH dependent reaching the best performance at lower pH values (Santra and Sarkar, 2016). X. Yu et al. (2013), synthesized multi-amino-functionalized cellulose with glycidyl methacrylate grafted onto the surface of cotton cellulose using ceric ammonium nitrate, and then the introduced epoxy groups reacted with tetraethylenepentamine to obtain it the multi-amino-functionalized adsorbent for inorganic arsenic removal from water. The adsorption process is pH dependent, the



optimal pH for the removal of arsenic was 7 for As(III) and 5 for As(V), the experimental data fit the Langmuir model and the adsorption capacities were 5.71 mg g<sup>-1</sup> and 75.13 mg g<sup>-1</sup> for As(III) and As(V) respectively, and the adsorbent show good reuse capabilities (Yu et al., 2013). Yousif et al. (2016) synthesized a copper containing modified cellulose for As(V) purification on different waters. The adsorption process show a fast (equilibrium adsorption at 5 min) and adsorption capacities of 1.32 mmol g<sup>-1</sup> towards As(V) from aqueous media at natural pH (8.4) (Yousif et al., 2016). Pereira et al. (2020) prepared a bioadsorbent by tosylation of microcrystalline cellulose and nucleophilic substitution of the tosyl group by ethylenediamine for the simultaneous removal of Cu(II) and As(V). The adsorption is dependent on the pH reaching the best performance for As(V) removal at pH 3, and the maximum adsorption capacity of the bioadsorbent for As(V) adsorption was 1.62 mmol g<sup>-1</sup>. Multicomponent adsorption experiments show that SO<sub>4</sub><sup>2-</sup> inhibited As(V) adsorption (Pereira et al., 2020). Singh et al. (2015) prepared a functionalized nanocrystalline cellulose by selective oxidation of the nanocrystalline cellulose with sodium periodate and then grafting of diethylene triamine to obtain their amine derivatives, for As(III) and As(V) removal from aqueous solution. The adsorption isotherms were best adjusted with Langmuir model and the maximum adsorption capacity were 10.56 mg g<sup>-1</sup> and 12.06 mg g<sup>-1</sup> for As(III) and As(V), respectively. The adsorption of the different species was proven to be dependent on the pH of the solution, optimum conditions were pH 7.5 for As(III) (92.84%) and 2.5 for As(V) (97.86%) removal (Singh et al., 2015).

In aqueous systems contaminated with arsenic, the removal of As(III) is typically more challenging than that of As(V). This phenomenon can be attributed to the

predominant neutral state of As(III) under natural water pH conditions (6-9), whereas As(V) is more commonly found in negatively charged forms (Guisela et al., 2022). The trivalent state of arsenic “As(III)” maintains a neutral charge up to pH 9.2, rendering it resistant to removal from contaminated water. Hence, most remediation technologies exhibit greater efficacy towards the pentavalent state of arsenic “As(V),” which typically exists in negatively charged in pH > 2.

#### **1.4.2. Adsorption methods using cellulose-base adsorbents for remediation and recovery of Pb**

There is some work in the literature from the past years, using cellulose as a base polymer to develop new absorbent materials for Pb remediation. Most of this work use chemical modification to incorporate new functional groups to improve their adsorption properties.

Modification with amino group is a common strategy, O’Connell et al. (2006) reported a glycidyl methacrylate-modified cellulose material functionalized with imidazole for the removal of Pb(II). This material showed selectivity towards Pb(II) ion over a wide pH range (pH 1–9), the adsorption process was best described by the Langmuir adsorption model and the maximum adsorption capacity was 72 mg g<sup>-1</sup> of Pb(II) from aqueous solution at 23°C (O’Connell et al., 2006). Barsbay et al. (2018) reported a  $\gamma$ -initiated grafting of poly(glycidyl methacrylate) from cellulose substrate and subsequent modification with iminodiacetic acid for Cd(II), Pb(II) and Cu(II) removal from aqueous media. Experimental results showed that pH 5 was the best condition for Pb(II) removal

and the adsorption capacity was  $52 \text{ mg g}^{-1}$  in batch adsorption condition (Barsbay et al., 2018). Wu et al. (2020) reported a multiple active sites cellulose-based adsorbent using epichlorohydrin cross-linking MCC with tetraethylenepentamine and grafting with bis(carboxymethyl) trithiocarbonate for the removal of low-level Cu(II), Pb(II) and Cr(VI). The experimental result showed the influence on the pH of the solution reaching 100% of Pb(II) adsorption at initial concentration of  $1 \text{ mg L}^{-1}$  at  $\leq \text{pH } 6$  (Wu et al., 2020). Sun et al. (2017) reported a cellulosic adsorbent prepared by halogenation of MCC and functionalized with pyridone diacid for the removal of Pb(II) and Co(II) from aqueous solutions. Results showed that the best Pb(II) adsorption performance occurred at  $\leq \text{pH } 4$ , the adsorption process could be described by the Langmuir adsorption model and the maximum adsorption capacity for Pb was  $177.75 \text{ mg g}^{-1}$ , with possibility of regeneration of the material (Sun et al., 2017). Huang et al. (2018) described the production of adsorbents based on cellulose acetate modified by polyethyleneimine grafting and subsequently by ethylenediamine, for Cu(II) and Pb(II) removal from water. The adsorbent show best adsorption performance for Pb(II), the process is best describe for Langmuir adsorption model achieving a maximum adsorption capacity of  $2.01 \text{ mg g}^{-1}$  at pH 4 (Huang et al., 2018). Kenawy et al. (2018) synthesized a guanyl-modified cellulose for the adsorption of Cu(II), Cd(II), Hg(II), Pb(II) and Zn(II) ions from aqueous solution. For the synthesis, cellulose was pretreated with periodate prior to its condensation with aminoguanidine for the formation of cellulose aldehyde-guanyl Schiff's. The adsorption of Pb(II) was carried out at pH 6 and the maximum adsorption capacity was  $52 \text{ mg g}^{-1}$ , obtained thought Langmuir isotherm model (Kenawy et al., 2018). Q. Wu et al. (2020) prepared a multiple active sites cellulose-based adsorbent with multiple active adsorption

sites (N, O, S) by using epichlorohydrin cross-linking microcrystalline cellulose with tetraethylenepentamine, followed by grafting with bis(carboxymethyl) trithiocarbonate for the removal of low-level Cu(II), Pb(II) and Cr(VI) from aqueous solutions. The adsorption mechanism studies indicated that the S and O atoms were the dominant adsorption sites for cationic potentially toxic elements ions Cu(II) and Pb(II), and N atoms were the dominant adsorption sites for the anion potentially toxic elements Cr(VI). The material exhibit a 100% removal of Pb(II) in pH above 6 (Wu et al., 2020). Sun et al. (2017) obtained a cellulose-base adsorbent by halogenation of microcrystalline cellulose and functionalized with pyridone diacid for removing Pb(II) and Co(II) from aqueous solutions. The maximum adsorption capacity described by the Langmuir model for the material towards Pb(II) was  $177.75 \text{ mg g}^{-1}$ . The adsorption process was pH dependent, reaching the best performance at pH range 4-6 (Sun et al., 2017). Kumar and Sharma (2019) prepared functional copolymers by graft copolymerization of cellulose extracted from rice husk with n-isopropylacrylamide and comonomer acrylic acid to obtain two materials for removal of Ni(II), Cu(II) and Pb(II) ions from aqueous solutions. The Pb(II) adsorption data was best fitted using Langmuir adsorption isotherm model and the maximum adsorption capacity for Pb(II) was  $118.3 \text{ mg g}^{-1}$  at pH 5 (Kumar and Sharma, 2019).

Some cases include nanoparticles and metallic oxides incorporation, Zhang et al. (2017) reported the use of cellulose fibers for substrates to induce the formation of nano-TiO<sub>2</sub> under microwave irradiation, to produce hierarchical mesoporous nano-TiO<sub>2</sub>/cellulose composites for Pb(II) adsorption. The adsorption rate is pH dependent and increase within the pH, reaching the highest adsorption at pH 6, the maximum adsorption capacity of  $42.5 \text{ mg g}^{-1}$  was reported (Zhang et al., 2017). Luo et al. (2016) produced a

magnetic cellulose-based nanocomposite beads, blending cellulose with the carboxyl-functionalized magnetite nanoparticles and acid-activated bentonite in NaOH/urea aqueous solution for Pb(II) removal from aqueous solution. The adsorption process was pH dependent and the removal efficiency decrease from pH 6 to 2, Freundlich isotherm model best adjust to the experimental data and the maximum adsorption capacity was estimated as 2,86 mg g<sup>-1</sup> (Luo et al., 2016). Fu and Xie (2020) synthesized a microcrystalline cellulose-manganese dioxide nanocomposite by the redox reaction between potassium permanganate and ethanol based on microcrystalline cellulose for removal of Pb(II) and Cd(II) from water. Experimental results show that the Pb(II) adsorption was a rapid process, and the maximum adsorption capacities of Pb(II) with Langmuir model was 290.8 mg g<sup>-1</sup>, at pH 6. The adsorption mechanism is mainly attributed to surface complexation and electrostatic attraction (Fu and Xie, 2020). Luo et al. (2016) prepared a magnetic cellulose nanocomposite beads via extrusion dropping technology by blending cellulose with the carboxyl-functionalized Fe<sub>3</sub>O<sub>4</sub> nanoparticles and acid-activated bentonite in NaOH/urea aqueous solution, for Pb(II) removal from water. They found that complexation, ion exchange, and electrostatic interactions are all involve in the adsorption mechanism of Pb(II) onto the magnetic cellulose beads, the adsorption is pH dependent and the best performance was obtain in a pH 4.5-6 and the maximum adsorption capacity was 2.862 mg g<sup>-1</sup> (Luo et al., 2016).

For carboxylic groups incorporation, Vadakkekara, Thomas, and Nair (2019) prepared a maleic acid modified cellulose in different fibrillary size (macro, micro and nano) by the reaction of cellulose with maleic anhydride followed by sodium exchange of protons for Pb(II) from contaminated waters. They demonstrated that the adsorption

occurred through chemisorption and the experimental data best adjust Freundlich model, the maximum chemisorption capacities of macro, micro and nano for Pb(II) were 20 mg g<sup>-1</sup>, 40 mg g<sup>-1</sup> and 115 mg g<sup>-1</sup>, respectively, at pH of 5.5 (Vadakkakara et al., 2019).

Combination of different polymers are common strategy, Vijayalakshmi et al. (2017) prepared a nanochitosan/sodium alginate/microcrystalline cellulose bead for the removal of Pb(II) from aqueous solution. The experimental results showed that the best pH condition to follow the adsorption was at pH 6, among various adsorption equilibrium isotherms models where applied and Freundlich was found as the best adjust, the maximum adsorption capacity was estimated as 114.47 mg g<sup>-1</sup> (Vijayalakshmi et al., 2017). Zhao et al. (2021) prepared beads of cellulose nanofiber and sodium alginate path, a simple cross-linking method for the removal of Pb(II). The adsorption process adjust Langmuir adsorption isotherm model, and the maximum adsorption capacity was 318.47 mg g<sup>-1</sup> and the best pH condition for the adsorption process was above pH 3 (Zhao et al., 2021). Y. Li et al. (2019) prepared an aerogel with oriented microchannel structure via a directional freeze-drying approach using chitosan and nanofibrillated cellulose for efficient removal of Pb(II) from aqueous solutions. The best adsorption performance was observed at pH 5, with maximum adsorption capacity of 248.5 mg g<sup>-1</sup>, Langmuir isotherm model best adjust the experimental data. The kinetic of the adsorption was relatively high reaching good removal after 5 min, the reusability of the material was achieve through desorption experiments using Na<sub>2</sub>EDTA, keeping 85% of removal after 5 cycles (Li et al., 2019). Qu et al. (2020) obtained a functionalized cellulose derived from rice husk, under microwave irradiation reaction with CS<sub>2</sub> in NaOH medium for adsorption of Pb(II), Cd(II) and Ni(II) and application for electroplating wastewater purification. The adsorbent exhibit

adsorption capacity of 295.20 mg g<sup>-1</sup> for Pb(II), within the equilibrium time of 30 min at pH 5.5. Experimental results show that both ion exchange and chelation were involve in the metal ions uptake, while physical interaction was also involved in the adsorption process (Qu et al., 2020). Qu, Yuan, et al. (2020) prepared a  $\beta$ -cyclodextrin functionalized rice husk-based cellulose using epichlorohydrin as the cross-linking agent for removal of atrazine and Pb(II). The adsorbent presented a pH-dependent adsorption performance for Pb(II) with best performance at pH range of 4-6, with an adsorption capacity of 283.00 mg g<sup>-1</sup>, adjusting the Langmuir model. The Pb(II) adsorption was associated with complexation and electrostatic interaction (Yuan et al., 2020). Xu et al. (2021) prepared carboxylated chitosan/carboxylated nanocellulose hydrogel beads for Pb(II) removal from aqueous solutions. The best pH for the adsorption was at pH 4, the adsorption data fitted the Langmuir model and the maximum adsorption capacity was 334.92 mg g<sup>-1</sup> (Xu et al., 2021). Hu et al. (2018) prepared a carboxylated cellulose nanocrystal-sodium alginate hydrogel beads using cross-linking method, first microcrystalline cellulose was treated with ammonium persulfate and citric acid under ultrasonic treatment to obtain the carboxylated cellulose nanocrystals and then mixed with the alginate solution to form the beads, the beads were used for adsorption of Pb(II) from aqueous solution. The equilibrium was reached after 3 h and the best pH condition for the adsorption took place was pH 5. The Langmuir model was used for determination of the maximum adsorption capacity that was 338.98 mg g<sup>-1</sup> (Hu et al., 2018). Mohammadabadi and Javanbakht (2020) prepared alginate/lignocellulosic compounds (cellulose, hemicellulose, and lignin extracted from barley straw) hybrid gel beads for removing Pb(II) ions from aqueous solution. The experimental data best fit Langmuir model and the maximum adsorption

capacities were obtained for the different materials 206.75 mg g<sup>-1</sup>, 244.50 mg g<sup>-1</sup>, and 365.43 mg g<sup>-1</sup> for cellulose, hemicellulose, and lignin-based biocomposites, respectively, and all presented best performance at pH > 3.5 (Mohammadabadi and Javanbakht, 2020).

In this way, it is possible to see that cellulose-based materials have been extensively studied as a base polymer to develop absorbent materials for the remediation of Pb from aqueous solutions. Researchers have used chemical modification techniques to incorporate new functional groups to improve their adsorption properties. Several studies have shown that the adsorption of Pb(II) ions on these materials is pH-dependent and that the Langmuir adsorption model is best suited for describing the adsorption process. Advantages of cellulose-based materials include their biodegradability, low cost, and high availability. However, a major limitation of these materials is their low mechanical strength, which can be addressed by incorporating reinforcement materials. Overall, these materials have demonstrated high selectivity and adsorption capacity for Pb(II) and others ions over a wide pH range, making them a promising candidate for water treatment applications.



## **2. Objective**

The goal of this project is to develop methods for lead separation and determination and fractionation and speciation of organic and inorganic arsenic species in different water samples using cellulose-base adsorbent and detection by inductively coupled plasma optical emission spectrometry (ICP OES) and graphite furnace atomic absorption spectrometry (GF AAS).

### **2.1. Specific Objective**

- ❖ Preparation and characterization of different cellulose-base adsorbent materials for Pb separation and determination, and As fractionation and speciation.
- ❖ Morphological characterization of the materials using Infrared Spectroscopy, Scanning Electron Microscopy, X-ray Photoelectron Spectroscopy and CNH elemental analysis.
- ❖ Optimization of the experimental adsorption parameters for the separation of Pb(II) from different water (potable, lake and saline) samples using ICP OES as detector.
- ❖ Optimization of the experimental parameters for the separation, pre-concentration, and determination of inorganic arsenic species from river water sample, using GF AAS as detector.

### 3. Experimental Section

#### 3.1. Instrumental

For As and Pb detection was used an inductively coupled plasma optical emission spectrometer (ICP-OES) (Thermo Fisher Scientific Inc.), model iCAP 7400 Duo, with dual view, CID (Charge Injection Device) detector, wavelength range from 166.4 to 847.0 nm, Echelle polychromator and focal length of 383 mm, that provides an optical resolution from 19 pm to 200 nm, and 27.12 MHz radiofrequency sources, being able to adjust the applied power from 750 to 1350 W. Argon (99.998% v v<sup>-1</sup>) (Air Liquid Brasil, São Paulo, Brazil) was used to generate and maintain the plasma and sample aerosol transportation. Table 1 shows the set up instrumental parameters for Pb determination by ICP OES.

Table 1. Instrumental set up of ICP OES for As and Pb detection.

Parameters	Selected condition
Power supply	1350 W
Nebulizer	Meinhard
Spray chamber	Cyclonic
Plasma gas-flow	12 L min <sup>-1</sup>
Auxiliary gas-flow	0.2 L min <sup>-1</sup>
Nebulizer gas-flow	0.5 L min <sup>-1</sup>
Sample introduction	2 mL min <sup>-1</sup>
Wavelength	As (I) 189.042 nm Pb (I) 220.353 nm

(I) Ionic emission

The determination of the limit of detection (LOD) and limit of quantification (LOQ) for ICP-OES measurements were calculated according to the International Union of Pure and Applied Chemistry (IUPAC),  $LOD=3S_B/m$ , and  $LOQ=10S_B/m$ , where  $S_B$  is the standard deviation of several consecutive measurements of the blank signal, and  $m$  is the calibration curve slope (Naught and Wilkinson 2019).

For As detection was also used a ZEE nit<sup>®</sup> 60 atomic absorption spectrometer (Analytik Jena AG, Jena, Germany), equipped with a transversely heated graphite atomizer automatic, an inverse and transversal 2- and 3-field mode Zeeman-effect background corrector, and an automatic sampling to deliver precise volumes of liquid analytical solutions into the graphite tube, pyrolytic graphite tube atomizer and boat-type platform were used throughout. The spectrometer was operated with a hollow cathode lamp for As (wavelength=193.6 nm, lamp current=6.0 mA, and bandpass=0.8 nm). The magnetic field strength used for 3-field mode Zeeman-effect background corrector was 0.8 T. All measurements were based on integrated absorbance values controlled by Windows NT+ software. Argon 99.998% (v v<sup>-1</sup>) (Air Liquid Brasil, São Paulo, Brazil) was used as protective and purge gas. The heating program of the graphite tube is showed in Table 2.

The heating program was set up pyrolysis an atomization temperature. Aliquots of 10  $\mu$ L of As solution was co-injected to the boat type platform with 10  $\mu$ l of a solution of 500 mg L<sup>-1</sup> of Pd<sup>2+</sup> (Pd(NO<sub>3</sub>)<sub>2</sub>) + 300 mg L<sup>-1</sup> Mg<sup>2+</sup> (Mg(NO<sub>3</sub>)<sub>2</sub>) as chemical modifier. The limit of detection (LOD) and limit of quantification (LOQ) for GFAAS were calculated according to IUPAC,  $LOD=3S_B/m$ , and  $LOQ=10S_B/m$ , as describe in previously for ICP-OES ( $S_B$  = standard deviation of blank, n=10, and  $m$  = curve slope).

Table 2. Heating program for the transversally heated graphite atomizer for As determination.

Step	Temperature (°C)	Ramp (°C s <sup>-1</sup> )	Hold time (s)	Argon flow-rate (L min <sup>-1</sup> )
Drying	80	10	10	1.0
Drying	130	20	5	1.0
Pyrolysis	450	50	10	1.0
Pyrolysis	1450	100	30	1.0
Auto Zero	1450	0	5	0
Atomization	2450	FP	5	0
Cleaning	2500	500	3	1.0

A Fourier Transform Infrared Spectrophotometer (FT-IR), model Frontier FT-IR (PerkinElmer) was used to identify the characteristic bands of beads produced by different approaches. KBr pellets containing dry powder of different materials were prepared for FT-IR analyses.

The morphology of beads was analyzed by scanning electron microscopy (SEM) in a model MEE JEOL Neoscope JCM-500). Dried beads were coated with a thin (~2 nm) gold nanoparticles layer prior to the analyses.

X-ray photoelectron spectroscopy (XPS) analyses were performed for beads before and after lead adsorption. The XPS spectra were obtained using Specs – XPS, with the instrumental configuration, Slit: 4:7x20c / C:mesh, Mode: Fixed Analyzer Transmission, Excitation Energy (1486.71 eV), Detector Voltage (1800 V), Bias Voltage (90.00 V). XPS high resolution spectra of C 1s, O 1s, and Pb 4f were obtained with a pass energy of 50 eV and 0.3 eV/step, accumulating 30 scans.

Elemental analysis using Elemental Analyzer - Perkin Elmer 2400 series II was used for CNH quantification. Its operation is based on the Pregl-Dumas method, in which the samples are subjected to combustion in an atmosphere of pure oxygen, and the resulting gases are released. Combustion is quantified in a TCD detector (thermal conductivity detector).

For the As speciation study, a chromatograph (Shimadzu Corporation, Kyoto, Japan) equipped with a degassing system (DGU-20 A3), reciprocating piston pumps (LC-6 AD) and a 100 $\mu$ L sampling loop. The separation of As species was carried out on an anion exchange column, model PRP X-100 (Hamilton, Reno, USA). The column output was connected directly to the ICP-OES nebulizer. The instrumental parameters of the ICP-OES for obtaining the As chromatograms were the same shown in Table 1.

To prepare solutions at different pHs, a pH meter, model DM-22 (Digimed Analytical Instrumentation) was used.

An IPC Series peristaltic pump (Ismatec, Switzerland) was used to prepare the beads and to control the flow through the columns.

### **3.2. Material and reagents**

All the chemicals and reagents used were analytical reagents. All the solutions were prepared with high purity water (18.2 M $\Omega$  cm), obtained from a Milli-Q<sup>®</sup> water purification system (Millipore Corporation, EUA).

Single-element standard solution containing 1,000  $\pm$  1 mg L<sup>-1</sup> of lead (PbNO<sub>3</sub>) in 5% (w v<sup>-1</sup>) in HNO<sub>3</sub> (Specpure<sup>®</sup>, Alfa Aesar, USA) and 1,000  $\pm$  1 mg L<sup>-1</sup> of arsenic (V) 5%

(w v<sup>-1</sup>) in HNO<sub>3</sub> (Specpure<sup>®</sup>, Alfa Aesar, USA) were used to prepare the references solution for analysis by dilution with deionized water. As(III) and As(V) standard solution were prepared by dissolving salts sodium arsenite (NaAsO<sub>2</sub>) and sodium arsenate hydrate (Na<sub>2</sub>HAsO<sub>4</sub>·7H<sub>2</sub>O), respectively, in deionized water.

Concentrated HNO<sub>3</sub> (65% w v<sup>-1</sup>) and HCl (35% w v<sup>-1</sup>), from Merck, were used. The pH of the solutions was adjusted using 0.1 mol L<sup>-1</sup> of NaOH solution (from Merck) and 0.1 mol L<sup>-1</sup> of HCl solution (from Merck).

Microcrystalline cellulose (MCC) with a particle size of less than 20 μm (SPEX SamplePrep) was used to prepare beads. For the modification of MCC was used Glycidyl trimethylammonium chloride (GTAC), purchased from Sigma Aldrich.

For the oxidation of As(III) was used Sodium Hypochlorite (NaClO), purchased from Sigma Aldrich.

### 3.3. Samples

- ✓ **High salinity water (HS water):** Sea water from the coast of the state of São Paulo, was collected and transported in polyethylene vials of 5 L. This water was filtered and HCl was added to adjust the pH at 2 for preservation of the dissolved ions, the water was kept in the refrigerator at temperature of 4-5 °C until analysis. This sample was diluted, used as a water sample with high salinity water (HSW), and tested for Pb separation.
- ✓ **Tap water:** Tap water was collected at the Chemical Institute at the São Paulo University previously to analysis. This sample was tested for Pb removal.

- ✓ **Dam water:** Dam water from the Guarapiranga dam, at the Embu-Guaçu sampling point was sampled and preserved as previously described (Mota, 2021). This sample was tested for Pb removal.
- ✓ **River water:** River water from “Corrego das Corujas” in the region of Vila Madalena state of São Paulo was collected and transported to the laboratory in polyethylene vials of 2 L. This water was filtered and HCl was added to adjust the pH at 2 for preservation, the water was kept in the freezer at temperature of 4-5 °C until analysis. This water was used for As species fractionation-speciation and inorganic As preconcentration.

### 3.4. Cellulose beads preparation

Cellulose beads are spherical particles with diameters in the micro to millimeter range and it has been used in many advanced applications such as adsorbent material, chromatography on solid supported synthesis and protein immobilization and delayed drug release. Beads preparation is easy, allowing large scale production of batches. Functional materials for specific applications have been reported, prepared by introducing chemical functionalities or by mixing cellulose with organic and inorganic compounds (Gericke et al., 2013).

Preparation of the cellulose beads was carried out according to the procedure previously described in the literature (Gericke et al., 2013). A solution of 7% (w v<sup>-1</sup>) of NaOH + 12% (w v<sup>-1</sup>) urea-water was added to 5% (w v<sup>-1</sup>) microcrystalline cellulose, MCC

solubilization; the mixture was agitated for 20 min, until a clean solution was obtained, and kept at 10 °C.

Afterward, the cellulose solution was dripped in an acidic coagulant bath, at 25°C, using an IPC Series peristaltic pump (100 pump rotation) with connection tubes of the Tygon type (1.6 mm inner diameter) for propulsion and a polypropylene tube (0.55 mm inner diameter) for dripping microcrystalline cellulose solution at the coagulating bath. As coagulating medium was used 0.1, 0.5, 1.0, 2.0 and 8 mol L<sup>-1</sup> HNO<sub>3</sub> and HCl 1 mol L<sup>-1</sup>. Figure 7 shows the schematic procedure for bead preparation and a photographic of final bead after formation in solution.

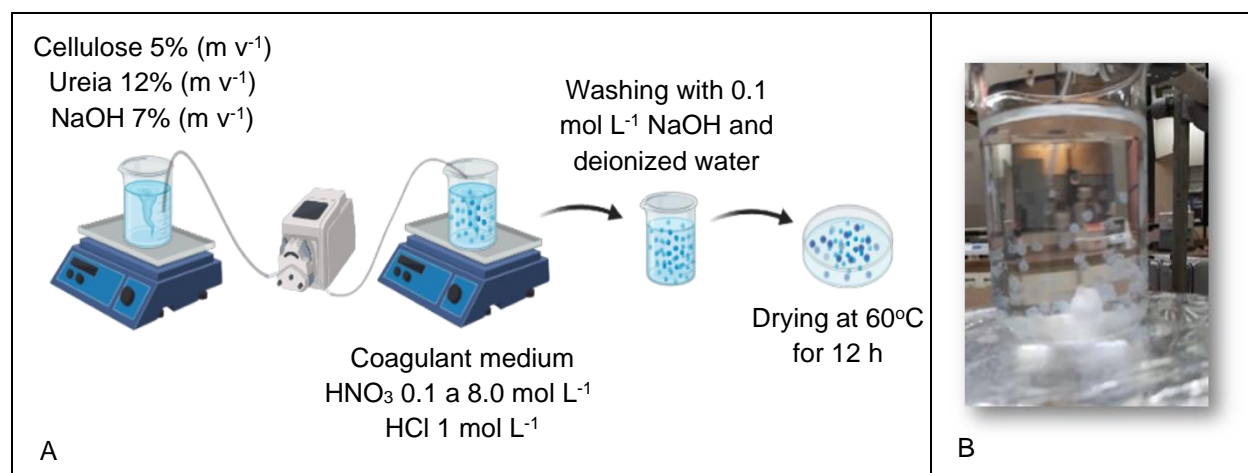


Figure 7. (A) Schematic setting up for the bead preparation and (B) photography of bead formation.

After formation of beads, they were separated by decantation and the supernatants were separated from the beads. The beads were washed with deionized water and neutralized with 0.1 mol L<sup>-1</sup> NaOH solution to eliminate the excess of acid on the beads



surface, which can affect adsorption experiments that are sensitive to pH changes, again washed with deionized water, dried in an oven at 60 °C and storage for further use.

### **3.5. Cellulose beads characterization**

Beads was characterized by Fourier transform infrared spectrophotometry (FT-IR), scanning electron microscopy (SEM), X-ray photoelectron spectroscopy (XPS), elemental analysis, as described in section 3.1.

#### **3.5.1. Point of zero charge determination for b-HNO<sub>3</sub>**

Point of zero charge (pzc) is defined as pH values for which one or more of the surface-charge components is equal to zero at a given temperature, pressure, and aqueous solution composition. The (pzc) of the b-HNO<sub>3</sub> adsorbents, prepared in 2.0 mol L<sup>-1</sup> of HNO<sub>3</sub>), was determined by potentiometric titration using a pH meter, model DM-22 (Digimed Analytical Instrumentation, São Paulo). Amounts of adsorbent (0.200 ± 0.001 g) were placed in Erlenmeyer flasks and added 25 ml of 0.05 mol L<sup>-1</sup> KNO<sub>3</sub> solution, which was used as the background electrolyte. The titration was carried out by adding aliquots of 0.02 mol L<sup>-1</sup> of HCl and 0.02 mol L<sup>-1</sup> of NaOH and stirring for 5 min in order to change the initial solution pH, which was measured with a glass electrode. The amount of protons (Q, in moles) consumed or released by each gram of adsorbent was calculated using equation 1 (Puziy et al., 2004):

$$Q = [(V_0+V_t)/m] \times ([H^+]_i - [OH^-]_i - [H^+]_e + [OH^-]_e) \quad \text{Equation 1}$$

where  $V_0$  and  $V_t$  are the volumes of the background electrolyte and the titrant, respectively, and  $m$  is the mass of the adsorbent. The subscripts “i” and “e” refer to the initial and equilibrium concentrations, respectively. The initial concentration of protons was calculated through the added amount of the titrant. The equilibrium proton concentration was calculated using the measured pH value. Background electrolyte (0.05 mol L<sup>-1</sup> KNO<sub>3</sub>) solution was also titrated, as reference.

### 3.5.2. Adsorption isotherm of Pb(II) onto b-HNO<sub>3</sub> in batch

Adsorption isotherms is a useful strategy to describe the relationship between the adsorbate concentration in solution (liquid phase) and the adsorbent (solid phase) at a constant temperature and design adsorption systems (Tran et al. 2017). To evaluate the performance of the different cellulosic materials (b-HCl and b-HNO<sub>3</sub>) on Pb(II) adsorption efficiency, batch experiment was carried out using the Equation 2 and Equation 3 to obtain the nonlinear and linear fit for Langmuir isotherm to estimation of different parameters) (Foo and Hameed 2010):

$$q_e = q_{max} * K_I * C_e / (1 + K_I * C_e) \quad \text{Equation 2}$$

$$C_e / q_e = 1/bQ_0 + C_e/Q_0 \quad \text{Equation 3}$$

where the  $C_e$  is the equilibrium concentration ( $\text{mg L}^{-1}$ ),  $q_e$  is the amount adsorbed at equilibrium ( $\text{mg g}^{-1}$ ),  $q_{max}$  is the maximum saturated monolayer adsorption capacity of an adsorbent ( $\text{mg g}^{-1}$ ), and  $KI$  is the equilibrium adsorption constant related to the affinity between an adsorbent and adsorbate ( $\text{L mg}^{-1}$ ).

The essential characteristics of the Langmuir isotherm model can be expressed by a dimensionless constant called the separation factor or equilibrium parameter  $RI$ , which is defined as follows (Tran et al. 2017):

$$RI = 1/(1+KI*C_0) \quad \text{Equation 4}$$

where  $RI$  is a constant separation factor (dimensionless) of the solid-liquid adsorption system,  $KI$  is the Langmuir equilibrium constant, and  $C_0$  ( $\text{mg L}^{-1}$ ) is the initial adsorbate concentration (Zhou et al. 2014). The value of  $RI$  describes the tendency of the adsorption process, which is either unfavorable ( $RI > 1$ ), linear ( $RI = 1$ ), favorable ( $0 < RI < 1$ ), or irreversible ( $RI = 0$ ). Greater affinity between the adsorbent and the adsorbate is inferred when  $RI$  is smaller (Zhou et al. 2014).

To evaluate the maximum Pb(II) adsorption capacity of the different materials (MCC and beads of MCC prepared in  $2.0 \text{ mol L}^{-1}$  of HCl (b-HCl) and  $2.0 \text{ mol L}^{-1}$  of  $\text{HNO}_3$  (b- $\text{HNO}_3$ ) media), adsorption experiments were carried out as follow. 2 mL of Pb(II) solutions with concentrations ranging from 1 to  $200 \text{ mg L}^{-1}$ , at pH 6, were put in contact with 8 mg of each different materials (b-HCl and b- $\text{HNO}_3$ ), and shaking for 24 h, in a horizontal rotary shaker, at 300 rpm. After centrifugation for 5 min, at 3000 rpm, the supernatant was analyzed by ICP OES.

### **3.6. Optimization of Pb(II) adsorption onto b-HNO<sub>3</sub> in a fixed-bed column**

Beads prepared in 2.0 mol L<sup>-1</sup> of HNO<sub>3</sub>, named b-HNO<sub>3</sub>, was used for Pb(II) separation and preconcentration in waters samples.

Continuous flow adsorption experiments were conducted with a polypropylene column (internal diameter of 0.8 cm) and porous polyethylene chips (0.8 cm in diameter; pore size <1 μm) filled with different beads (b-HCl and b-HNO<sub>3</sub>). The cartridges used were from Eichrom Technologies Inc. (Darien, IL, USA). The columns were prepared using 150 mg of each bead. For packaging of column, a suspension of the bead was prepared in water and subsequently added to the top of column and the packing occurs only by gravity. The column output was connected to silicone Tygon<sup>®</sup> tubes attached to a peristaltic pump (Ismatec, Switzerland). The experiments were performed in flow, for the optimization of the column adsorption process were evaluated different experimental conditions such as pH, flow rate of solution passing through the column, repeatability, and reusability.

#### **3.6.1. Adsorption rate as function of pH**

To evaluate the Pb(II) separation using b-HNO<sub>3</sub> against different pH, solutions of 1 mg L<sup>-1</sup> of Pb(II) in different pH (2 to 8) were prepared. The pH values were adjusted using HCl (0.1 mol L<sup>-1</sup>) or NaOH (0.1 mol L<sup>-1</sup>) solutions. The experiment was carried out using 10 ml of the different solutions that were passed through the column with a flow-

rate of 1 ml min<sup>-1</sup>. Subsequently, the eluate solution was analyzed by ICP OES for the determination of Pb(II). The separation capacity was calculated as:

$$Separation (\%) = \frac{C_o - C_e}{C_o} \times 100 \quad \text{Equation 5}$$

where  $C_o$  is the initial concentration and  $C_e$  is the concentration at the eluate. A solution of HCl (1 mol L<sup>-1</sup>) was used for desorbing, after that the concentration of Pb(II) desorbed was analyzed by ICP-OES and the recovery (%) was calculated as:

$$Recovery(\%) = \frac{C_o - C}{C_o} \times 100 \quad \text{Equation 6}$$

where  $C_o$  is the initial concentration and  $C$  is the concentration eluted after desorption.

### 3.6.2. Flow-rate optimization

To evaluate the influence of flow-rate on the Pb(II) adsorption using b-HNO<sub>3</sub>, 10 mL of 1 mg L<sup>-1</sup> of Pb(II) solution, at pH 6, was passed through the column at different flow-rate (0.5 to 2 ml min<sup>-1</sup>). Subsequently, the eluate solution was analyzed by ICP OES for the determination of lead.

### 3.6.3. Intra e inter column repeatability and type of eluent for desorption

To evaluate the repeatability of the adsorption process, 5 b-HNO<sub>3</sub> columns were prepared with the same masses of beads (150 mg) and in each one was passed through 10 mL of 1 mg L<sup>-1</sup> of Pb(II) solution, at pH 6, with a flow-rate of 0.5 ml min<sup>-1</sup>. Volumes of 2 mL of 1 mol L<sup>-1</sup> of HCl were used for desorbing and the eluates were analyzed by ICP-OES for the recoveries' calculation.

For the reusability investigation, in each of these 5 b-HNO<sub>3</sub> column (150 mg) was passed 10 mL of 1 mg L<sup>-1</sup> of Pb(II) solution, at pH 6, with a flow-rate of 0.5 ml min<sup>-1</sup>. A volume of 2 mL of 1 mol L<sup>-1</sup> of HCl was used as desorbing solution and the eluate was analyzed by ICP-OES. The process (loaded and desorption) was repeated 9 times for the same b-HNO<sub>3</sub> column.

Different acids were evaluated as desorbing solutions at different concentration for lead desorption from the column, such as sodium citrate (10<sup>-4</sup> mol L<sup>-1</sup> and 10<sup>-5</sup> mol L<sup>-1</sup>), HCl (1 mol L<sup>-1</sup> and 2 mol L<sup>-1</sup>), HNO<sub>3</sub> (1 mol L<sup>-1</sup> and 2 mol L<sup>-1</sup>) and H<sub>2</sub>SO<sub>4</sub> (1 mol L<sup>-1</sup> and 2 mol L<sup>-1</sup>). After the adsorption process using b-HNO<sub>3</sub> column (10 mL of 1 mg L<sup>-1</sup> of Pb(II) solution, at pH 6) and a flow-rate of 0.5 ml min<sup>-1</sup>), 2 ml of each desorbing were used for desorption and the concentration on the eluent solutions was analyzed using ICP OES, to evaluate the elution efficiency.

#### 3.6.4. Breakthrough curve for Pb(II) adsorption onto b-HNO<sub>3</sub> column

In practical applications of full-scale adsorption processes, continuous-flow fixed bed columns are commonly favored. These systems exhibit spatial and temporal variations in concentration profiles within the liquid and adsorbent phases. Consequently, designing and optimizing fixed bed columns in advance without a quantitative modeling approach becomes challenging. Process modeling allows us to describe the dynamic behavior of a fixed bed column in terms of the effluent concentration-time profile, commonly known as the breakthrough curve. The breakthrough curve represents the ratio of the effluent concentration ( $C_t$ ) to the influent concentration ( $C_0$ ) plotted against time or throughput volume. The shape of this curve is determined by the equilibrium isotherm and is influenced by the distinct transport processes occurring within the column and the adsorbent material (K. H. Chu 2004). A polluted stream undergoes adsorption as it passes through a fixed bed column packed with adsorbent particles. The adsorbent particles attract and retain the pollutants, resulting in the production of a purified stream at the exit of the column. As the adsorption capacity of the bed is finite, the concentration of pollutants in the column effluent progressively increases with time. The breakthrough experiment holds significant importance as it represents the most probable mode of operation for any potential commercialized adsorbent. Therefore, conducting dynamic column breakthrough experiments plays a critical role in evaluating newly developed adsorbents (Tan and Hameed 2017).

The breakthrough curve was obtained by *online* coupled b-HNO<sub>3</sub> column (150 mg of bead) to the ICP-OES for the determination of the Pb(II) concentration until the

saturation of the adsorption column. A volume of 120 mL of 5 mg L<sup>-1</sup> of Pb(II) solution, at pH 6, was prepared and passed through the column at flow rate of 1 mL min<sup>-1</sup> and the eluate directly introduced at the ICP nebulizer system. Thomas model was used for data treatment (Khim Hoong Chu 2020).

$$\frac{C_t}{C_o} = \frac{1}{1 + \exp\left[\frac{K_{Th}}{v} q_o m - K_{Th} C_o t\right]} \quad \text{Equation 7}$$

were  $K_{Th}$  is the rate constant (L mg<sup>-1</sup> min<sup>-1</sup>),  $m$  is the mass of adsorbent,  $q_o$  is the maximal adsorption capacity (mg g<sup>-1</sup>) and  $v$  is the flow rate (mL min<sup>-1</sup>).

### 3.7. Separation-removal of Pb(II) from water samples using b-HNO<sub>3</sub> column

According to the “Conselho Nacional do Meio Ambiente – CONAMA” of the Minister of the Environment, through the Resolution CONAMA No. 430, from May 13, 2011, the maximum concentration of Pb that can be discarded into the environment is 0.5 mg L<sup>-1</sup> (CONAMA, 2011). In this way, tests using water samples with distinct matrix composition were investigated to evaluate the performance of b-HNO<sub>3</sub> column for separation and preconcentration of Pb(II).

After optimizing the different parameters for separation of Pb(II) onto b-HNO<sub>3</sub> (150 mg of bead, pH 6 and flow-rate 0.5 mL min<sup>-1</sup>), different samples (tap water, dam water, and high salinity water) as described in section 3.3 were spiked with 1 mg L<sup>-1</sup> of Pb(II) and passed through the column to investigate the efficiency of separation processes



using these real samples. For this, 10 mL or 25 mL of each sample, without and with spikes, was passed through the separation b-HNO<sub>3</sub> column and then the adsorbed Pb(II) was desorbing with 2 mL of HCl 1 mol L<sup>-1</sup> and analyzed by the ICP-OES.

Standard solutions of concentration 0.5, 1.0, 2.5, and 5.0 mg L<sup>-1</sup> of Pb(II) in 2.0 mol L<sup>-1</sup> of HCl were prepared and used for ICP-OES calibration. The LOD and LOQ were calculated as describe in section 3.1. Also, standard calibration using preconcentration of 25 mL of low concentrations (2.0, 5.0, 10, 20 and 50 µg L<sup>-1</sup>) of Pb(II) solutions were used for calibration the ICP-OES. After de adsorption process the desorbing was carried out with 1 mL of HCl 1 mol L<sup>-1</sup> and analyzed by the ICP-OES. The concentration of Pb(II) was determined in the eluate solution and calculated the percentage of separation/removal and the recovery of each sample.

### **3.8. Microcrystalline cellulose with glycidyl trimethylammonium chloride (MCC-GTA) preparation for As fractionation and speciation**

The first part of process was to increase the reactivity of the hydroxyl groups of MCC to guarantee the best efficiency of modification with glycidyl trimethylammonium groups. For this, 10 % (w v<sup>-1</sup>) of NaOH and 2.5 % (w v<sup>-1</sup>) of MCC was added in a flask under constant stirring (5 rpm) at 25 ± 1 °C for two days (Siqueira Petri et al. 1999). For the second part of modification, a procedure describe elsewhere (Najib and Christodoulatos 2019) was follow. After two days (48 h), to the suspension (10 % (w v<sup>-1</sup>) of NaOH and 2.5 % (w v<sup>-1</sup>) of MCC) was added 9% (w v<sup>-1</sup>), 18 % (w v<sup>-1</sup>) and 36 % (w v<sup>-1</sup>) of glycidyl trimethylammonium group (GTA) under constant stirring (5 rpm) and keep at

75 °C for 8 h. At the end of the reaction, the mixture was neutralized with HCl, filtered and then, washed with deionized water and centrifuged at 5000 rpm, for five consecutive cycles. The MCC-GTA was freeze-drying at -40°C for 2 days before further use. Figure 8 shows the schematic procedure for MCC-GTA preparation and a photographic of final product.

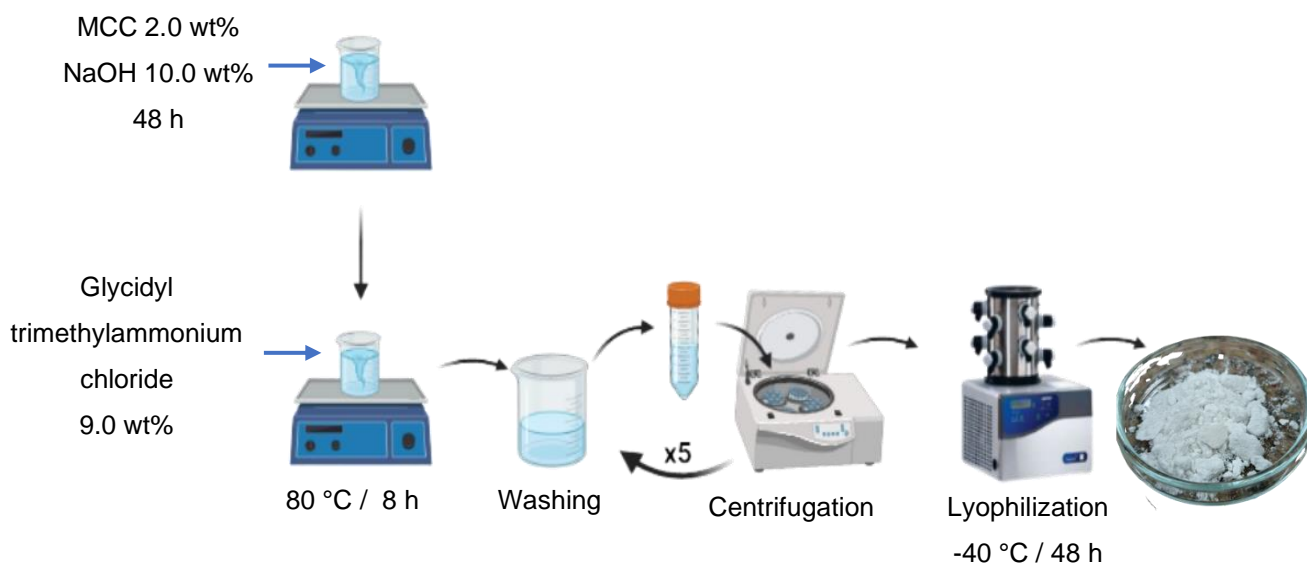


Figure 8. Schematic setting up for the MCC-GTA preparation.

### 3.9. Macrocrystalline cellulose with glycidyl trimethylammonium chloride (MCC-GTA) characterization

Macrocrystalline cellulose with glycidyl trimethylammonium chloride (MCC-GTA) was characterized by Fourier transform infrared spectrophotometry (FT-IR), and elemental analysis (CNH), as described in section 3.1.

### **3.10. Optimization of As species adsorption onto MCC-GTA in batch**

#### **3.10.1. Adsorption rate as function of pH**

To evaluate the arsenic species adsorption rate at different pH (2-8), 2 mL of 0.1 mg L<sup>-1</sup> of arsenic species (As(III), As(V), AsB, MMA and DMA) solutions were prepared and put in contact with MCC-GTA for 30 min, under stirring using a 360° motion homogenizer at 8rpm. Then centrifuged for 10 min at 5000 rpm and the supernatant solution was separated and analyzed by GF AAS to determine the non-adsorbed concentration of As species.

#### **3.10.2. Contact time and adsorbent mass**

To evaluate the influence of contact time (1-60 min) and adsorbent mass (10-20 mg) on the adsorption efficiency of the different arsenic species (As(III), As(V), AsB, MMA and DMA) onto MCC-GTA, 2 mL of 0.1 mg L<sup>-1</sup> of each species of arsenic, at pH 6-7, were put in contact with different masses or during different contact times. For contact time investigation, a mass of 10 mg of MCC-GTA was kept constant and for mass investigations, the contact time was kept constant at 1 min. After centrifugation for 5 min at 5000 rpm, the supernatants of these solutions were separated and analyzed in GF AAS.

### 3.10.3. Oxidation of arsenic species and monitoring by LC-ICP-OES

As the As(V) species had the best adsorption efficiency, a procedure to investigate the influence of As(III) oxidation was investigated. For this, NaClO in different molar ratios ( $R_{\text{NaClO}/t_{\text{As}}} = 1, 2 \text{ and } 3$ ) was investigated to the preoptimized adsorption conditions (pH 6-7, contact time = 1 min, adsorbent mass = 10 mg). The oxidation efficiency of As(III) to As(V) and the influence on the other arsenic species were followed by liquid chromatography coupled to the inductively coupled plasma optical emission spectrometry (LC-ICP-OES).

Speciation of As was done for  $10 \text{ mg L}^{-1}$  of each species or using a mixture of As III  $10 \text{ mg L}^{-1}$  + As V  $10 \text{ mg L}^{-1}$ , AsB  $10 \text{ mg L}^{-1}$ , MMA  $10 \text{ mg L}^{-1}$  and DMA  $10 \text{ mg L}^{-1}$  before and after the oxidation process with NaClO in different molar ratios ( $R_{\text{NaClO}/t_{\text{As}}} = 1, 2 \text{ and } 3$ ). Species separation was performed on an anion exchange column (PRP X-100, Hamilton), using a  $100 \mu\text{L}$  sampling loop and a phosphate buffer ( $30 \text{ mmol L}^{-1}$  - pH 6.0 adjusted with  $\text{NH}_4\text{OH}$ ) as mobile phase, with a flow rate of  $1.0 \text{ mL min}^{-1}$ . The column output was connected to the ICP-OES nebulizer for online detection in transient mode. Ammonium acetate buffers (pH = 4.7) with concentrations of 10 mM (phase A) and 250 mM (phase B) were used as a mobile phase with gradient elution (0 - 5 min: 0% B; 5-15 min: 0% - 100% B; 25 - 26 min: 100% - 0% de B; 26 - 35 min: 100% B) and flow rate of  $1.5 \text{ mL min}^{-1}$ .

### 3.11. Arsenic speciation and fractioning using MCC-GTA in batch

After optimizing the different parameters for adsorption (pH 6-7, contact time = 1 min, adsorbent mass = 10 mg, and  $R_{\text{NaClO}/\text{As}} = 2$ ), the optimization of fractionation and speciation was applied to standard solutions and a river water samples spiked with different concentration ( 20-100 mg L<sup>-1</sup>) of As(III), As(V), MMA, DMA and AsB. The sequence of procedure followed for As fractionation is depicted in Figure 9.

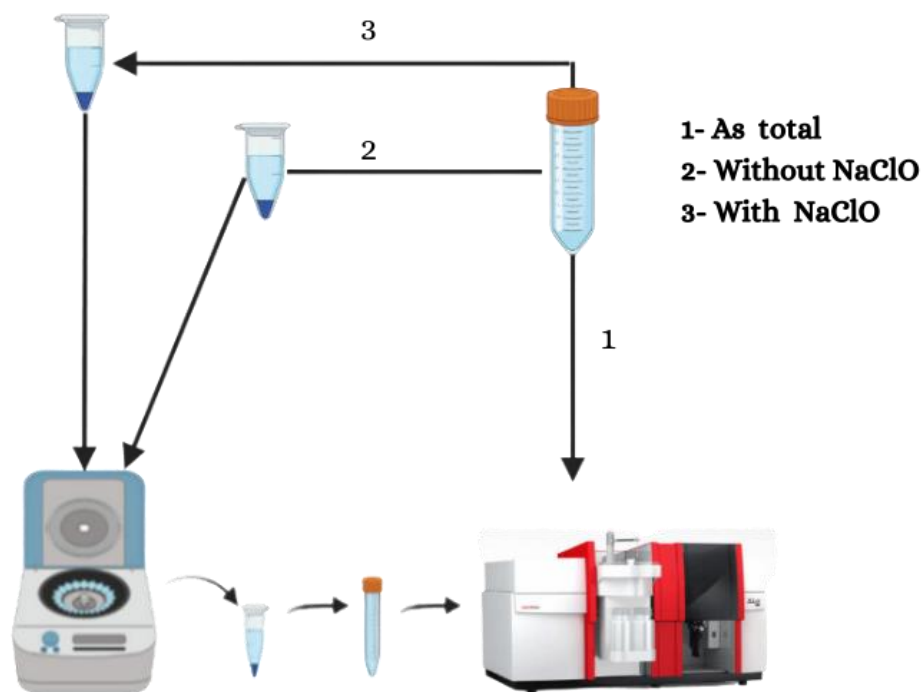


Figure 9. Experimental set up used for arsenic fractionation and speciation: 1. Total determination of As by GF AAS; 2. Separation of arsenic species and determination by GFT AAS before addition of NaClO; and 3. Separation of arsenic species and determination by GF AAS after addition of NaClO.

In the first step, the total concentration of all species of As was determined by GF AAS (Fig. 10.1). Afterwards, an aliquot of the mixture of As species was put in contact with MCC-GTA, using optimized conditions (pH 6-7, contact time = 1 min, adsorbent mass = 10 mg) for adsorption procedure without oxidation, then centrifugated for 10 min at 5000 rpm for separation of MCC-GTA from the solution with a micropipette. The MCC-GTA was washed with 1 mL of deionized water and subsequently subjected to desorption with 1 mL of HCl (1 mol L<sup>-1</sup>). The supernatants of these solutions and desorption HCl solution were analyzed in GF AAS (Fig. 10.2). In the third step, an aliquot of the mixture of As species was put in contact with MCC-GTA, using optimizing conditions (pH 6-7, contact time = 1 min, adsorbent mass = 10 mg) for adsorption procedure after addition of NaClO (R<sub>NaClO/As</sub> = 2) as oxidant. After centrifugation for 5 min at 5000 rpm for separation of MCC-GTA from the solution. The supernatants of these solutions were analyzed in GF AAS (Fig. 10.3). With these results it is possible to estimate the contents of the different species in the samples, by the difference between the total concentration and the concentration after different adsorption steps, following Equation 8 to Equation 12 described later in section 4.8. The mass balance for total arsenic concentration was calculated as followed:

### **3.12. Preconcentration and speciation of inorganic arsenic in water samples using MCC-GTA**

Figure 10 show the procedure for preconcentration of inorganic arsenic species using MCC-TA in water samples (standard solutions and river water described in section

3.3) containing different amounts of As(III) and As(V) in low concentrations ( $2 \mu\text{g L}^{-1}$ ) were prepared, 25 mL of solution at pH 6-7 were placed in 50 mL falcon tubes containing 50 mg of MCC-TA, the procedure was repeated for each sample adding NaClO allowing preconcentration of both iAs species (As(III) and As(V)) and without addition of NaClO only preconcentrating or As(V) present in the solution.

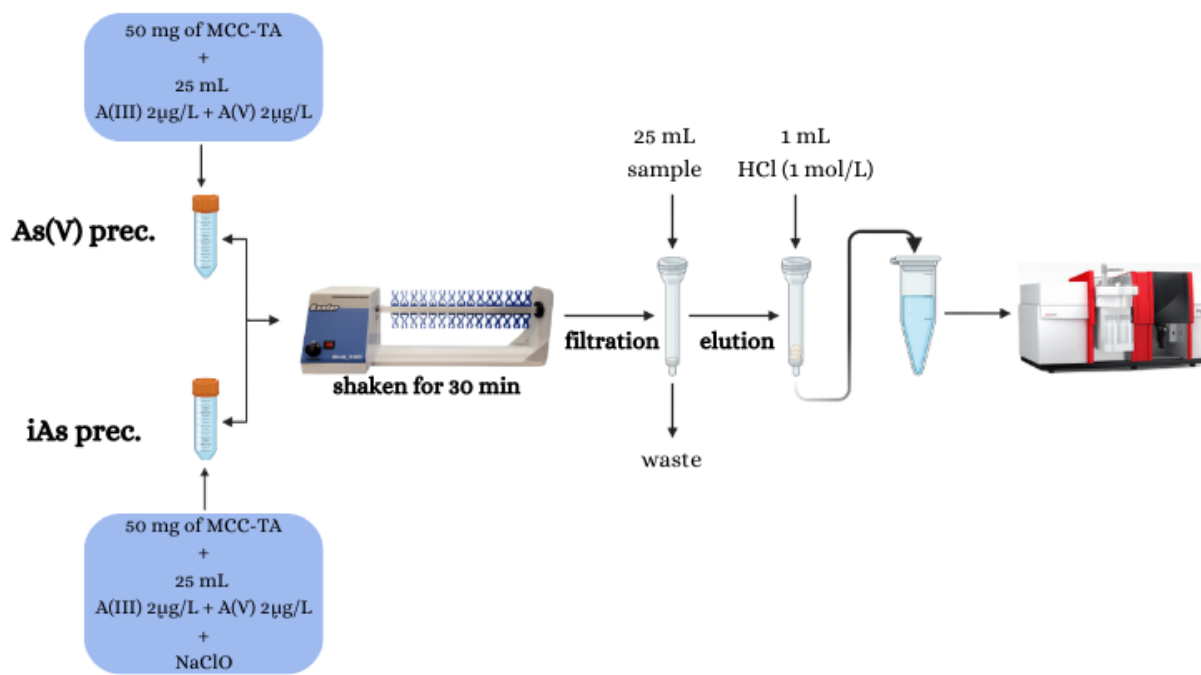


Figure 10. Schematic setting up for preconcentration of inorganic As species in water.

The tubes were shaken for 30 min and later filtered using a polypropylene column (internal diameter of 0.8 cm) and at the bottom a porous polyethylene frits (0.8 cm in diameter; pore size  $<1 \mu\text{m}$ ) to separate the solution from the solid. The material was washed with 1 mL of deionized water and subsequently subjected to elution with 1 mL of HCl ( $1 \text{ mol L}^{-1}$ ). The concentration of As in the eluate was determined using GF AAS.

## **4. Results and Discussion**

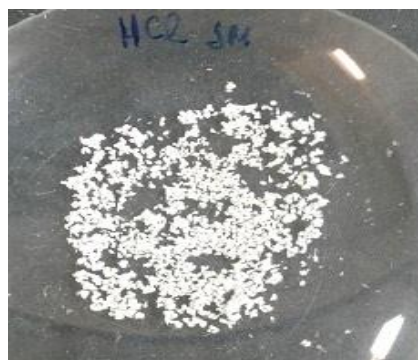
### **4.1. Preparation and characterization of microcrystalline cellulose beads**

Cellulose beads were prepared according to the procedure proposed previously (Gericke et al., 2013), however, some adjustments were made in order to obtain particles with the smallest possible sizes. In this way, the optimization of the peristaltic pump rotation and the diameter of the Tygon and the polypropylene tubes, which dispense the cellulose solution in the coagulant medium were mandatory to obtain beads with diameters size around of 0.5 mm to 1 mm (before drying) and smaller than 0.5 mm (after drying in an oven, at 60 °C for 12 hours). Figure 11 shows the photographic register of the beads prepared in 1 mol L<sup>-1</sup> of HCl and 2 mol L<sup>-1</sup> HNO<sub>3</sub> media before and after drying. In this composition of coagulant media, both materials have a droplet shape and rough surface area as seen in the picture.





(a)



(b)



(c)



(d)

Figure 11. Photo of cellulose beads prepared in  $1 \text{ mol L}^{-1}$  of HCl (a and b) and  $2 \text{ mol L}^{-1}$  of  $\text{HNO}_3$  (c and d) media, wet (a and c) and after drying at  $60 \text{ }^\circ\text{C}$  for 12 hours (b and d).

#### 4.1.1. Characterization using SEM

To evaluate the morphological structure and correlate with the material adsorption rate, high-resolution images from surface morphology were obtained by (SEM), using 6 mA and 10 kV-accelerated electrons sputter coating with golden (Figure 12). Different concentration of  $\text{HNO}_3$  ( $0.5$ ,  $1$ ,  $2$ ,  $4$ , and  $8 \text{ mol L}^{-1}$ ) were evaluated to optimize the beads formation process.

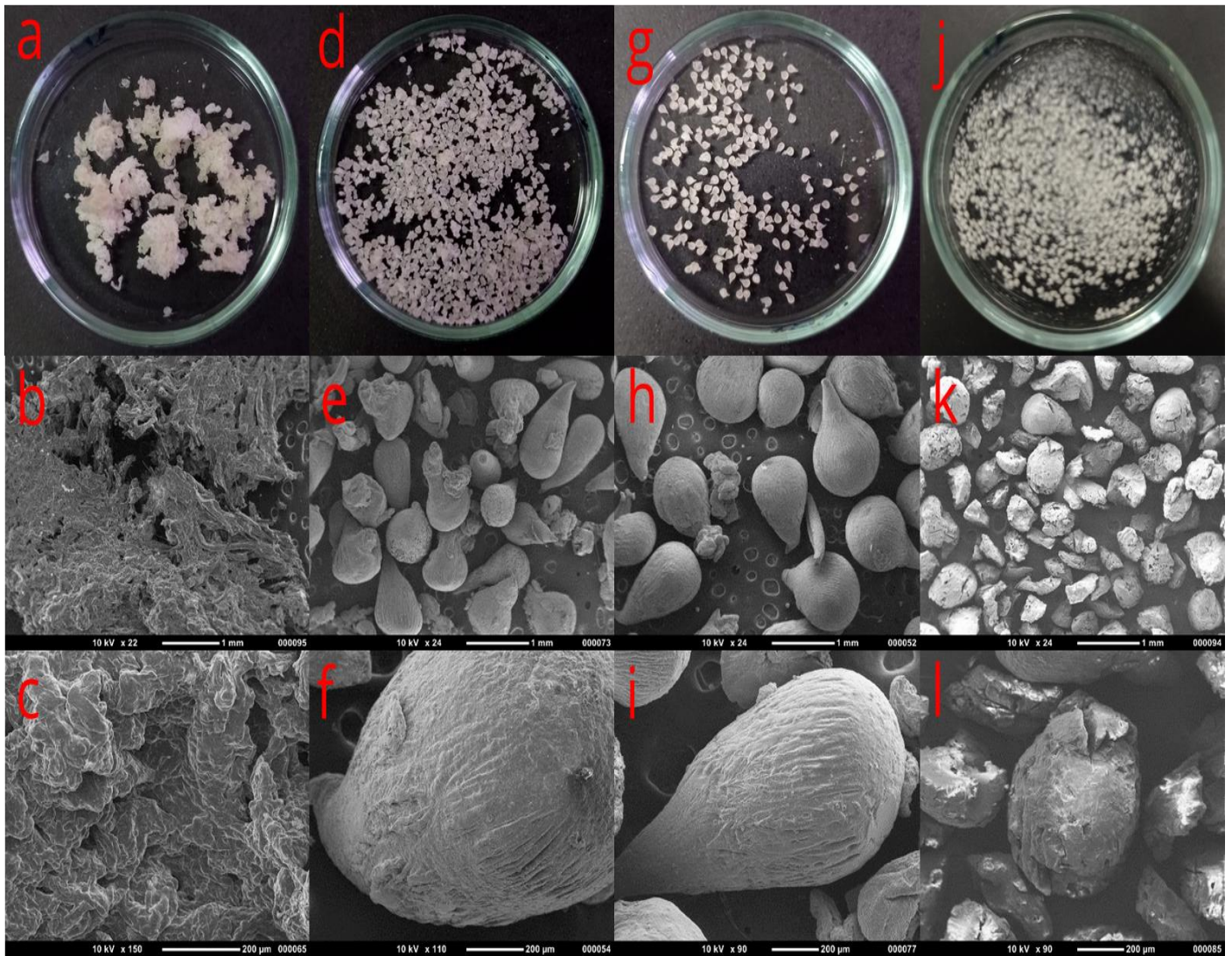


Figure 12. Photography of beads prepared in different acid concentrations (a,d,g,j) and SEM images of dry microcrystalline cellulose beads prepared in 0.5 mol L<sup>-1</sup> of HNO<sub>3</sub> (a, b, c), in 1 mol L<sup>-1</sup> of HNO<sub>3</sub> (d, e, f), in 2 mol L<sup>-1</sup> of HNO<sub>3</sub> (g, h, i), and in 8 mol L<sup>-1</sup>.

Figure 12 shows the photographic register of the beads prepared in different acid concentrations (a,d,g,j) and SEM images at different magnification of 1 mm (b,e,h,k) and 200 μm (c,f,i,l). As it can be seeing the beads obtained at 1 and 2 mol L<sup>-1</sup> of HNO<sub>3</sub> has a droplet shape and rough surface area. At 8 mol L<sup>-1</sup> of HNO<sub>3</sub> the beads formed where

brittle and has irregular shape. The beads formed in 2 mol L<sup>-1</sup> of HNO<sub>3</sub> have a more regular and uniform shape, therefore were selected for the following experiments, and are designated as b-HNO<sub>3</sub>.

#### 4.1.2. Characterization using FTIR

Figure 13 shows the FTIR spectra of microcrystalline cellulose (MCC) as a control sample for comparison purpose, and using beads prepared in 2.0 mol L<sup>-1</sup> of HNO<sub>3</sub> (b-HNO<sub>3</sub>) and b-HNO<sub>3</sub> loaded with 100 mg L<sup>-1</sup> of Pb(II), with 1 h of contact time in the wavenumber range of 500-4000 cm<sup>-1</sup>. The three spectra have similar characteristic bands corresponding to microcrystalline cellulose.

Previous study reported the oxidation of microcrystalline cellulose using 45-55% of HNO<sub>3</sub>, acting as a deposited form of catalyst of cellulose oxidation (Gert et al. 2006). It can be seen in the Figure 13 that it is not possible to identify new bands with difference from the MCC spectrum. In view of this, there is no evidence of the formation of new identifiable functional groups during the bead formation process in HNO<sub>3</sub> media. It is important to emphasize that modification was not observed even in the 8 mol L<sup>-1</sup> of HNO<sub>3</sub> as coagulant medium.

Peaks at approximately 3500-3300 cm<sup>-1</sup> are due to the O-H stretching vibrations, at ~2900 cm<sup>-1</sup> belong to C-H stretching vibrations, at 1000–1100 cm<sup>-1</sup> due to stretching vibrations (Wang et al., 2017), at 1000–1100 cm<sup>-1</sup> due to stretching vibrations of C–O, and 1250–1420 cm<sup>-1</sup> due to bending vibrations of O–H (Kenawy et al., 2018).

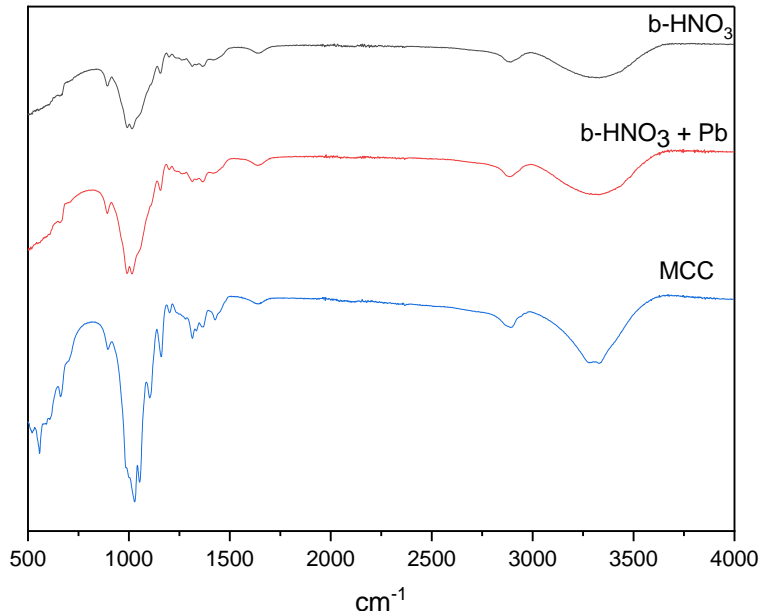


Figure 13. FTIR spectra of beads prepared in 2,0 mol L<sup>-1</sup> of HNO<sub>3</sub> (b-HNO<sub>3</sub>) beads, beads loaded with Pb (b-HNO<sub>3</sub> +Pb) and pure MCC.

#### 4.1.3. Characterization using XPS

To clarify the adsorption mechanism on the beads, XPS analysis was done using beads prepared in 2.0 mol L<sup>-1</sup> of HNO<sub>3</sub> (b-HNO<sub>3</sub>) and b-HNO<sub>3</sub> loaded with 100 mg L<sup>-1</sup> of Pb(II), with 1 h of contact. Figure 14(a) shows a XPS spectrum of the beads before and after the lead adsorption experiments. Before lead adsorption there are only typical signals of carbon (C 1s) and oxygen (O 1s), which are atoms that correspond to the cellulose molecule. After the lead adsorption experiments, it is possible to see that the lead signal (Pb 4f) is present, indicating that a sorption process has taken place. Figure 14(b), (c) and (d) shows high resolution XPS spectra for Pb 4f, O1s, before lead

adsorption and O 1s after leads adsorption, respectively. These signals were curve fitting by Gauss-Lorentz and the background eliminated using the Shirley method (Sheng et al. 2004).

Two energy peaks for Pb 4f are show at Figure 14(b), at 137.93 eV and 142.84 eV, assigned to Pb 4f<sub>7/2</sub> and Pb 4f<sub>5/2</sub>, respectively, corresponding with divalent state of Pb. Similar results are reported by Li et al. and these peaks are attributed to the formation of Pb–O bond between Pb(II) and function groups of the material (Li et al. 2011). Figure 14(c) and (d) shows that O1s spectra, could be splitted into two peaks of C-OH, and C-O-C. After Pb(II) adsorption, peaks of C-OH and C-O-C shifted from 531.09 eV and 529.92 eV to higher binding energy of 531.3 eV and 530.2 eV, respectively. These increase in the binding energies infers that hydroxyl and ester groups are involved in the adsorption of Pb(II) on the beads through dipole-induced dipole attraction and surface complex (Yu et al. 2020).

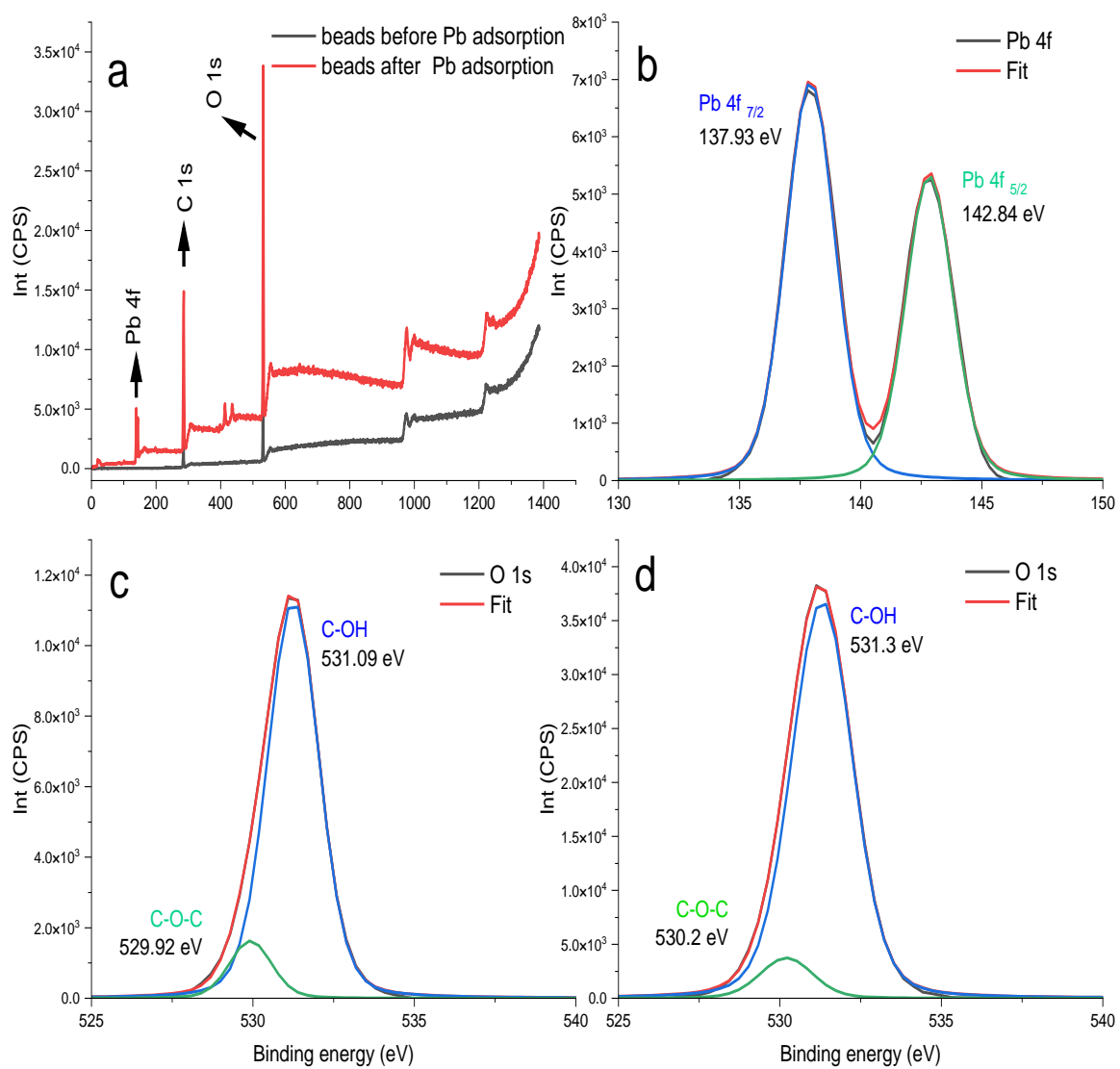


Figure 14. XPS survey spectrum of the beads (a) before (black) and after (red) the lead adsorption (a). XPS high resolution spectra of Pb 4f (b) for beads after lead adsorption, O 1s (c) before lead adsorption and O 1s (d) after lead adsorption.

#### 4.1.4. Characterization using PZC

Figure 15 shows the experimental potentiometric titration curves obtained for the background electrolyte ( $0.05 \text{ mol L}^{-1}$  of  $\text{KNO}_3$ ) (red) and for the b- $\text{HNO}_3$  sample (black), being (a) titration with  $0.02 \text{ mol L}^{-1}$  of  $\text{NaOH}$  and (b) titration with  $0.02 \text{ mol L}^{-1}$  of  $\text{HCl}$ .

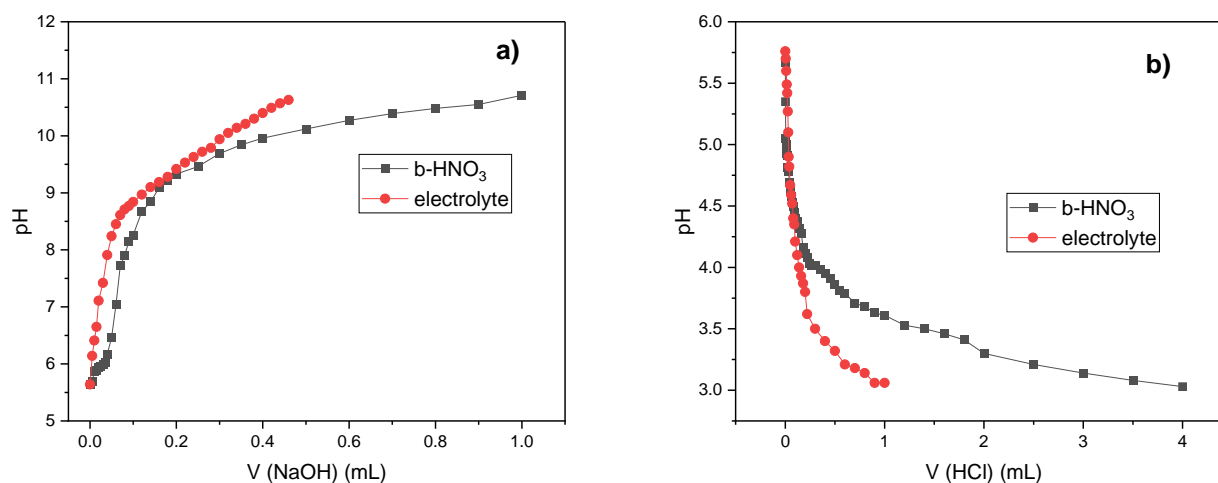


Figure 15. Experimental potentiometric titration curves with (a)  $0.02 \text{ mol L}^{-1}$  of  $\text{NaOH}$  and (b) with  $0.02 \text{ mol L}^{-1}$  of  $\text{HCl}$ , obtained for background electrolyte ( $0.05 \text{ mol L}^{-1}$  of  $\text{KNO}_3$ ) (red) and for the b- $\text{HNO}_3$  sample (black).

The pH in which the number of protons consumed or released ( $Q$ ) is zero define the point of zero charges (pzc), that means at this point there is a balance between the adsorption and release of protons, and there is no excess of positive or negative charge on the material surface (Ogeda 2011). Figure 16 shows the isotherm of number of protons released or adsorbed resulting from the potentiometric titration of the background electrolyte and b- $\text{HNO}_3$  ( $Q/ \text{mmol L}^{-1} \times \text{pH}$ ), calculated according to equation 1 (section 3.5.1). The point of zero charge of  $4,90 \pm 0,05$  was determined for b- $\text{HNO}_3$ . Positive

values of  $Q$  indicate that there is adsorption of protons, while negative values of  $Q$  represent release of protons. At pH values above 4.90, the surface of the material is negatively charged, favoring the adsorption of positive ions such as Pb(II) through electrostatic interactions between the ions and b-HNO<sub>3</sub>.

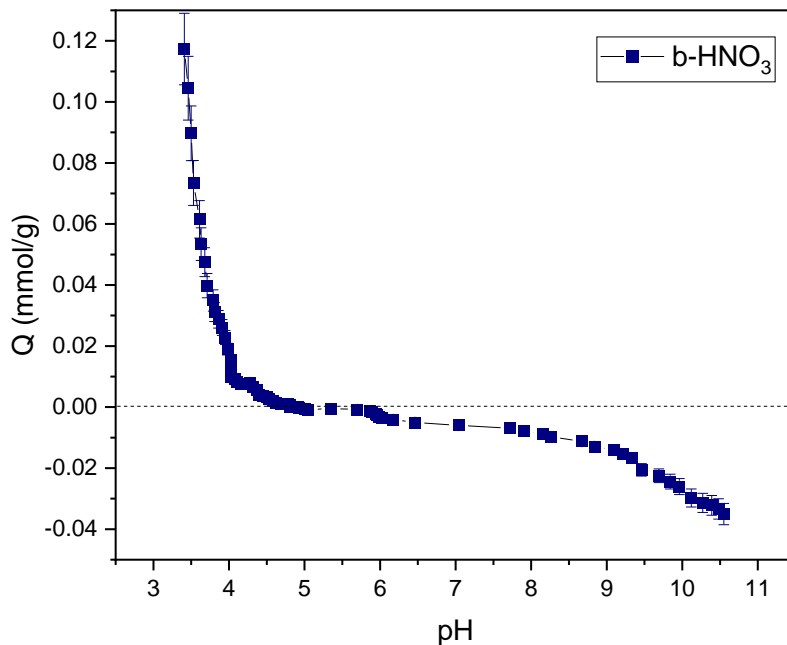


Figure 16. Isotherm of the number of protons released or adsorbed obtained for b-HNO<sub>3</sub>.

#### 4.1.5. Adsorption isotherm of Pb(II)

The adsorption studies of 1 to 200 mg L<sup>-1</sup> of Pb(II), at pH 6, on 8 mg of bead prepared in 2.0 ml L<sup>-1</sup> of HNO<sub>3</sub> (b-HNO<sub>3</sub>) and 2.0 mol L<sup>-1</sup> of HCl (b-HCl) as coagulant media and pure MCC were done keeping the contact time constant as 24 hour, and supernatant analyzed by ICP OES. Figure 17 shows the Pb(II) adsorption isotherm on b-HNO<sub>3</sub>, b-HCl and pure MCC with nonlinear fitting for Langmuir isotherm and the estimated



parameter are show at Table 3. Figure 18 shows the Pb(II) adsorption isotherm on b-HNO<sub>3</sub>, b-HCl, and MCC with linear fitting for Langmuir isotherm and the estimated parameters are show at

Table 4. The parameters determined from the nonlinear fittings with the Langmuir model, showed that the b-HNO<sub>3</sub> presented the best fitting quality, yielding  $q_{max}$  value of  $108.4 \pm 7.7 \text{ mg g}^{-1}$ , affinity constant of  $0.5 \pm 0.1 \text{ L mg}^{-1}$  and separation factor of 0.69. The parameters determined from the linear fittings with the Langmuir model, showed that the b-HNO<sub>3</sub> presented the best fitting quality too, yielding  $q_{max}$  value of  $110.5 \text{ mg g}^{-1}$ , affinity constant of  $0.4 \text{ L mg}^{-1}$  and separation factor of 0,72. The affinity constant of b-HNO<sub>3</sub> using the linearized adjust is greater than MCC and b-HCl, indicating a more efficient interaction between lead ions and the surface of the b-HNO<sub>3</sub>, therefore based on the  $q_{max}$  and KI values b-HNO<sub>3</sub> was selected as the best material for lead adsorption.

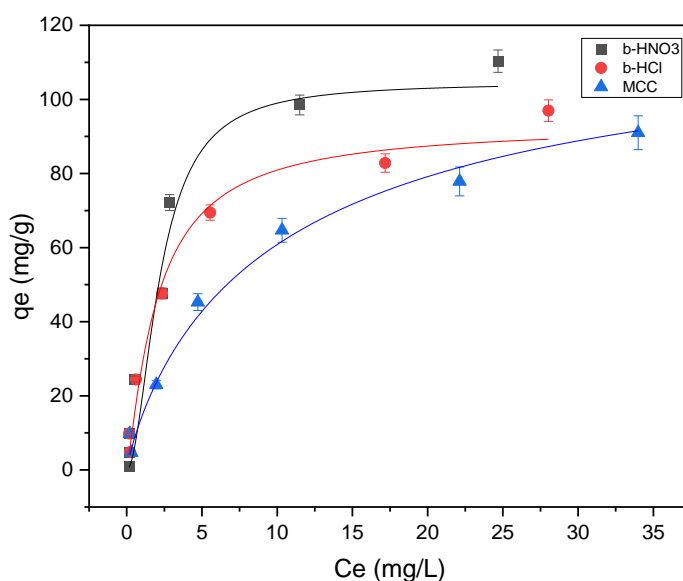


Figure 17. Adsorption isotherms Langmuir nonlinear adjusted for b-HNO<sub>3</sub>, b-HCl, and pure MCC.

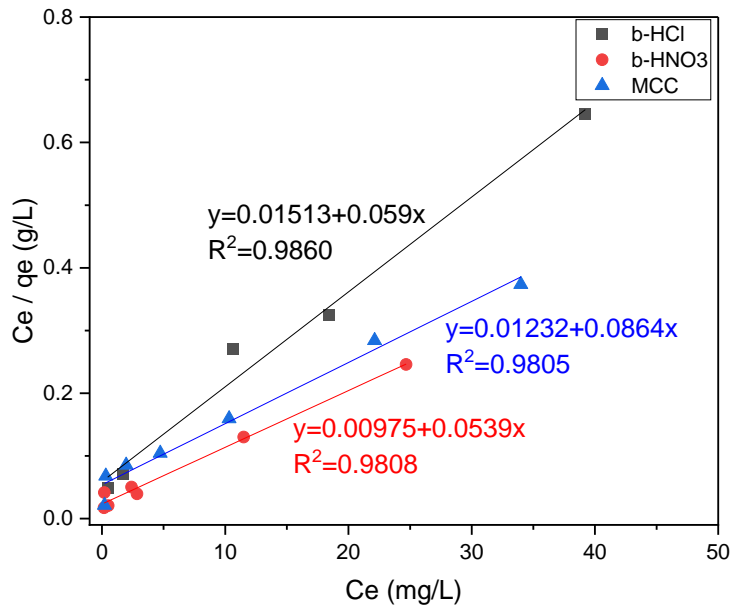


Figure 18. Adsorption isotherms Langmuir linear adjusted for b-HNO<sub>3</sub>, b-HCl, and pure MCC.

Table 3. Adsorption isotherms Langmuir nonlinear adjust parameters.

	pure MCC	b- HNO <sub>3</sub>	b- HCl
<i>Model</i>	qe = qmax*KI*Ce/(1+KI*Ce) (Foo and Hameed 2010)		
<i>q<sub>max</sub></i>	101.4 ± 6.4	108.4 ± 7.7	100.2 ± 4.4
<i>KI</i>	0.403 ± 0.045	0.455 ± 0.112	0.411 ± 0.069
<i>R-Square</i>	0.98325	0.97129	0.96821
<i>RI</i>	0.76	0.69	0.71

Table 4. Adsorption isotherms Langmuir linear adjust parameters.

	pure MCC	b- HNO <sub>3</sub>	b- HCl
<i>Equation</i>	Ce /qe =1/bQ <sub>0</sub> + Ce/Q <sub>0</sub> (Foo and Hameed 2010)		
<i>qmax</i>	102.6	110.5	91.2
<i>Kl</i>	0.181	0.390	0.143
<i>R-Square</i>	0.98088	0.98779	0.98056
<i>Rl</i>	0.84	0.72	0.87

The adsorption capacity for Pb(II) removal obtained for b-HNO<sub>3</sub> is comparable or better than previously reported cellulosic materials. Vijayalakshmi *et al.* (2017) prepared a nanochitosan/sodium alginate/microcrystalline cellulose bead with maximum adsorption capacity of 114.47 mg g<sup>-1</sup>; Zhang *et al.* (2017) reported mesoporous nano-TiO<sub>2</sub>/cellulose composites with maximum adsorption capacity of 42.5 mg g<sup>-1</sup>; Luo *et al.* (2016) prepared a magnetic cellulose-based nanocomposite beads with maximum adsorption capacity of 2.86 mg g<sup>-1</sup>; Vadakkekara, Thomas, and Nair (2019) prepared a maleic acid modified cellulose (macro, micro and nano) with maximum chemisorption capacities of macro, micro and nano for Pb(II) of 20 mg g<sup>-1</sup>, 40 mg g<sup>-1</sup> and 115 mg g<sup>-1</sup>, respectively; Kumar and Sharma (2019) prepared cellulose extracted from rice husk with N-isopropylacrylamide with maximum adsorption capacity for Pb(II) of 118.3 mg g<sup>-1</sup>. The adsorption capacity obtained demonstrates that b-HNO<sub>3</sub> could be a promising adsorbent material for Pb(II) to be used for water treatment especially given its easy production with no chemical modifications and an eco-friendly material. Additionally, b-HNO<sub>3</sub> showed very

good performance for separation and preconcentration of Pb(II) from water with a considerable amount of concomitants.

## **4.2. Optimization of Pb(II) adsorption onto b-HNO<sub>3</sub> in a fixed-bed column**

### **4.2.1. Effect of pH on the Pb(II) adsorption**

The effect of pH on the Pb(II) removal was investigated using b-HNO<sub>3</sub> at Pb(II) concentration of 1 mg L<sup>-1</sup> and a flow rate through the column of 1 ml min<sup>-1</sup>. The pH values were adjusted using HCl (0.1 mol L<sup>-1</sup>) and NaOH (0.1 mol L<sup>-1</sup>) solutions before the adsorption experiments. Figure 19 shows that the optimal pH was  $\geq 6$ . At pH values above the point of zero charges ( $4,90 \pm 0,05$ ) the surface of the material had an excess of negative charge that favor the adsorption of Pb(II). One reason for low removal efficiency at low pH can be attribute to the surface protonation of the adsorbent. At low pH value, high concentrations of hydrogen ions will compete with free lead ions for the same adsorption sites in the solution (Fu and Xie 2020). Other crucial factor is the chemical form of Pb in the solution that also depend on the pH. Pb(II) species varies in proportion based on their hydrolysis constants ( $\log k_1 = 6.48$ ,  $\log k_2 = 11.16$ , and  $\log k_3 = 14.16$ ). Typically, when the pH is below 7.0, the solution is predominantly composed of divalent free Pb(II) ions (Al-Degs, Khraisheh, and Tutunji 2001). The pH in the range 6 was selected to perform the subsequent adsorption experiments, preventing the formation of Pb(OH)<sub>2</sub>, therefore, limiting the adsorption process to divalent free Pb(II) ions.

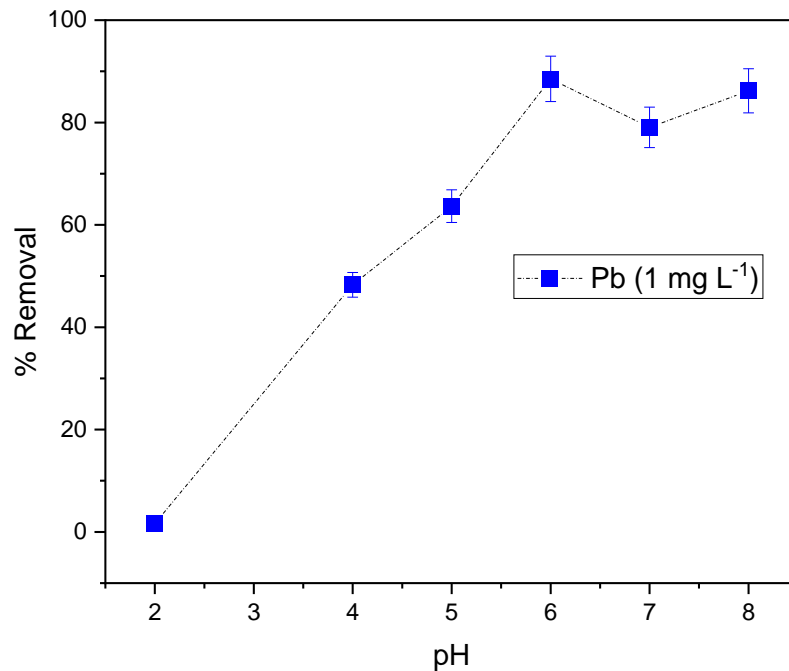


Figure 19. Effect of pH on adsorption of Pb(II) ( $1 \text{ mg L}^{-1}$ ,  $1 \text{ ml min}^{-1}$ ) onto 150 mg of b- $\text{HNO}_3$  column, at pH=6.

#### 4.2.2. Effect of flow rate through the column on the Pb(II) adsorption

The flow rate of the solution through the column is an experimental parameter that contributes to the equilibrium between analyte and adsorbent. Moreover, the sample solution flow rate influences the analyte contact with the adsorbent and directly affects the application of solid-phase extraction processes (Ozdemir et al. 2021). The impact of the flow rate on the removal of Pb(II) on b- $\text{HNO}_3$  was examined between the range of  $0.25\text{--}2.0 \text{ mL min}^{-1}$  at pH 6.

Figure 20 shows that  $0.5 \text{ ml min}^{-1}$ , reaching 100 % of removal with relatively low standard deviation ( $n=3$ ), was the best condition to perform the following experiments. At

a flow rate higher than  $0.5 \text{ mL min}^{-1}$ , there was a reduction in the removal due to not having enough contact time to reach equilibrium between Pb(II) and b-HNO<sub>3</sub>.

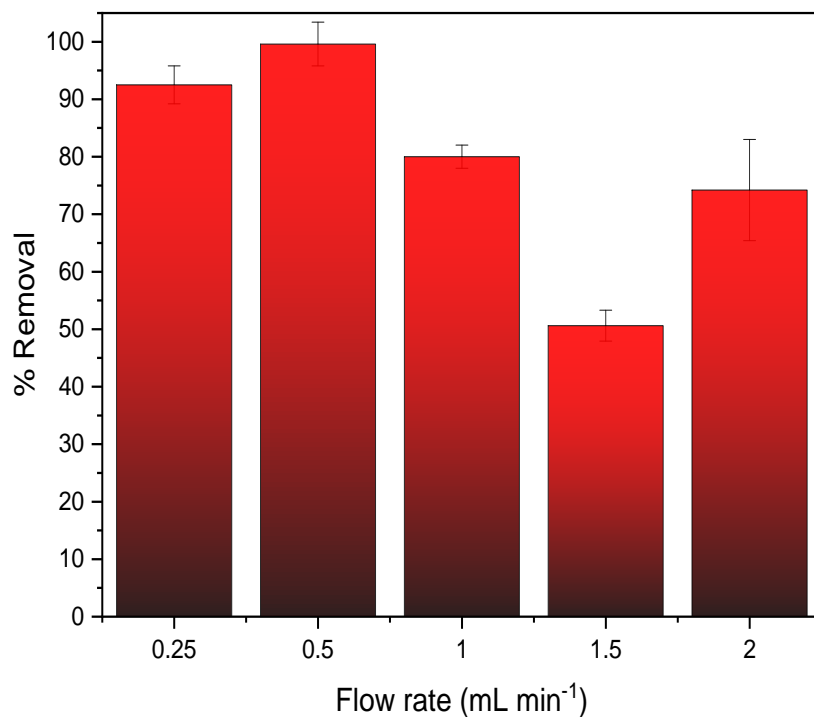


Figure 20. Flow rate optimization of Pb(II) ( $1 \text{ mg L}^{-1}$ ) onto  $150 \text{ mg}$  of b-HNO<sub>3</sub> column, at pH=6.

Considering this, pH = 6 and flow-rate of  $0.5 \text{ mL min}^{-1}$  was chosen as the best conditions to investigate the repeatability and the type of effluent to release the Pb(II) adsorbed over b-HNO<sub>3</sub> column.

#### 4.2.3. Intra and inter column repeatability and type of eluent for desorption

Adopting the best pH (6) and flow rate ( $0.5 \text{ mL min}^{-1}$ ), experiments were executed to investigate the performance of adsorption of  $1 \text{ mg L}^{-1}$  of Pb(II) using 5 different columns (inter) and in the same time the repeatability using 2 adsorption-desorption cycle ( $n=2$ ) for each one (intra). Figure 21 shows the repeatability (adsorption-desorption cycle) and performance obtained using columns with  $150 \text{ mg}$  of b- $\text{HNO}_3$ .

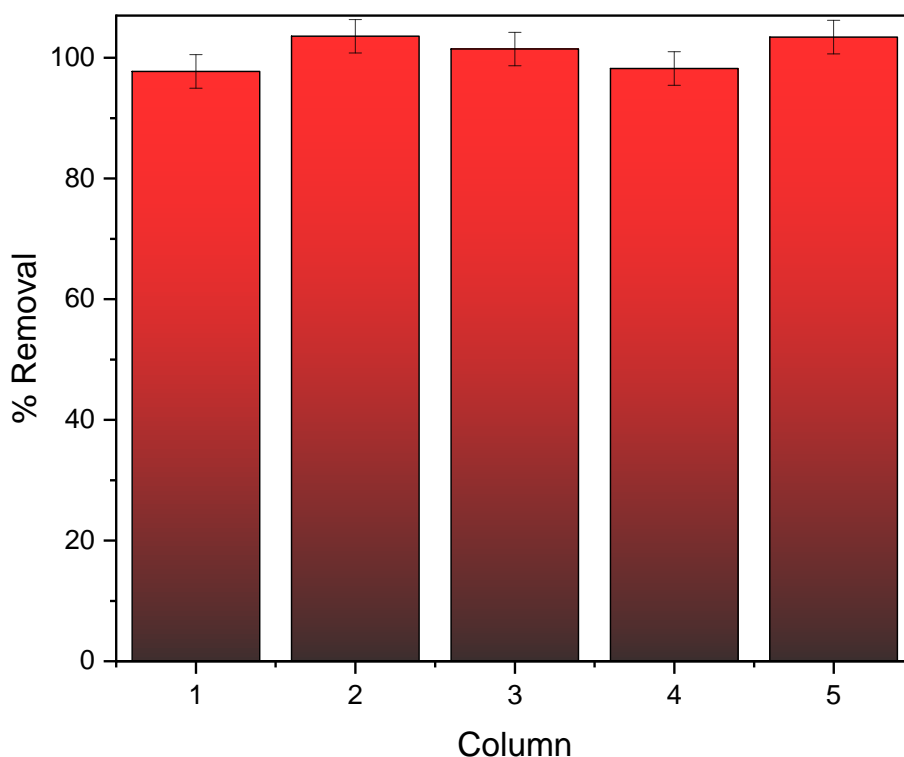


Figure 21. Inter repeatability using 5 different columns and intra repeatability for adsorption-desorption ( $n=2$ ):  $1 \text{ mg L}^{-1}$  of Pb(II), mass  $150 \text{ mg}$  of b- $\text{HNO}_3$ , flow rate  $0.5 \text{ mL L}^{-1}$ , and pH 6.

The performance of  $1 \text{ mg L}^{-1}$  of Pb(II) adsorption was practically the same between the 5 columns ( $100.9 \pm 2.8$ ), showing the good repeatability inter b- $\text{HNO}_3$  columns. The

overall adsorption/desorption cycles ( $n=2$  for each column) also showed good performance with relative standard deviation below 2%.

The repeatability of the adsorption process promoted by the adsorbent is an important characteristic for analytical or separation/removal in an industrial applications based on cost benefit of the system for practical use in real operation (Awual et al. 2015). For this matter, it is preferable the elution of the adsorbed Pb(II) from the adsorbent and perform the regeneration for several cycles without losing its adsorption capacity. Additionally, separation allows pollutants removal and for valuable materials (*c.a.*, metallic elements) the recovery for reusability in technological industry, protecting the environment. The reuse for one b-HNO<sub>3</sub> column was evaluated for nine adsorption-desorption cycle as shown in Figure 22. After adsorption and desorption with 2.0 mol L<sup>-1</sup> of HCl, the b-HNO<sub>3</sub> column was regenerated with deionized water into the initial pH conditions (pH 6). The removal efficiency was calculated for each cycle and after nine reuse cycle, using the same column, was observed only 5% of loss in the separation-removal capacity.

The correct choice of eluent for analyte desorption is important for the quantitative elution and regeneration of the column, allowing practical applications and reuse of with efficiency and selectivity. In Figure 23 is showed the results of elution using 2 mL of different acids solutions (HCl, HNO<sub>3</sub> and H<sub>2</sub>SO<sub>4</sub>) and citrate as complexing ligand.



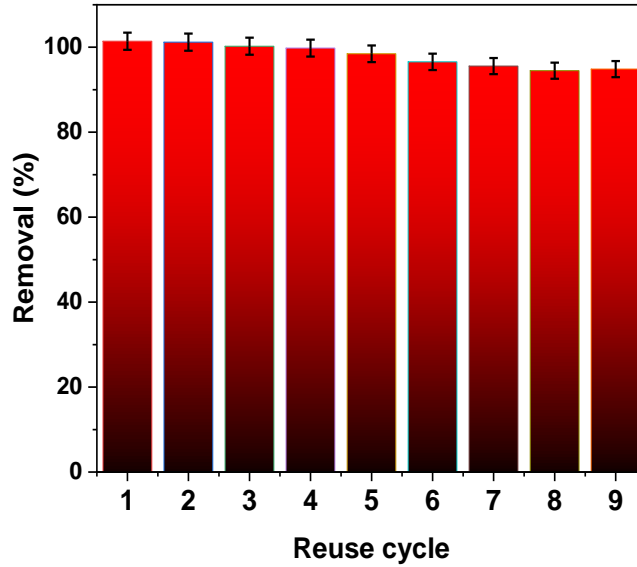


Figure 22. Reuse cycle of Pb(II) separation for nine adsorption-desorption cycle: 2 mL of eluent, 1 mg L<sup>-1</sup> of Pb(II), mass 150 mg of b-HNO<sub>3</sub>, flow rate 0.5 ml L<sup>-1</sup>, and pH 6.

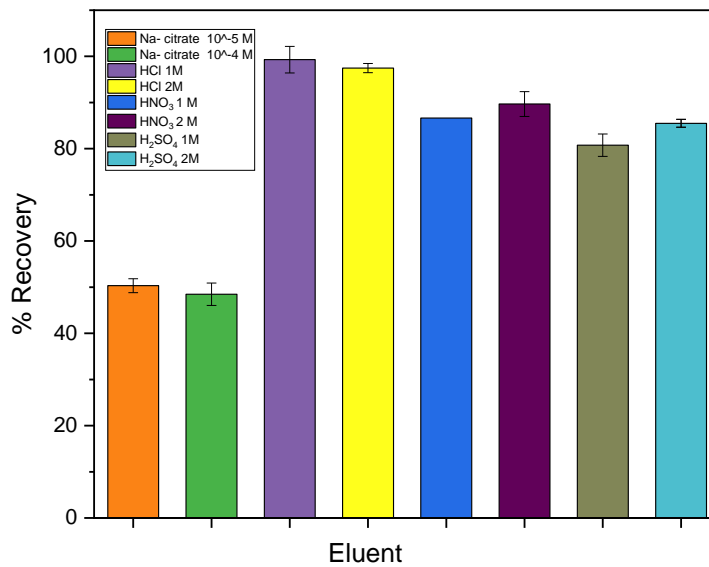


Figure 23. Recoveries of Pb after adsorption/desorption using different type of eluent for Pb(II) desorption: 2 mL of eluent, 1 mg L<sup>-1</sup> of Pb(II), mass 150 mg of b-HNO<sub>3</sub>, flow rate 0.5 ml L<sup>-1</sup>, and pH 6.

The eluent should be able to quantitatively desorb the analyte of interest and not interfere with the detection method. The choice of eluent can also affect the stability of the column and its lifetime (Liu 2021). Metals adsorbed in cellulosic materials can be eluted using various eluents such as HNO<sub>3</sub>, HCl, H<sub>2</sub>SO<sub>4</sub>, NaOH, EDTA (Nag and Biswas 2021; Malik, Jain, and Yadav 2017), depends on the type of metal ions being adsorbed and the type of cellulosic material used.

Different concentrations sodium citrate, HCl, HNO<sub>3</sub> and H<sub>2</sub>SO<sub>4</sub> were evaluated as eluent solution for Pb desorption from the columns, using 2 mL of each and making the experiment in duplicate. Sodium citrate at pH 8 is a good complexing agent for Pb(II) ions, but as eluant showed the lower performance with recovery around 50 % (Figure 23). All acid eluent showed good performance, with recoveries of Pb(II) ranging to 83% to 100%. The better recoveries were found for 1.0 mol L<sup>-1</sup> of HCl with standard deviation around 2% (n=3).

#### **4.2.4. Breakthrough curve for Pb(II) on b-HNO<sub>3</sub>**

The capacity of adsorption of higher concentration of Pb(II) (5 mg L<sup>-1</sup>) onto 0.150 g of b-HNO<sub>3</sub> column and using a continuous flow rate (1 ml min<sup>-1</sup>) was tested using the breakthrough curve (Figure 24). The end of the column was coupled to the ICP OES nebulizer and Pb emission was continuously monitored. As can be seen in the Figure 24, the plateau considering the total concentration measured by ICP OES (Ct) and the initial concentration (Co) was reached after 40 min.

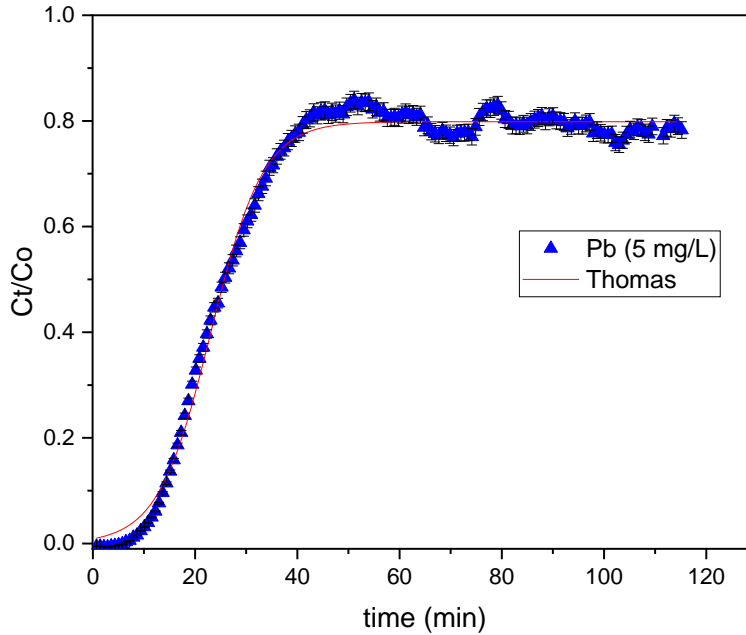


Figure 24. The breakthrough curve for Pb(II) onto b-HNO<sub>3</sub> showing nonlinear fittings for the Thomas model: 5 mg L<sup>-1</sup> Pb(II) (C<sub>0</sub>), mass 150 mg of b-HNO<sub>3</sub>, flow rate 0.5 ml L<sup>-1</sup>, and pH 6.

The experimental data was fitted for the Thomas model to gain insight into the dynamic behavior of the column. The Thomas model, which assumes Langmuir adsorption characteristics, is more realistic and provides a better fit to breakthrough data (Tan and Hameed 2017), according equation 7.

The parameters determined from nonlinear fitting with Thomas model are K<sub>Th</sub> value (0.353×10<sup>-3</sup> L mg<sup>-1</sup> min<sup>-1</sup>) and the q<sub>max</sub> value (7.00 mg g<sup>-1</sup>) was smaller than that estimated from the Langmuir model (108.4 mg g<sup>-1</sup>). In continuous processes the sorption capacity depends on several factors such as initial concentration, bed height, flow-rate, etc.(Cruz-Olivares et al. 2010)

### 4.3. Analytical characteristics for the detection of Pb using ICP OES

External calibration was applied for lead determination in ICP OES, using standard solution of 0.5, 1, 2.5, and 5 mg L<sup>-1</sup> of Pb(II) at pH 6 without preconcentration, and using 25 mL of standard solutions of 2.0, 5.0, 10, 20 and 50 µg L<sup>-1</sup> of Pb(II) at pH 6 with adsorption-preconcentration, as depicted in Figure 25.

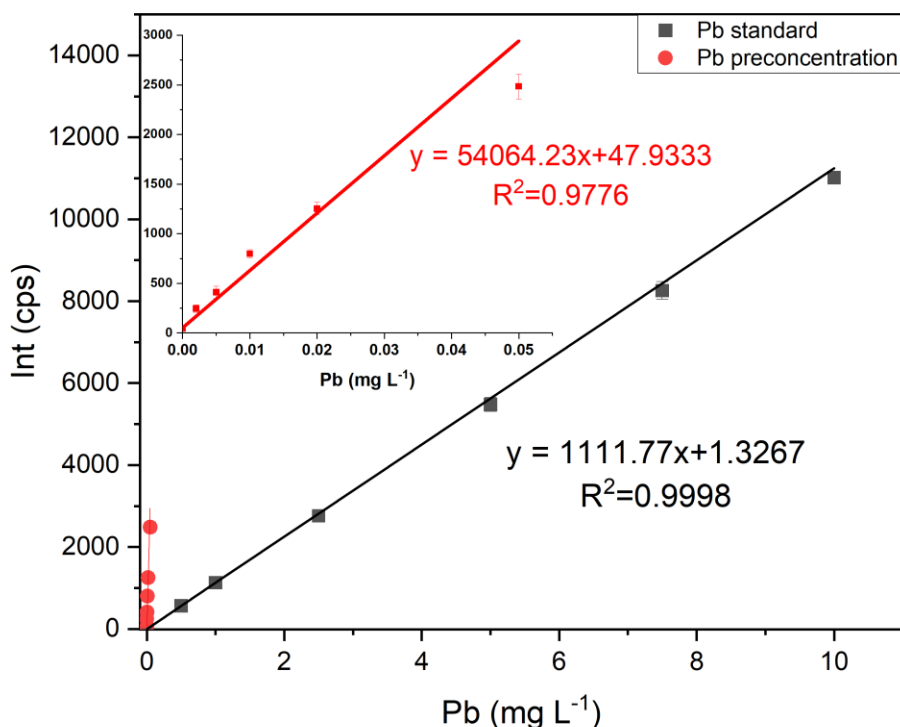


Figure 25. Calibration curves of Pb without (black) and with preconcentration step (red) for the ICP OES.

After the adsorption process the elution of the adsorbed Pb was carried out with 1 mL HCl (1 mol L<sup>-1</sup>). The LOD and LOQ were calculated as describe in section 3.1 and

the found values were  $\text{LOD} = 4 \mu\text{g L}^{-1}$  and  $\text{LOQ} = 12 \mu\text{g L}^{-1}$  without preconcentration. After preconcentration the LOD and LOQ were  $0.4 \mu\text{g L}^{-1}$  and  $1.2 \mu\text{g L}^{-1}$ , respectively.

The enrichment factor refers to the concentration of the components adsorbed and retained on the solid phase, which was eluted by a small volume of eluent and whose concentration was measured from the eluent after the preconcentration step. The enrichment factor (EF) can be calculated from the division of the slope of the standard calibration without and the slope of the calibration using preconcentration as follow  $\text{EF} = B_{\text{prec}}/B_{\text{std}}$ , being  $B_{\text{std}}$  the slope of the standard calibration and  $B_{\text{prec}}$  the slope of the standard calibration after preconcentration. The enrichment factor was 48.6, demonstrating the efficiency of the adsorption system for determination of low concentration of Pb(II).

#### **4.4. Separation-removal of Pb(II) from water using b-HNO<sub>3</sub> column**

The optimized adsorption procedure using b-HNO<sub>3</sub> column ( $m = 0.150 \text{ mg}$ , flow rate =  $1 \text{ ml min}^{-1}$ , and  $\text{pH} = 6$ ) was applied for the removal of Pb(II) in drinking water, dam water, and high salinity water (HS water, diluted sea water x 4), using addition and recovery method, as showed in Figure 26. The removal presented in Figure 26 represents the concentration of Pb determined in the eluate (after percolate through the column) and the recovery was obtained after adsorption and desorption using  $1 \text{ mol L}^{-1}$  of HCl and determined by ICP OES.

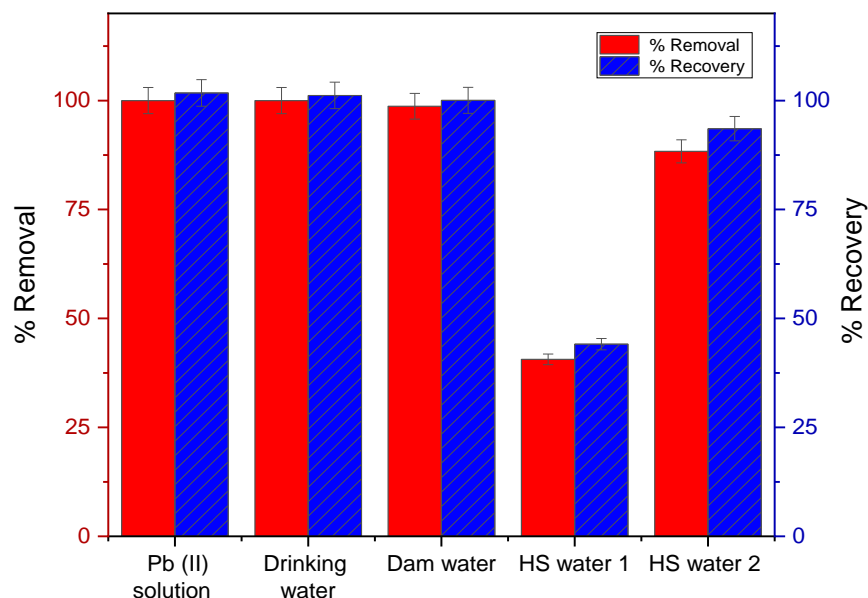


Figure 26. Removal and recovery in water samples spiked with  $1 \text{ mg L}^{-1}$  and Pb(II), using  $0.150 \text{ g}$  of  $\text{b-HNO}_3$  column, pH 6, desorption with  $1 \text{ mol L}^{-1}$  HCl: Drinking water, Dam water, and HS water 1 with flow rate  $0.5 \text{ mL min}^{-1}$  and HS water 2 with flow rate  $0.25 \text{ mL min}^{-1}$ .

For all samples spiked with  $1 \text{ mg L}^{-1}$  of Pb(II), removal was 100% for standard solution, 100% for drinking water, 98.6% for dam water, and 40.6% for HS water 1 (seawater four-time diluted) with flow rate  $0.5 \text{ mL min}^{-1}$  and 88.4% HS water 2 (seawater four-time diluted) with flow rate  $0.25 \text{ mL min}^{-1}$ . This result shows that increase of the contact time with the diminution in the flow rate improves the removal of Pb(II) in more complex matrixes such as water with high salinity.

To obtain more information about the influence of the salinity on the adsorption of Pb(II), sea water samples with different dilutions factor of 2, 4, 8, and 10 (conductivity of  $7.13$ ,  $6.38$ ,  $5.40$  and  $4.99 \text{ } \mu\text{S cm}^{-1}$ , respectively) were spiked with  $1 \text{ mg L}^{-1}$  of Pb(II), using

flow rate  $0.5 \text{ mL min}^{-1}$  through the column during the adsorption step. The result is shown in Figure 27.

The removal of different dilution (2, 4, 8, e 10) were in the range of 25.33%, 40.46%, 85.01%, and 87.49% respectively. With a decrease in the conductivity the recovery values increase until stabilization above 8-time dilution. Similar result were reported by Yang et al. (W. Yang et al. 2019) showed that an increase in solution salinity led to a significant decrease in Cu(II) and Pb(II) adsorption by *Enteromorpha* derived biochar. A decrease in adsorption with increasing salinity can be attributed to the competition of ions in the solution. Seawater have high concentrations of ions, such as  $\text{Cl}^-$  with a medium concentration of  $38,4 \text{ g L}^{-1}$  (Shehata and Nasr-EI-Din 2015). The distribution for the Pb(II) species was simulated using the Visual MINTEQ software, taking into account the pH conditions and seawater dilution with an estimated  $\text{Cl}^-$  concentration of  $9 \text{ mg L}^{-1}$  for the adsorption experiments. Chloride ions could form different complex with Pb(II) such as,  $\text{PbCl}^+$ ,  $\text{PbCl}_2 (\text{aq})$ ,  $\text{PbCl}_3^-$ ,  $\text{PbCl}_4^{2-}$ , competing with the adsorption of Pb(II) on the b- $\text{HNO}_3$  column.

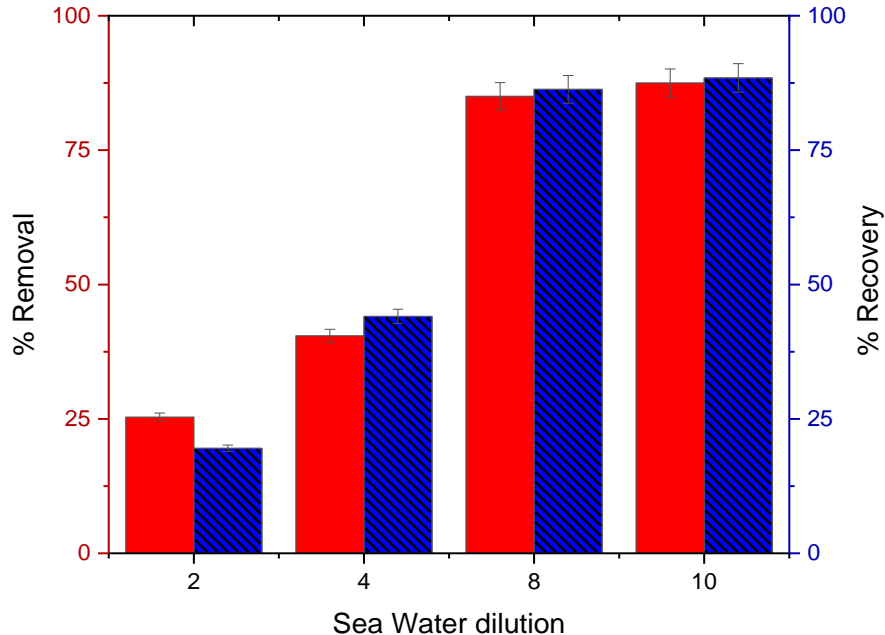


Figure 27. Performance of Pb(II) removal and recovery in different dilutions of HS water samples using b-HNO<sub>3</sub> column: 0.150 g b-HNO<sub>3</sub>, samples spiked with 1 mg L<sup>-1</sup> Pb(II), pH 6 and flow rate 0.5 mL min<sup>-1</sup>.

The influence of Cl<sup>-</sup> concentration (1 to 20 mg L<sup>-1</sup>) on the Pb(II) adsorption process is shown at Figure 28. As can be seen, with the increase of the Cl<sup>-</sup> concentrations the removal of Pb(II) decreases up to 46.7 % at Cl<sup>-</sup> concentration of 20 mg L<sup>-1</sup>. Although the concentration of Cl<sup>-</sup> employed is lower than the natural seawater concentration, its impact on Pb(II) adsorption is discernible. Notably, the influence of Cl<sup>-</sup> on adsorption is more pronounced in a simplified system compared to a real sample. Furthermore, the presence of other ions in the sample can induce synergistic or antagonistic effects on the interference caused by Cl<sup>-</sup> in Pb(II) adsorption. However, comparing the results obtained in the Figure 28, it can be considered that the greatest influence is related to the presence of high concentrations of Cl<sup>-</sup>.



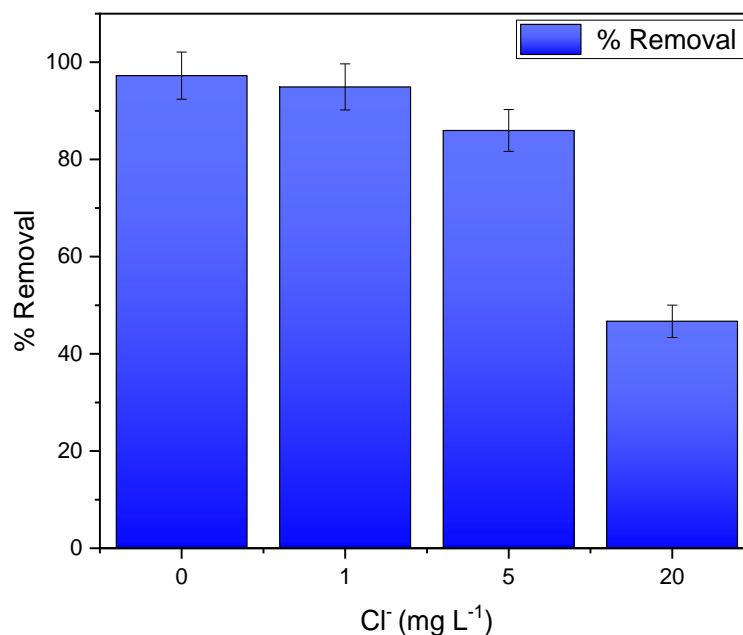
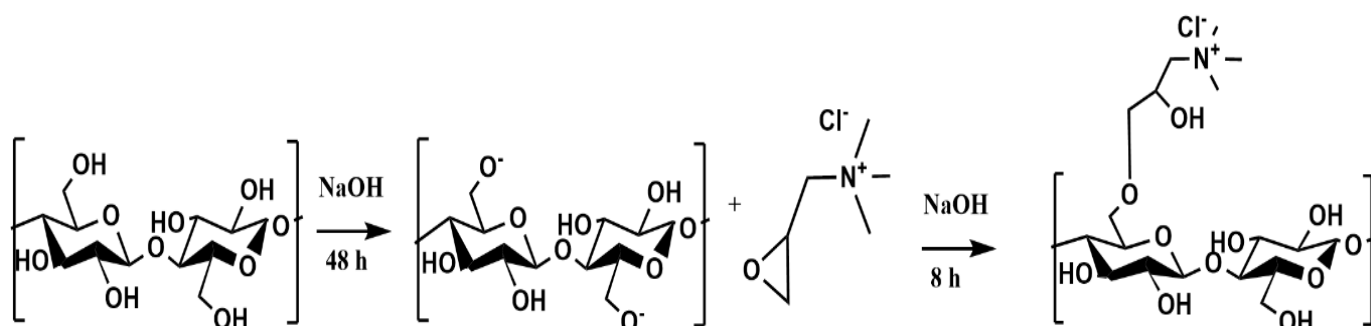


Figure 28. Influence of Cl<sup>-</sup> concentration on the removal of Pb(II) using b-HNO<sub>3</sub> column, solutions with 1 mg L<sup>-1</sup> Pb(II) and different Cl<sup>-</sup> (1-20 mg L<sup>-1</sup>) with flow rate 0,5 mL min<sup>-1</sup>.

These results show that in the case of high salinity water samples analysis, two strategies can be applied to improve the recovery of Pb(II), reduce a flow rate or increase the dilution factor lowering the salinity, demonstrating that the proposed method is suitable for the removal of Pb(II) in environmental waters. At the same time, the high enrichment factor observed, and the good recovery obtained demonstrate that the method can also be used for the determination of trace Pb concentrations by ICP OES.

#### 4.5. Preparation of modified MCC with Glycidyl trimethylammonium chloride (MCC-GTA)

The functionalization of microcrystalline cellulose with glycidyl trimethylammonium was started using a fixed amount of MCC in a mild alkaline solution with 5 % (w v<sup>-1</sup>) of NaOH. The suspension was then subjected to sonication at 20 kHz for 10 h. Sonication was used to enhance the reactivity of hydroxyl groups (OH<sup>-</sup>) of MCC and increase the amount of trimethylammonium groups introduced onto the final material (Najib and Christodoulatos 2019). However, it was not possible to reproduce this procedure, because after sonication an amorphous mass of the MCC was yield, making it impossible to obtain fine particles for further studies. In addition, e procedure involving 10 % (w v<sup>-1</sup>) of NaOH and 2.5 % (w v<sup>-1</sup>) of MCC with constant stirring during 48h showed the best results (Siqueira Petri et al. 1999). The reaction for functionalization of de MCC-GTA is represented below:



*Scheme 1.* Reaction for MCC functionalization with Glycidyl trimethylammonium chloride (MCC-GTA)

Figure 29 shows the FTIR spectrum of microcrystalline cellulose (MCC) as a control sample for comparison purpose, and MCC-GTA prepared using different amounts of glycidyl trimethylammonium chloride (GTAC) (9%, 18% and 36%). The three spectra have similar characteristic bands for that observed for pure microcrystalline cellulose (MCC). The most prominent bands are the O-H stretching at around  $3340\text{ cm}^{-1}$ , the C-H stretching band at around  $2900\text{ cm}^{-1}$ , the C-O-C stretching band at around  $1050\text{ cm}^{-1}$ , and O-H bending vibrations  $1250\text{--}1420\text{ cm}^{-1}$  (Momzyakova et al. 2021). Glycidyl trimethylammonium has several characteristic bands that could overlap characteristics band of MCC, N-H stretching band at around  $3300\text{ cm}^{-1}$ , the C-H stretching band at around  $2900\text{ cm}^{-1}$ , and the C-N stretching band at around  $1000\text{--}1200\text{ cm}^{-1}$  (M. Wang et al. 2022). It is also possible that the modification caused a change in the crystallinity of the cellulose, which could affect the intensity of the absorption bands (Momzyakova et al. 2021), this was observe in slightly decrease in the intensity of the bans at  $3340\text{ cm}^{-1}$  and  $1050\text{ cm}^{-1}$ .

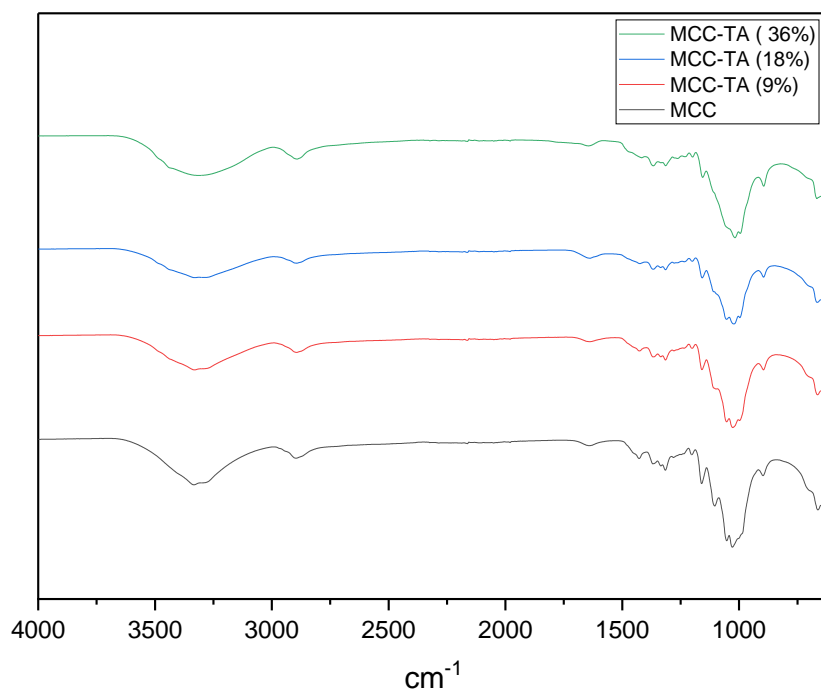


Figure 29. FTIR spectra of pure MCC and after functionalization with different amounts of glycidyl trimethylammonium chloride (9%, 18% and 36%).

Although it was not possible to clearly identify the modification of MCC with CTAC by FTIR, elemental analysis showed promised results (Table 5). In Table 5 is showed the elemental analysis of carbon (%C), hydrogen (%H), and nitrogen (%N) in MCC and its derivatives, varying percentages of modifications using GTAC. The results indicate that as the percentage of modification increases, there is a gradual decrease in the %C and %H content. This suggests that the modification process leads to a reduction in the carbon and hydrogen composition in the modified compounds.

Table 5. CNH elemental analysis of MCC and MCC-GTA with different % of GTAC

	%C	%H	%N
<i>MCC</i>	41.47±0.13	6.55±0.01	0.02±0.01
MCC-GTA (9%)	41.02±0.01	6.67±0.11	0.31±0.01
MCC-GTA (18%)	40.60±0.02	6.48±0.18	0.62±0.03
MCC-GTA (36%)	36.29±0.08	6.75±0.08	0.65±0.02

Additionally, the %N content shows a significant increase with increasing modification percentage until stabilization over 18% ( $m v^{-1}$ ), indicating that the introduction of quaternary ammonium group on the cellulose structure resulting in a higher nitrogen content in the modified compounds. For this reason, the functionalization material using 18% ( $m v^{-1}$ ) was selected to continue with the adsorption experiments. These findings provide valuable insights into the structural changes occurring during the modification process and highlight the impact of GTAC on the elemental composition of the resulting MCC-GTA derivatives.

#### 4.6. Arsenic species adsorption optimization

It is important to highlight that all the experiments of fractionation and speciation of As was done using batch mode separation.

##### 4.6.1. Arsenic species removal as a function of pH onto MCC-GTA

The effect of pH on the adsorption of arsenic species (AsIII, AsV, AsB, MMA and DMA) onto MCC-GTA is showed in Figure 30. Each of the systems with the different species studied, presents a different behavior depending on the pH of the solution. MCC-GTA shows a high affinity for As(V) between pH 6 and 7. In this interval, it can be seen that almost 100% of adsorption of As(V), since concentration of As in the supernatant was below LOD. A similar behavior of As(V) adsorption on cellulosic materials modified with amino groups is also reported in the literature (Anirudhan et al. 2012). However, these experiments did not explore the possibility to apply for speciation analysis of As.

At pH 8, the percentage of desorption of As(V) decreased to 75% and at pH 10 it already decreased to almost 60%. Taking into account the speciation of As(V), it is important to considerer the formation of  $\text{H}_3\text{AsO}_4$ ,  $\text{H}_2\text{AsO}_4^-$ ,  $\text{HAsO}_4^{2-}$  and  $\text{AsO}_4^{3-}$ , which are the dominant species of As(V) in water in the pH ranges of <2.0, 2.0–6.1, 6.1–11.5, and >11.6, respectively (Najib and Christodoulatos 2019).

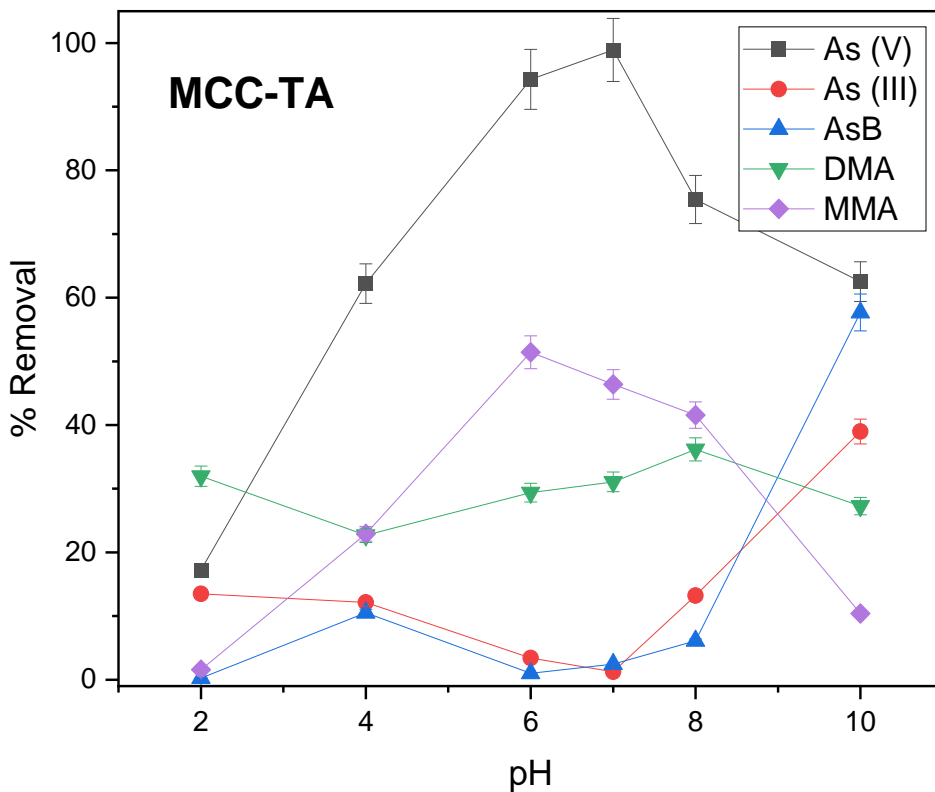


Figure 30. Arsenic species adsorption as a function of pH using 10 mg of MCC-GTA at pH 2-10.

In a pH range of 6-7,  $\text{H}_2\text{AsO}_4^-$  is the predominant As(V) species and can be electrostatically attracted by the positively charged amine groups on MCC-GTA. At pH > 8, the number of OH- groups increases and they can compete with the adsorption of As(V) on the material. In this pH range 6-7 where the adsorption of As(V) is maximum, species such as As(III) and AsB present a completely different behavior with adsorption % values close to 0 for As(III), and the methylated species MMA and DMA, present adsorption of 30% and 50%, respectively. For the optimization of the adsorption parameters for the

development of arsenic fractionation and speciation procedure the pH was maintained between 6-7.

For comparison, experiments were carried out to verify the adsorption efficiency of the different As species on MCC without treatment and the MCC after the activation process using NaOH ( $10 \text{ mol L}^{-1}$ ), but without modification with GTA and the results are shown in Figure 31 and Figure 32, respectively. Both materials present a low adsorption for the species studied in the different pH conditions. These results are evidence that the MCC modification process with the introduction of quaternary amino groups was satisfactory and that these groups are directly related to the adsorption mechanism of As species on the modified MCC-GTA.

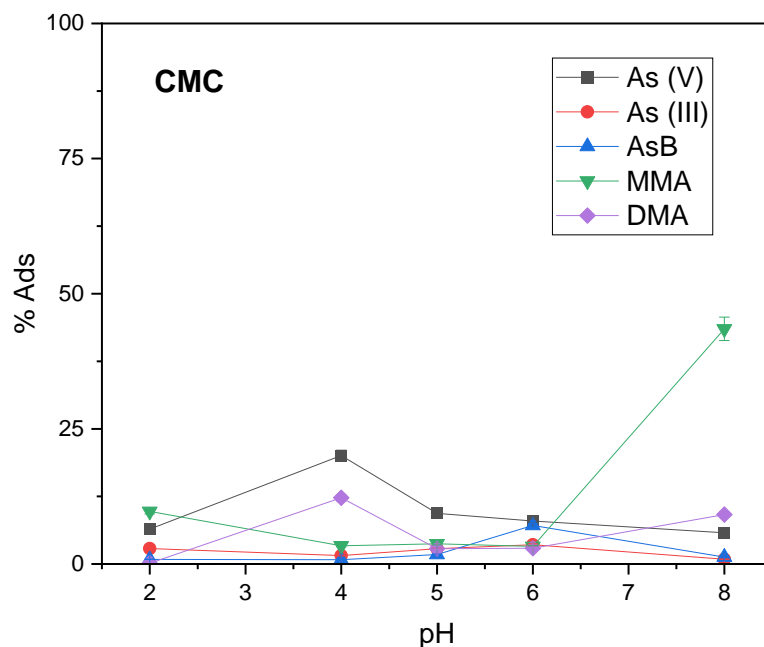


Figure 31. Arsenic species adsorption as a function of pH using pure MCC, mass 10 mg and at pH 6-7.



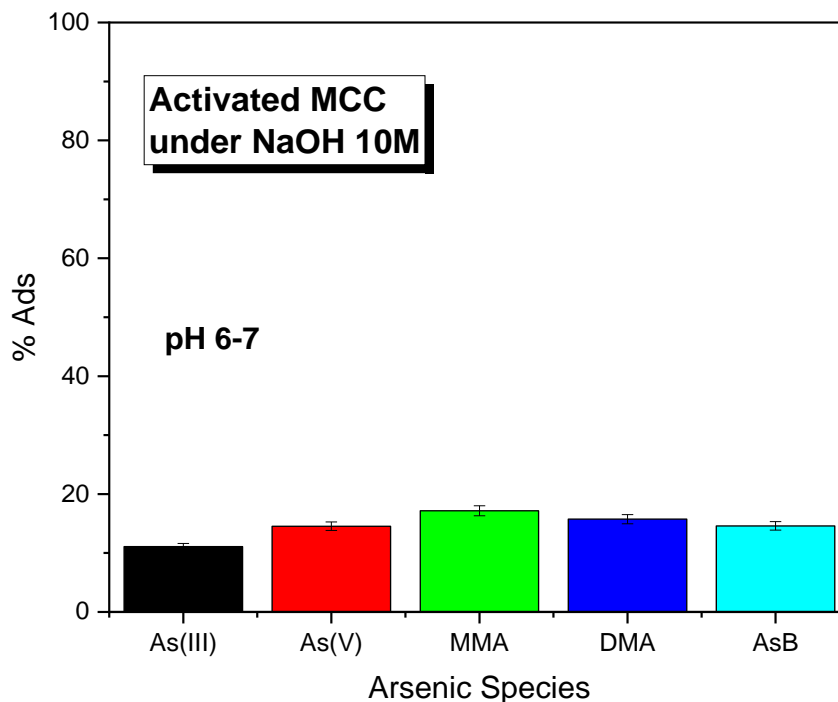


Figure 32. Arsenic species adsorption as a function of pH using activated MCC with NaOH (10 mol L<sup>-1</sup>), without modification with GTA, mass 10 mg and at pH 6-7.

#### 4.6.2. Contact time and adsorbent mass for arsenic species adsorption onto MCC-GTA

The contact time and the mass of adsorbent are important parameters to be evaluated, which are related to the kinetics of the adsorption process and the adsorption capacity of the material, respectively. The experimental results shown in Figure 33 show that there were no significant differences in the adsorption of 100 µg L<sup>-1</sup> of the different species in different contact times of 1 - 60 min. It can be seen that the adsorption for As(V), at pH 6-7, is fast and efficient (almost 100% adsorption).

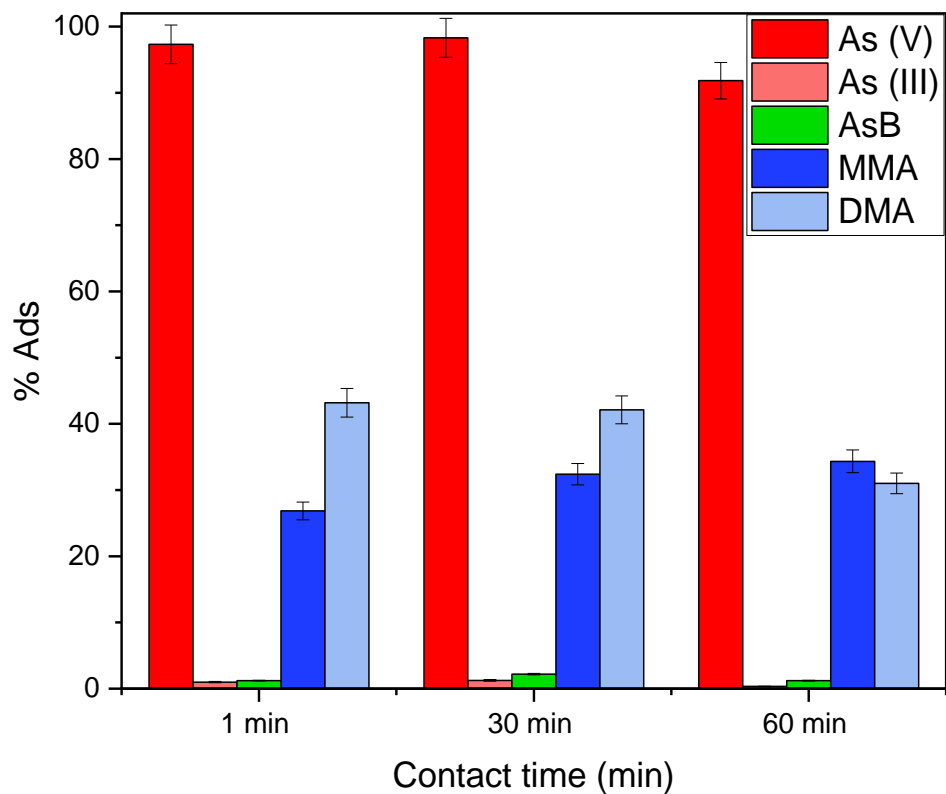


Figure 33. Contact time for arsenic species adsorption using 10 mg MCC-GTA, initial concentration  $100 \mu\text{g L}^{-1}$  of As species, at pH 6-7.

The variation in the adsorbent mass (Figure 34) from 10 mg to 20 mg did not present significant differences in the adsorption profile of the varied species. For the following experiments, the experimental parameters were set at 1 min of contact time and adsorbent dose of 10 mg.

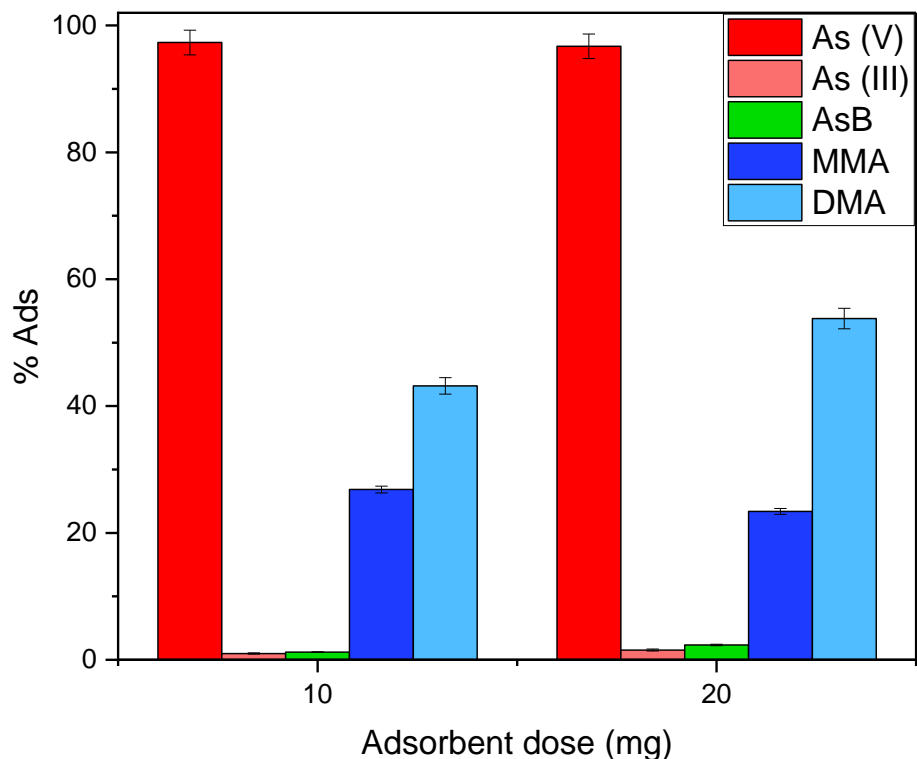


Figure 34. Adsorbent dose for arsenic species adsorption using MCC-GTA, initial concentration 0,1 mg/L and pH 6-7.

#### 4.6.3. LC-ICP OES arsenic species monitoring and oxidation process

Some of the strategies for As remediation, such as precipitation combined with reverse osmosis or ion exchange, achieve good removal rates only if As(III) is oxidized (Sorlini and Gialdini 2010). With the results obtained at pH 6-7, the adsorption efficiency of As(V) was maximum while As(III) and AsB practically did not adsorb on the material under these conditions. The fractionation of the inorganic arsenic species (iAs) would be possible if, prior to adsorption, through an oxidation process, transforming As(III) to As(V),

thus allowing the adsorption of the iAs species. For this reason, the need to find some oxidizing agent that can provide the oxidation of As(III) without interfering in the adsorption and in the adsorbent structure is a challenge. Some oxidants have been previously reported such as chlorine dioxide, hypochlorite, potassium permanganate, and monochloramine for the oxidation of As(III) species to As(V) (Sorlini and Gialdini 2010). In this study, NaClO was selected as the oxidizing agent.

Figure 35 shows the chromatogram for the arsenic species using anion exchange column PRP X-100 and ICP OES as detector. First, the elution of As(III) and AsB with similar retention time occurs, followed by the elution of DMA after MMA and finally As(V), similar results are reported in the literature (Carioni et al. 2017; Minami F. 2017).

The oxidation of As(III) was monitored in the presence of the other species. Figure 36 shows the chromatogram of the mixture of the arsenic species (As(III), As(V), AsB, MMA and DMA) before and after the oxidation process with different molar ratio between NaClO and the concentration of total As ( $R_{NaClO/As}$ ). As can be seen, after the oxidation process, occurs the decrease of the first peak ( $t = 120$  sec) and an increase in the last peak ( $t = 350$  sec) corresponding to the oxidation of As(III) to As(V). The peaks corresponding to AsB, MMA, and DMA appear unchanged after the oxidation process, which indicates that the oxidizing agent does not affect the stability of these species. The redox reaction involved in this process can be find below:



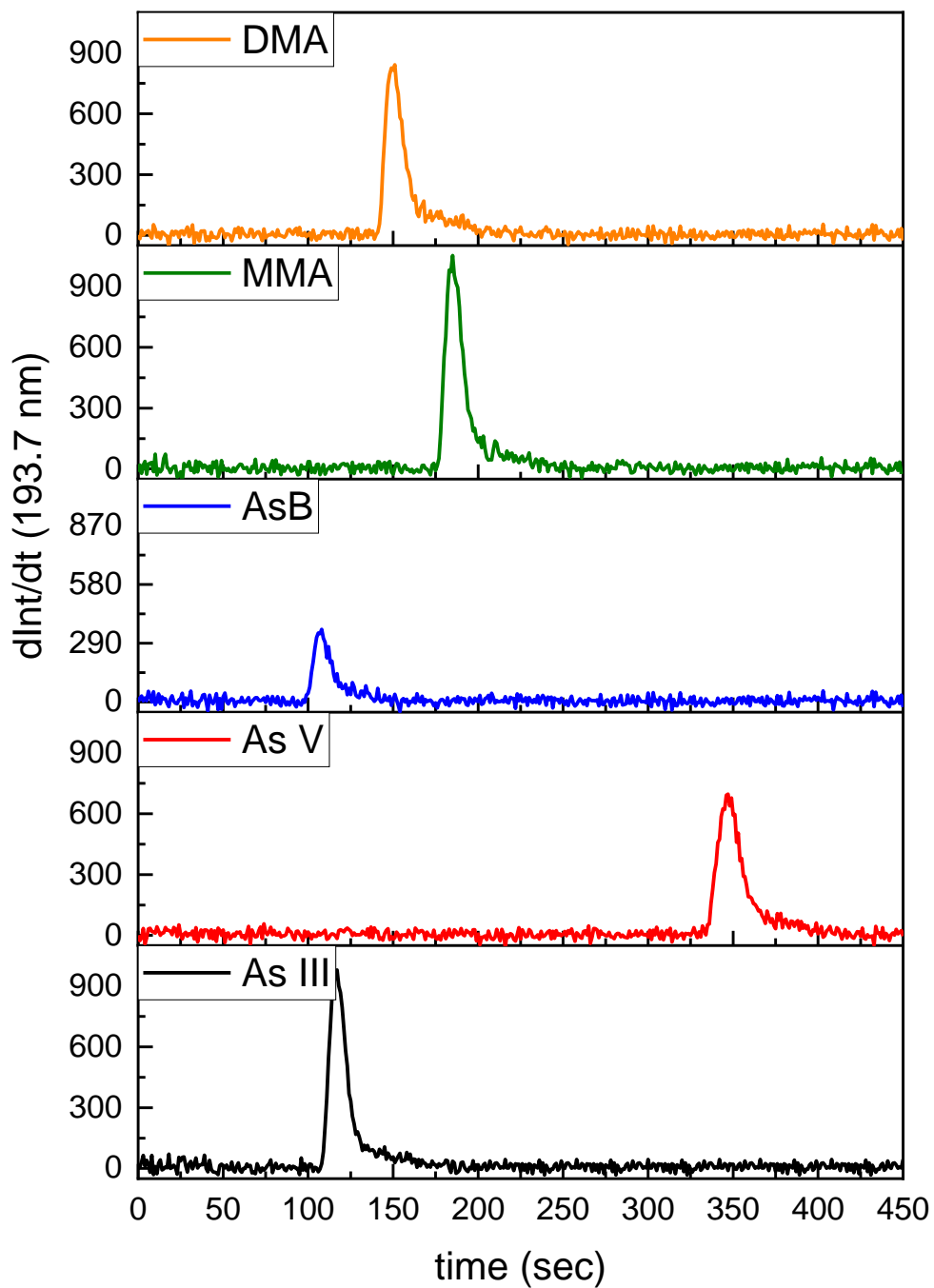


Figure 35. Anion exchange chromatogram of As species by LC-ICP OES: dimethyl arsenic (DMA), monomethyl arsenic (MMA), arsenobetaine AsB), As(V) and As(III).

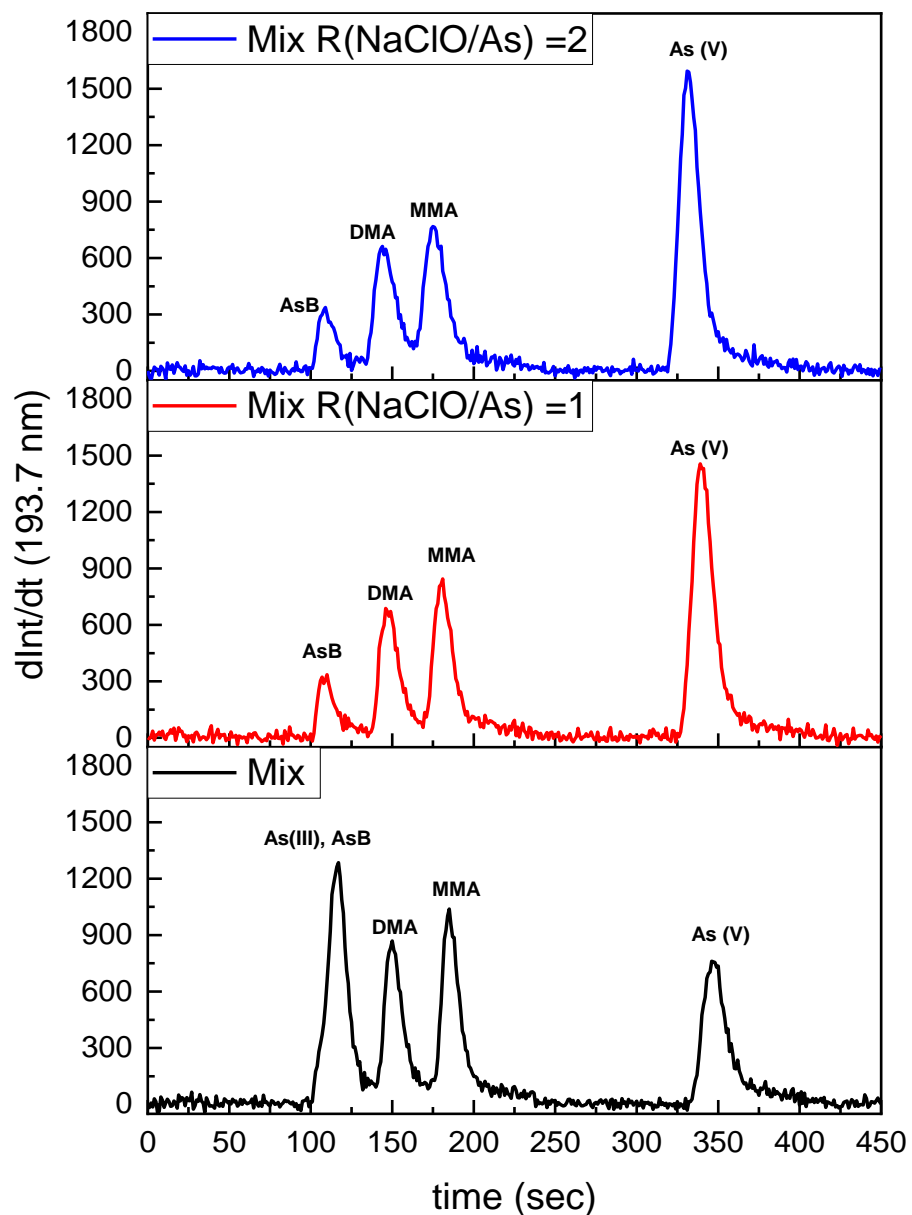


Figure 36. Anion exchange chromatogram of As species mixture by LC-ICP OES: Mix (without oxidant), Mix  $R_{NaClO/As}=1$  (after oxidation with same molar ratio between NaClO and As species) and Mix  $R_{NaClO/As}=2$  (after oxidation with twice molar ratio between NaClO and As species).

#### 4.6.4. Influence of sodium hypochlorite as oxidant agent on the adsorption of As species on MCC-GTA

To verify the results obtained by LC-ICP OES for the oxidation of As(III) to As(V) with NaClO and using the optimized conditions for the adsorption process, the adsorption of the different species was studied using MCC-GTA before and after the oxidation with different conditions of  $R_{NaClO/As}$  and the results are in the Figure 37.

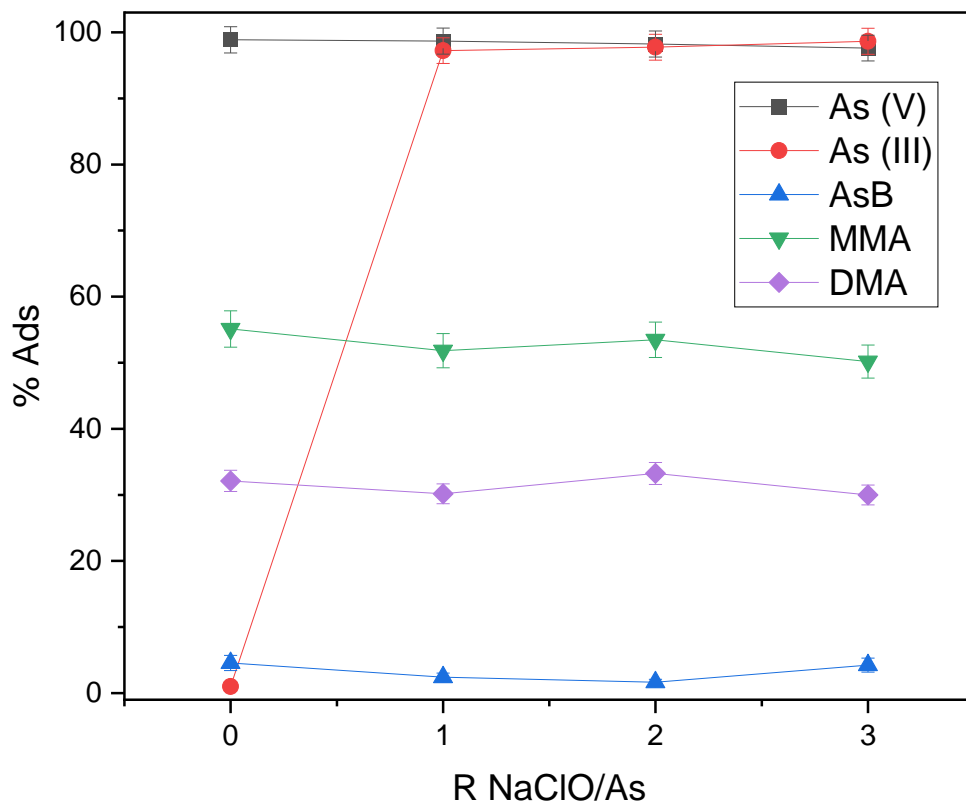


Figure 37. Arsenic species adsorption using MCC-GTA at pH 6-7: 0 (without oxidant) and 1, 2 and 3 (after oxidation with NaClO).

The presence of NaClO does not affect the adsorption of As(V) since both in the absence or in different concentrations of oxidant the percentage of adsorption remains close to 100%, the MMA and DMA methylated seems to be unaffected by NaClO keeping the percentage of adsorption around 50% and 30%, respectively. In the case of AsB, the sorption is not influenced by the presence of NaClO and is kept below 5% under different conditions. As expected, the adsorption of As(III) without NaClO is insignificant, in the presence of oxidant in different molar ratios the adsorption increases to almost 100% adsorption. With these results, we can conclude that the selective separation of the iAs species is possible through a previous oxidation process that allows transforming As(III) into As(V) and adsorbed on MCC-GTA.

However, the methylated species of arsenic are not completely adsorbed, however, throughout the various experiments was observed systematic maintenance of absorption of MMAs and DMAs, which allowed proposing a fractionation and semiquantitative analysis of the set of the most toxic species (AsIII, AsV , MMAs, and DMAs) from the non-toxic specie (AsB).

#### **4.7. Analytical characteristics for the detection of As using GF AAS**

The optimization of GF AAS was done and standard calibration using 5, 10, 20, 40, 60, 80 and 120  $\mu\text{g L}^{-1}$  in pH 6-7 was used for arsenic determination. Figure 38 (blue) show the calibration using the standard solutions above mentioned. The LOD and LOQ were calculated according to IUPAC recommendations ( $\text{LOD}=3S_B/m$  and  $\text{LOQ}=10S_B/m$ ). The obtained values were  $\text{LOD}= 7 \mu\text{g L}^{-1}$  and  $\text{LOQ}= 22 \mu\text{g L}^{-1}$ .



The high efficiency of adsorption observed for As(V) and none for As(III) on the MCC-GTA allowed the speciation of inorganic arsenic (iAs). The calibration was performed in absence and presence of NaClO, as As(III) oxidant. The calibration using preconcentration procedure was done using a mixture of 0.25, 0.5, 1, 2 and 3  $\mu\text{g L}^{-1}$  of As(III) plus 0.25, 0.5, 1, 2 and 3  $\mu\text{g L}^{-1}$  of As(V) in pH 6-7. For calibration using As(V) preconcentration, volumes of 25 mL of standard solution was put in contact with 50 mg of MCC-TA, manually agitated for 1 min, separated, washed with 1 mL of deionized water and subsequently desorption was carried out with 1 mL of HCl (1 mol  $\text{L}^{-1}$ ). The concentration of As(V) in the eluate of standards was determined using GF AAS and results are show in Figure 38 (black). Afterwards, NaClO was added in all standards and again put in contact with 50 mg of MCC-GTA, manually agitated for 1 min, separated, washed with 1 mL of deionized water and subsequently desorption was carried out with 1 mL of HCl (1 mol  $\text{L}^{-1}$ ). The concentration of As(III) + As(V) in the eluate of standards was determined using GF AAS and results are show in Figure 38 (red).

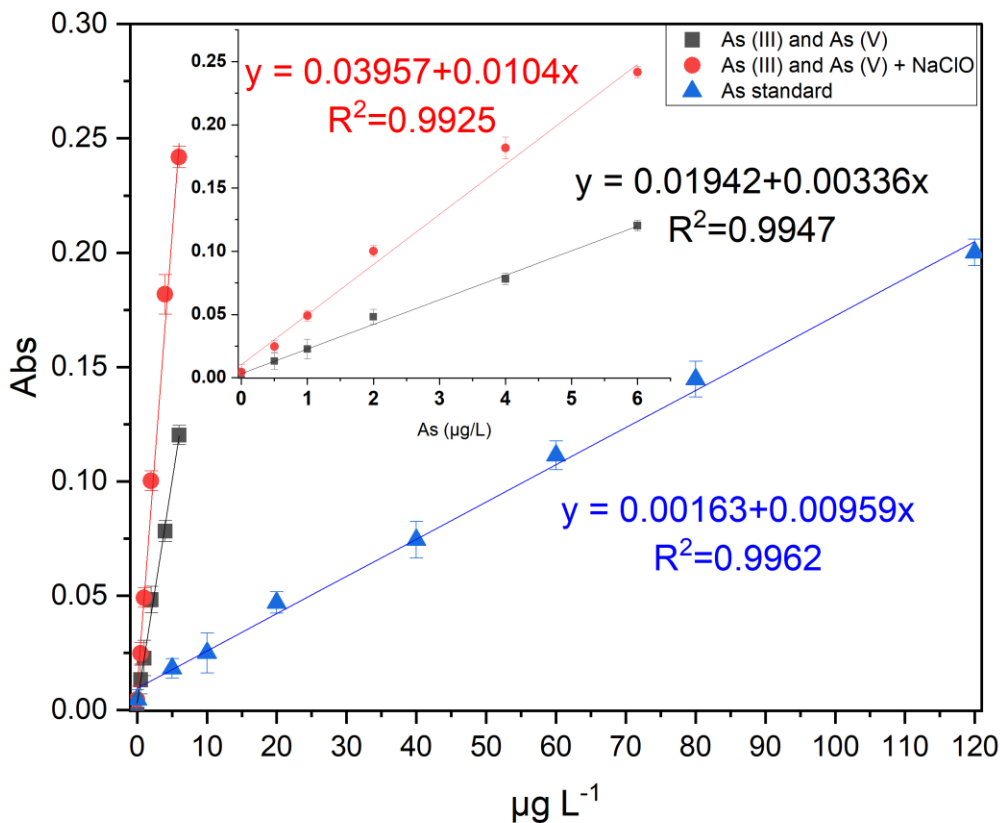


Figure 38. GF AAS standard calibration of As (blue) without preconcentration, with preconcentration of As(V) (black) and with preconcentration of As(III) and As(V) after oxidation of As(III) with NaClO (red).

As can be seen in Figure 38 (red) the slope of calibration curve (0.04) from the preconcentration of As(III) + As(V) is almost twice the slope of calibration curve (0.02) observed for the preconcentration of As(V) (Figure 38, black), demonstrating the efficiency of the oxidation and As(V) adsorption. The LOD and LOQ were calculated according to IUPAC recommendations ( $LOD=3S_B/m$  and  $LOQ=10S_B/m$ ) and the values for the preconcentration without NaClO, that refer only to As(V) were  $LOD= 0.6 \mu\text{g L}^{-1}$  and

LOQ= 2  $\mu\text{g L}^{-1}$ , and for the preconcentration with NaClO, that refer As(III) + As(V) were LOD= 1  $\mu\text{g L}^{-1}$  and LOQ= 3.4  $\mu\text{g L}^{-1}$ . Comparing the slope of calibration curve without preconcentration with the slope of calibration curve after preconcentration, using NaClO (AsIII + AsV), the enrichment factor was 24.3, demonstrating the capacity of concentration and trace analyses of inorganic species of As.

#### **4.8. Fractionation of arsenic species in water samples using MCC-GTA as adsorbent**

The identification and quantification of individual arsenic species is essential for understanding the distribution, environmental fate and behavior, metabolism, and toxicity of arsenic. Understanding arsenic speciation in water is important for managing the potential health risks associated with chronic arsenic exposure. Most arsenic monitoring studies to date include measured total arsenic and some looking at arsenic species (Rajakovic and Rajakovic-Ognjanovic 2018). Determination of arsenic species is of crucial importance to define the limits and safety of drinking water as well as in selection of arsenic removal technology for groundwater applications.

By using the NaClO treatment in the fractionation of arsenic in water samples, it becomes possible to determine the class of species that are adsorbed or not after each process. Since the adsorption of the different species (AsV, MMA, DMA and AsB) onto MCC-GTA keep the same profile without and with the use of NaClO, and As(III) was only adsorbed after the oxidation to As(V) with NaClO, was possible to establish equations to estimate the concentration of some species on each phase.

$$C_{As(total)} = C_{As(ads)} + C_{As(sol)} \quad \text{Equation 8}$$

By using Equation 9 is possible to obtain the concentration of As remained in the solution and by Equation 10 is possible to determine the concentration of As adsorbed onto MCC-GTA without the use on NaClO:

$$C_{As(sol)} (I) = C_{As(III)} + C_{AsB} + 50\% C_{MMA} + 70\% C_{DMA} \quad \text{Equation 9}$$

$$C_{As(ads)} = C_{As(V)} + 50\% C_{MMA} + 30\% C_{DMA} \quad \text{Equation 10}$$

were  $C_{As(sol)}$  is the arsenic concentration non-adsorbed onto the MCC-GTA and reminded in solution,  $C_{As(ads)}$  is the arsenic concentration adsorbed onto the MCC-GTA, and  $C_{As(III)}$ ,  $C_{As(V)}$ ,  $C_{MMA}$ ,  $C_{DMA}$ , and  $C_{AsB}$  is the concentration of As(III), As(V), MMA, DMA and AsB, respectively. After use of NaClO the concentration of different species of arsenic adsorbed and in the solution was calculated using the same way:

$$C_{As(sol\ NaClO)} (II) = C_{AsB} + 50\% C_{MMA} + 70\% C_{DMA} \quad \text{Equation 11}$$

$$C_{As(ads\ NaClO)} = C_{As(V)} + C_{As(III)} + 50\% C_{MMA} + 30\% C_{DMA} \quad \text{Equation 12}$$

were  $C_{As(sol\ NaClO)}$  is the arsenic concentration non-adsorbed onto the MCC-GTA and reminded in solution, after NaClO addition,  $C_{As(ads\ NaClO)}$  is the arsenic concentration adsorbed onto the MCC-GTA, after NaClO addition and  $C_{As(III)}$ ,  $C_{As(V)}$ ,  $C_{MMA}$ ,  $C_{DMA}$ , and  $C_{AsB}$  is the concentration of As(III), As(V), MMA, DMA and AsB, respectively. Combining Equation 9 and Equation 11 it is possible to estimate the concentration of As(III) in the sample:

$$C_{As(III)} = C_{As\ sol} (I) - C_{As\ sol} (II)$$

Equation 13

By employing these equations and analyzing the concentrations of different arsenic species, it becomes possible to determine which species are adsorbed onto MCC-GTA and which ones remain in solution through Equation 8 to Equation 12. Additionally, the concentration of As(III) can be determined using Equation 13, and the recoveries were calculated for the determined concentration of As(III) in the sample providing insights into the presence and distribution of this specific arsenic species in the water samples and the results are show in Table 6.

Table 6. Concentrations of As after fractionation in aqueous solution and water samples.

Solutions or River Sample	$\mu\text{g L}^{-1}$ added						Without NaClO ( $\mu\text{g L}^{-1}$ )		With NaClO ( $\mu\text{g L}^{-1}$ )		After addition of NaClO	
	As total	As(III)	As(V)	MMA	DMA	AsB	C <sub>As ads</sub> <sup>1</sup>	C <sub>As sol</sub> <sup>2</sup>	C <sub>As ads</sub> <sup>3</sup>	C <sub>As sol</sub> <sup>4</sup>	As(III) <sup>5</sup>	As III Recovery %
Aqueous solution	100	100	-	-	-	-	1.6	98.4	100	< LOD	98.4	98.4
Aqueous solution	100	-	100	-	-	-	100	< LOD	100	< LOD	-	-
Aqueous solution	50	-	-	50	-	-	24.3	25.7	24.2	25.8	-	-
Aqueous solution	50	-	-	-	50	-	15.4	34.6	15.2	34.8	-	-
Aqueous solution	100	-	-	-	-	100	2.1	97.9	1.7	98.3	-	-
Aqueous solution	100	50	50	-	-	-	49.7	50.3	100	< LOD	50.3	101
Aqueous solution	200	50	50	-	-	100	46.9	153.1	102.5	97.5	55.1	110
Aqueous solution	100	-	-	50	50	-	48.1	51.9	46.0	54.0	-	-
Aqueous solution	75	-	-	24	27	24	18.4	56.6	13.1	61.9	-	-
Aqueous solution	100	25	25	-	25	25	34.0	66.0	61.9	38.1	27.9	112
Aqueous solution	100	24	24	16	19	17	28.8	72.2	53.5	47.5	24.8	95
River water	-	-	-	-	-	-	-	< LOD	-	< LOD	-	-
River water	50	50	-	-	-	-	0.3	49.7	50.0	< LOD	49.7	99.4
River water	50	-	50	-	-	-	50	< LOD	50	< LOD	-	-
River water	45	-	-	45	-	-	22.71	22.29	21.28	23.72	-	-
River water	50	-	-	-	50	-	16.22	33.78	15.6	34.4	-	-
River water	42	-	-	-	-	42	0.13	41.87	0.03	41.97	-	-
River water	100	50	50	-	-	-	44.9	55.1	100	< LOD	55.1	110
River water	149	52	52	45	-	-	73.6	75.4	124.66	24.34	51.06	98.2
River water	199	52	52	45	50	-	88.9	110.1	141.09	57.91	52.19	100
River water	241	52	52	45	50	42	90.5	150.5	142.7	98.3	52.2	100

1 Equation 10 (without NaClO)  $C_{As\ sol\ (I)} = C_{As(III)} + C_{AsB} + 50\% C_{MMA} + 70\% C_{DMA}$

2 Equation 9 (without NaClO)  $C_{As(sol)} = C_{As(III)} + C_{AsB} + 50\% C_{MMA} + 70\% C_{DMA}$

3 Equation 12 (with NaClO)  $C_{As\ ads\ NaClO} = C_{As(V)} + C_{As(III)} + 50\% C_{MMA} + 30\% C_{DMA}$

4 Equation 11 (with NaClO)  $C_{As\ sol\ (II)} = C_{AsB} + 50\% C_{MMA} + 70\% C_{DMA}$

5 Equation 13  $C_{As(III)} = \text{Equation 9} - \text{Equation 11} = C_{As\ sol\ (I)} - C_{As\ sol\ (II)}$

The results in Table 6 show that the recovery of As(III) occurs with high efficiency when the oxidant is used. The effective oxidation of As(III) by NaClO allows to determine quantitatively the concentration of As(III) in a sample.

The concentration of As in the River Sample was below to the LOD. However, even considering a complex sample, the recoveries of As(III) in the sample are between 98%-111%. Since AsB is not toxic and did not adsorb on the MCC-GTA, and after oxidation As(V) and As(III) (the more toxic species) are fully adsorbed on the solid phase and a 50% of MMA and 30% of DMA (less toxic than iAs) are adsorbed on the MCC-GTA it is possible to do the fractionation and speciation of arsenic using a non-chromatographic method for screening. Important qualitative information on the arsenic toxicity present in the sample could be inferred from that and using this information a decision can be made about performing a more thorough speciation analysis.

#### **4.9. Preconcentration and speciation of iAs from water samples using MCC-TA**

Preconcentration of inorganic arsenic in water prior to detection is important because the concentration of inorganic arsenic in water is often extremely low and can be below the detection limit of the analytical method used for detection. The results of the iAs preconcentration and speciation analysis in water samples are presented in the Table 7. The table provides information on the concentration of arsenic species (As(III) and As(V)) in the samples, both before and after the addition of known amounts of arsenic.

These results demonstrate the effectiveness of the preconcentration and speciation analysis method for arsenic in water samples. The method allows for accurate quantification and differentiation of As(III) and As(V) species, and the recoveries indicate a high level of accuracy in the analysis with values between 93%-109% for As(III) and 96%-103% for As(V). The findings provide valuable information for assessing the contamination levels and potential risks associated with inorganic arsenic in water sources.



Table 7. iAs preconcentration and speciation analysis in water samples.

<i>Samples</i>	<i>μg L<sup>-1</sup> Added</i>		<i>μg L<sup>-1</sup> Found</i>		<i>% Recovery</i>	
	<i>As(III)</i>	<i>As(V)</i>	<i>As(III)</i>	<i>As(V)</i>	<i>As(III)</i>	<i>As(V)</i>
<i>Aqueous solution</i>	2	-	1.88 ± 0.06	-	94.0	-
<i>Aqueous solution</i>	-	2	-	2.07 ± 0.08	-	103.5
<i>Aqueous solution</i>	2	2	2.19 ± 0.09	1.92 ± 0.04	109.6	96.2
<i>River water</i>	-	-	< LOD	< LOD	-	-
<i>River water</i>	2	-	1.87 ± 0.12	-	93.6	-
<i>River water</i>	-	2	-	1.92 ± 0.02	-	95.9
<i>River water</i>	2	2	2.18 ± 0.14	1.94 ± 0.05	109.2	96.9

## 5. Conclusions

Microcrystalline cellulose beads (b-HNO<sub>3</sub>) were prepared in HNO<sub>3</sub> coagulant medium for removal of Pb in water. The adsorption process is pH dependent, the best condition to carry out the removal process is at pH 6. The reusability of b-NHO<sub>3</sub> was demonstrated for nine cycles and the material showed excellent results with only a 5% loss in removal efficiency. For complex samples (high salinity), the adsorption process is dependent on the flow rate of the solution through the column and the salinity of the sample. A decrease in flow rate and salinity increases the Pb removal efficiency. Different samples of Pb(II) enriched water were tested, using the optimized conditions for adsorption, obtaining recoveries between 94% and 102%. Cellulose beads proved to be efficient for separating Pb(II) from natural water samples, and can be used for removal and pre-concentration for analytical determinations. The beads has an easy preparation as an eco-friendly material, for its use in water treatment applications.

Microcrystalline cellulose modified with glycidyl trimethylammonium chloride (MCC-TA) exhibits selective adsorption to As(V) at pH 6-7. NaClO is a suitable oxidizing agent for the transformation of As (III) into As (V), allowing the selective separation of the iAs species through a previous oxidation process that allows transforming As (III) into As (V) and adsorbed on MCC-TA. The fractionation and speciation of As in water samples allows obtaining important quantitative and qualitative information about the toxicity of As present in the samples. MCC-TA demonstrated efficiency in the quantitative separation of As(V), and can be used as adsorbent material for removal and preconcentration aiming at analytical determinations. Quantitative oxidation of As(III) to As(V) with subsequent

adsorption on MCC-TA can be applied as a method of speciation of iAs. The non-adsorption of AsB and partial adsorption of MMA and DMA by cellulose modified with glycidyl trimethylammonium allows the fractionation of toxic species (As(III), As(V), MMA and DMA) from non-toxic ones, and can be applied as a screening method. The preconcentration and speciation analysis of iAs from water samples using MCC-TA demonstrated accurate quantification and differentiation of As(III) and As(V) species, with high recovery percentages ranging from 93% to 109% for As(III) and 96% to 103% for As(V). These results validate the effectiveness of the developed non chromatographic method for assessing inorganic arsenic contamination levels and potential risks in water sources.

## 6. Bibliography

- Adeloju, Samuel B., Shahnoor Khan, and Antonio F. Patti. 2021. "Arsenic Contamination of Groundwater and Its Implications for Drinking Water Quality and Human Health in Under-Developed Countries and Remote Communities—A Review." *Applied Sciences* 11 (4): 1926. <https://doi.org/10.3390/app11041926>.
- Aktar, Sanjida, Shamim Mia, Tomoyuki Makino, Mohammad Mahmudur Rahman, and Anushka Upamali Rajapaksha. 2023. "Arsenic Removal from Aqueous Solution: A Comprehensive Synthesis with Meta-Data." *Science of The Total Environment* 862 (March): 160821. <https://doi.org/10.1016/j.scitotenv.2022.160821>.
- Al-Degs, Y., M. A.M. Khraisheh, and M. F. Tutunji. 2001. "Sorption of Lead Ions on Diatomite and Manganese Oxides Modified Diatomite." *Water Research* 35 (15): 3724–28. [https://doi.org/10.1016/S0043-1354\(01\)00071-9](https://doi.org/10.1016/S0043-1354(01)00071-9).
- Ali Redha, Ali. 2020. "Removal of Heavy Metals from Aqueous Media by Biosorption." *Arab Journal of Basic and Applied Sciences* 27 (1): 183–93. <https://doi.org/10.1080/25765299.2020.1756177>.
- Alila, Sabrine, and Sami Boufi. 2009. "Removal of Organic Pollutants from Water by Modified Cellulose Fibres." *Industrial Crops and Products* 30 (1): 93–104. <https://doi.org/10.1016/j.indcrop.2009.02.005>.
- Altowayti, W. A.H. H., N. Othman, S. Shahir, A. F. Alshalif, A. A. Al-Gheethi, F. A.H. H. AL-Towayti, Z. M. Saleh, and S. A. Haris. 2022. "Removal of Arsenic from Wastewater by Using Different Technologies and Adsorbents: A Review." *International Journal of Environmental Science and Technology* 19 (9): 9243–66. <https://doi.org/10.1007/s13762-021-03660-0>.

- Anand, Vandana, Jasvinder Kaur, Sonal Srivastava, Vidisha Bist, Pallavi Singh, and Suchi Srivastava. 2022. "Arsenotrophy: A Pragmatic Approach for Arsenic Bioremediation." *Journal of Environmental Chemical Engineering*. Elsevier.  
<https://doi.org/10.1016/j.jece.2022.107528>.
- Anirudhan, T.S. S., J. Nima, S. Sandeep, and V.R.N. R.N. Ratheesh. 2012. "Development of an Amino Functionalized Glycidylmethacrylate-Grafted-Titanium Dioxide Densified Cellulose for the Adsorptive Removal of Arsenic(V) from Aqueous Solutions." *Chemical Engineering Journal* 209 (October): 362–71. <https://doi.org/10.1016/j.cej.2012.07.129>.
- Arana Juve, Jan Max, Frederick Munk S. Christensen, Yong Wang, and Zongsu Wei. 2022. "Electrodialysis for Metal Removal and Recovery: A Review." *Chemical Engineering Journal* 435 (May): 134857. <https://doi.org/10.1016/J.CEJ.2022.134857>.
- Arora, Rajeev. 2019. "Adsorption of Heavy Metals—A Review." *Materials Today: Proceedings* 18: 4745–50. <https://doi.org/10.1016/j.matpr.2019.07.462>.
- Asere, Tsegaye Girma, Christian V. Stevens, and Gijs Du Laing. 2019. "Use of (Modified) Natural Adsorbents for Arsenic Remediation: A Review." *Science of The Total Environment* 676 (August): 706–20. <https://doi.org/10.1016/j.scitotenv.2019.04.237>.
- ATSDR. 2002. "Toxicological Profile for Lead." In *ATSDR's Toxicological Profiles*. Atlanta, Georgia. [https://doi.org/10.1201/9781420061888\\_ch106](https://doi.org/10.1201/9781420061888_ch106).
- . 2022. "Substance Priority List." Substance Priority List. 2022.  
<https://www.atsdr.cdc.gov/spl/index.html#2022spl>.
- Awual, Md Rabiul, Tsuyoshi Yaita, Shinichi Suzuki, and Hideaki Shiwaku. 2015. "Ultimate Selenium(IV) Monitoring and Removal from Water Using a New Class of Organic Ligand Based Composite Adsorbent." *Journal of Hazardous Materials* 291 (June): 111–19.

<https://doi.org/10.1016/j.jhazmat.2015.02.066>.

B'Hymer, C., and J. A. Caruso. 2004. "Arsenic and Its Speciation Analysis Using High-Performance Liquid Chromatography and Inductively Coupled Plasma Mass Spectrometry." *Journal of Chromatography A* 1045 (1–2): 1–13.

<https://doi.org/10.1016/J.CHROMA.2004.06.016>.

Baer, Ines, Malcolm Baxter, Vicenta Devesa, Dinoraz Vélez, Georg Raber, Roser Rubio, Toni Llorente-Mirandes, Jens J Sloth, Piotr Robouch, and Beatriz de la Calle. 2011.

"Performance of Laboratories in Speciation Analysis in Seafood – Case of Methylmercury and Inorganic Arsenic." *Food Control* 22 (12): 1928–34.

<https://doi.org/https://doi.org/10.1016/j.foodcont.2011.05.005>.

Barakat, M.A. 2011. "New Trends in Removing Heavy Metals from Industrial Wastewater."

*Arabian Journal of Chemistry* 4 (4): 361–77. <https://doi.org/10.1016/j.arabjc.2010.07.019>.

Barsbay, Murat, Pınar Akkaş Kavaklı, Serhad Tilki, Cengiz Kavaklı, and Olgun Güven. 2018.

"Porous Cellulosic Adsorbent for the Removal of Cd (II), Pb(II) and Cu(II) Ions from Aqueous Media." *Radiation Physics and Chemistry* 142: 70–76.

<https://doi.org/https://doi.org/10.1016/j.radphyschem.2017.03.037>.

Başaran Kankılıç, Gökben, and Ayşegül Ülkü Metin. 2020. "Phragmites Australis as a New Cellulose Source: Extraction, Characterization and Adsorption of Methylene Blue." *Journal of Molecular Liquids* 312: 113313.

<https://doi.org/https://doi.org/10.1016/j.molliq.2020.113313>.

Bellinger, David C. 2005. "Teratogen Update: Lead and Pregnancy." *Birth Defects Research Part A: Clinical and Molecular Teratology* 73 (6): 409–20.

<https://doi.org/10.1002/BDRA.20127>.

- Brewer, Aaron, Elliot Chang, Dan M. Park, Tianyi Kou, Yat Li, Laura N. Lammers, and Yongqin Jiao. 2019. "Recovery of Rare Earth Elements from Geothermal Fluids through Bacterial Cell Surface Adsorption." *Environmental Science & Technology* 53 (13): 7714–23. <https://doi.org/10.1021/acs.est.9b00301>.
- Brewer, Aaron, Justyna Florek, and Freddy Kleitz. 2022. "A Perspective on Developing Solid-Phase Extraction Technologies for Industrial-Scale Critical Materials Recovery." *Green Chemistry* 24 (7): 2752–65. <https://doi.org/10.1039/D2GC00347C>.
- Bundschuh, Jochen, Maria Aurora Armienta, Nury Morales-Simfors, Mohammad Ayaz Alam, Dina L. López, Valeria Delgado Quezada, Sebastian Dietrich, et al. 2021. "Arsenic in Latin America: New Findings on Source, Mobilization and Mobility in Human Environments in 20 Countries Based on Decadal Research 2010-2020." *Critical Reviews in Environmental Science and Technology* 51 (16): 1727–1865. <https://doi.org/10.1080/10643389.2020.1770527>.
- Cabral, Milton de Vasconcelos Neto, Thales Brendon Castano Silva, Vânia Eloísa de Araújo, and Scheilla Vitorino Carvalho de Souza. 2019. "Lead Contamination in Food Consumed and Produced in Brazil: Systematic Review and Meta-Analysis." *Food Research International* 126 (December): 108671. <https://doi.org/10.1016/j.foodres.2019.108671>.
- Cao, Jie, Dongtao Fei, Xiaoling Tian, Yuejun Zhu, Shanshan Wang, Yadong Zhang, Qiangqiang Mao, and Mingbo Sun. 2017. "Novel Modified Microcrystalline Cellulose-Based Porous Material for Fast and Effective Heavy-Metal Removal from Aqueous Solution." *Cellulose* 24 (12): 5565–77. <https://doi.org/10.1007/S10570-017-1504-6/FIGURES/11>.
- Carioni, V. M.O., J. A. McElroy, J. M. Guthrie, R. A. Ngwenyama, and J. D. Brockman. 2017. "Fast and Reliable Method for As Speciation in Urine Samples Containing Low Levels of As by LC-ICP-MS: Focus on Epidemiological Studies." *Talanta* 165 (April): 76–83.

<https://doi.org/10.1016/J.TALANTA.2016.12.036>.

- Carvalho, Fernando Martins, Alessandra Santana Aguiar, Luciana Araújo Vieira, Henrique Ribeiro Gonçalves, and Angela Cristina Andrade Costa Costa. 2000. "Anemia, Deficiência de Ferro e Intoxicação Pelo Chumbo Em Crianças de Uma Creche de Salvador, Bahia." *Rev. Baiana Saúde Pública*, 32–41.
- Chakrabarti, Dipankar, Sushant K. Singh, Md Harunur Rashid, and Mohammad Mahmudur Rahman. 2019. "Arsenic: Occurrence in Groundwater." *Encyclopedia of Environmental Health*, January, 153–68. <https://doi.org/10.1016/B978-0-12-409548-9.10634-7>.
- Choi, Hyeong Yeol, Jong Hyuk Bae, Yohei Hasegawa, Sol An, Ick Soo Kim, Hoik Lee, and Myungwoong Kim. 2020. "Thiol-Functionalized Cellulose Nanofiber Membranes for the Effective Adsorption of Heavy Metal Ions in Water." *Carbohydrate Polymers* 234: 115881. <https://doi.org/https://doi.org/10.1016/j.carbpol.2020.115881>.
- Chu, K. H. 2004. "Improved Fixed Bed Models for Metal Biosorption." *Chemical Engineering Journal* 97 (2–3): 233–39. [https://doi.org/10.1016/S1385-8947\(03\)00214-6](https://doi.org/10.1016/S1385-8947(03)00214-6).
- Chu, Khim Hoong. 2020. "Breakthrough Curve Analysis by Simplistic Models of Fixed Bed Adsorption: In Defense of the Century-Old Bohart-Adams Model." *Chemical Engineering Journal* 380 (January): 122513. <https://doi.org/10.1016/j.cej.2019.122513>.
- Cruz-Olivares, J., C. Pérez-Alonso, C. Barrera-Díaz, G. López, and P. Balderas-Hernández. 2010. "Inside the Removal of Lead(II) from Aqueous Solutions by De-Oiled Allspice Husk in Batch and Continuous Processes." *Journal of Hazardous Materials* 181 (1–3): 1095–1101. <https://doi.org/10.1016/j.jhazmat.2010.05.127>.
- Deng, Sheng, Guangshan Zhang, Shuwei Chen, Yanei Xue, Zhaolin Du, and Peng Wang. 2016. "Rapid and Effective Preparation of a HPEI Modified Biosorbent Based on Cellulose Fiber



- with a Microwave Irradiation Method for Enhanced Arsenic Removal in Water.” *Journal of Materials Chemistry A* 4 (41): 15851–60. <https://doi.org/10.1039/C6TA06051J>.
- Dias, Fabio de S., Lucília A. Meira, Candice N. Carneiro, Lucas F.M. dos Santos, Leonardo B. Guimarães, Nívia M.M. Coelho, Luciana M. Coelho, and Vanessa N. Alves. 2023. “Lignocellulosic Materials as Adsorbents in Solid Phase Extraction for Trace Elements Preconcentration.” *TrAC Trends in Analytical Chemistry* 158 (January): 116891. <https://doi.org/10.1016/J.TRAC.2022.116891>.
- Du, Kai-Feng, Min Yan, Quan-Yi Wang, and Hang Song. 2010. “Preparation and Characterization of Novel Macroporous Cellulose Beads Regenerated from Ionic Liquid for Fast Chromatography.” *Journal of Chromatography A* 1217 (8): 1298–1304. <https://doi.org/https://doi.org/10.1016/j.chroma.2009.12.037>.
- Fakhre, Nabil A, and Bnar M Ibrahim. 2018. “The Use of New Chemically Modified Cellulose for Heavy Metal Ion Adsorption.” *Journal of Hazardous Materials* 343: 324–31. <https://doi.org/https://doi.org/10.1016/j.jhazmat.2017.08.043>.
- Ferreira, Sergio L.C., Joao B.Pereira Junior, Lucas C. Almeida, Luana B. Santos, Valfredo A. Lemos, Cleber G. Novaes, Olivia M.C. de Oliveira, and Antonio F.S. Queiroz. 2020. *Strategies for Inorganic Speciation Analysis Employing Spectrometric Techniques–Review. Microchemical Journal*. Vol. 153.
- Ferron, Mariana Maleronka, André Klafke de Lima, Paulo Hilário Nascimento Saldiva, and Nelson Gouveia. 2012. “Environmental Lead Poisoning among Children in Porto Alegre State, Southern Brazil.” *Revista de Saúde Pública* 46 (2): 226–33. <https://doi.org/10.1590/S0034-89102012000200004>.
- Foo, K. Y., and B. H. Hameed. 2010. “Insights into the Modeling of Adsorption Isotherm Systems.” *Chemical Engineering Journal* 156 (1): 2–10.

<https://doi.org/https://doi.org/10.1016/j.cej.2009.09.013>.

French, Alfred D. 2017. "Glucose, Not Cellobiose, Is the Repeating Unit of Cellulose and Why That Is Important." *Cellulose* 24 (11): 4605–9. <https://doi.org/10.1007/s10570-017-1450-3>.

Fu, Binbin, and Fencun Xie. 2020. "Facile in Situ Synthesis of Cellulose Microcrystalline-Manganese Dioxide Nanocomposite for Effective Removal of Pb(II) and Cd(II) from Water." *Environmental Science and Pollution Research* 27 (5): 5108–21.

<https://doi.org/10.1007/s11356-019-07159-7>.

Gall, Jillian E., Robert S. Boyd, and Nishanta Rajakaruna. 2015. "Transfer of Heavy Metals through Terrestrial Food Webs: A Review." *Environmental Monitoring and Assessment* 187 (4): 1–21. <https://doi.org/10.1007/s10661-015-4436-3>.

Garba, Zaharaddeen N., Ibrahim Lawan, Weiming Zhou, Mingxi Zhang, Liwei Wang, and Zhanhui Yuan. 2020. "Microcrystalline Cellulose (MCC) Based Materials as Emerging Adsorbents for the Removal of Dyes and Heavy Metals – A Review." *Science of the Total Environment* 717 (May): 135070. <https://doi.org/10.1016/j.scitotenv.2019.135070>.

Gericke, Martin, Jani Trygg, and Pedro Fardim. 2013. "Functional Cellulose Beads: Preparation, Characterization, and Applications." *Chemical Reviews* 113 (7): 4812–36. <https://doi.org/10.1021/cr300242j>.

Gert, E. V., V. I. Torgashov, O. V. Zubets, and F. N. Kaputskii. 2006. "Combination of Oxidative and Hydrolytic Functions of Nitric Acid in Production of Enterosorbents Based on Carboxylated Microcrystalline Cellulose." *Russian Journal of Applied Chemistry* 79 (11): 1896–1901. <https://doi.org/10.1134/S1070427206110309>.

Grandjean, Philippe, and Philip J. Landrigan. 2014. "Neurobehavioural Effects of Developmental Toxicity." *The Lancet Neurology* 13 (3): 330–38. <https://doi.org/10.1016/S1474->

4422(13)70278-3/ATTACHMENT/57D395F7-EE37-492C-926A-343A58D302C6/MMC1.PDF.

Güell, Raquel, Enriqueta Anticó, Spas D. Kolev, Juana Benavente, Victòria Salvadó, and Clàudia Fontàs. 2011. "Development and Characterization of Polymer Inclusion Membranes for the Separation and Speciation of Inorganic As Species." *Journal of Membrane Science* 383 (1–2): 88–95. <https://doi.org/10.1016/J.MEMSCI.2011.08.037>.

Guisela B, Zambrano, De Almeida Ohana N, Duarte Dalvani S, Velasco Fermin G, Luzardo Francisco HM, and Nieto-González González Luis. 2022. "Adsorption of Arsenic Anions in Water Using Modified Lignocellulosic Adsorbents." *Results in Engineering* 13 (March): 100340. <https://doi.org/https://doi.org/10.1016/j.rineng.2022.100340>.

Gupta, Archana, Vishal Sharma, Kashma Sharma, Vijay Kumar, Sonal Choudhary, Priyanka Mankotia, Brajesh Kumar, et al. 2021. "A Review of Adsorbents for Heavy Metal Decontamination: Growing Approach to Wastewater Treatment." *Materials* 14 (16). <https://doi.org/10.3390/MA14164702>.

Han, Yangyang, Xinxing Zhang, Xiaodong Wu, and Canhui Lu. 2015. "Flame Retardant, Heat Insulating Cellulose Aerogels from Waste Cotton Fabrics by in Situ Formation of Magnesium Hydroxide Nanoparticles in Cellulose Gel Nanostructures." *ACS Sustainable Chemistry & Engineering* 3 (8): 1853–59. <https://doi.org/10.1021/acssuschemeng.5b00438>.

Hokkanen, Sanna, Amit Bhatnagar, and Mika Sillanpää. 2016. "A Review on Modification Methods to Cellulose-Based Adsorbents to Improve Adsorption Capacity." *Water Research* 91 (March): 156–73. <https://doi.org/https://doi.org/10.1016/j.watres.2016.01.008>.

Hokkanen, Sanna, Eveliina Repo, Song Lou, and Mika Sillanpää. 2015. "Removal of Arsenic(V) by Magnetic Nanoparticle Activated Microfibrillated Cellulose." *Chemical Engineering Journal* 260 (January): 886–94. <https://doi.org/10.1016/j.cej.2014.08.093>.

- Hu, Zhao-Hong, Ahmed Mohamed Omer, Xiao-kun Ouyang, and Di Yu. 2018. "Fabrication of Carboxylated Cellulose Nanocrystal/Sodium Alginate Hydrogel Beads for Adsorption of Pb(II) from Aqueous Solution." *International Journal of Biological Macromolecules* 108 (March): 149–57. <https://doi.org/10.1016/j.ijbiomac.2017.11.171>.
- Huang, Zhujian, Zhiyan Huang, Lijing Feng, Xuewen Luo, Pingxiao Wu, Lihua Cui, and Xiaoyun Mao. 2018. "Modified Cellulose by Polyethyleneimine and Ethylenediamine with Induced Cu(II) and Pb(II) Adsorption Potentialities." *Carbohydrate Polymers* 202 (December): 470–78. <https://doi.org/10.1016/j.carbpol.2018.08.136>.
- Hughes, Michael F. 2002. "Arsenic Toxicity and Potential Mechanisms of Action." *Toxicology Letters* 133 (1): 1–16. [https://doi.org/10.1016/S0378-4274\(02\)00084-X](https://doi.org/10.1016/S0378-4274(02)00084-X).
- IARC. 2023. "IARC Monographs on the Identification of Carcinogenic Hazards to Humans. World Health Organization." 1–133. <https://monographs.iarc.who.int/list-of-classifications/>.
- Kenawy, I M, M A H Hafez, M A Ismail, and M A Hashem. 2018. "Adsorption of Cu(II), Cd(II), Hg(II), Pb(II) and Zn(II) from Aqueous Single Metal Solutions by Guanyl-Modified Cellulose." *International Journal of Biological Macromolecules* 107: 1538–49. <https://doi.org/https://doi.org/10.1016/j.ijbiomac.2017.10.017>.
- Korak, Julie A., Annabel L. Mungan, and Landon T. Watts. 2023. "Critical Review of Waste Brine Management Strategies for Drinking Water Treatment Using Strong Base Ion Exchange." *Journal of Hazardous Materials* 441 (January): 129473. <https://doi.org/10.1016/J.JHAZMAT.2022.129473>.
- Kumar, Amit, Amit Kumar, M. Cabral-Pinto, Ashish K. Chaturvedi, Aftab A. Shabnam, Gangavarapu Subrahmanyam, Raju Mondal, et al. 2020. "Lead Toxicity: Health Hazards, Influence on Food Chain, and Sustainable Remediation Approaches." *International Journal of Environmental Research and Public Health* 17 (7): 2179.

<https://doi.org/10.3390/IJERPH17072179>.

Kumar, Rajesh, and Rajeev Kr Sharma. 2019. "Synthesis and Characterization of Cellulose Based Adsorbents for Removal of Ni(II), Cu(II) and Pb(II) Ions from Aqueous Solutions." *Reactive and Functional Polymers* 140: 82–92.

<https://doi.org/https://doi.org/10.1016/j.reactfunctpolym.2019.04.014>.

Lee, Ju-Wook, Hoon Choi, Un-Ki Hwang, Ju-Chan Kang, Yue Jai Kang, Kwang Il Kim, and Jun-Hwan Kim. 2019. "Toxic Effects of Lead Exposure on Bioaccumulation, Oxidative Stress, Neurotoxicity, and Immune Responses in Fish: A Review." *Environmental Toxicology and Pharmacology* 68 (May): 101–8. <https://doi.org/10.1016/j.etap.2019.03.010>.

Levin, Ronnie, Mary Jean Brown, Michael E. Kashtock, David E. Jacobs, Elizabeth A. Whelan, Joanne Rodman, Michael R. Schock, Alma Padilla, and Thomas Sinks. 2008. "Lead Exposures in U.S. Children, 2008: Implications for Prevention." *Environmental Health Perspectives* 116 (10): 1285–93. <https://doi.org/10.1289/EHP.11241>.

Li, Jiaying, Shuyu Chen, Guodong Sheng, Jun Hu, Xiaoli Tan, and Xiangke Wang. 2011. "Effect of Surfactants on Pb(II) Adsorption from Aqueous Solutions Using Oxidized Multiwall Carbon Nanotubes." *Chemical Engineering Journal* 166 (2): 551–58. <https://doi.org/10.1016/J.CEJ.2010.11.018>.

Li, Jingxi, Chengjun Sun, Li Zheng, Fenghua Jiang, Shuai Wang, Zhixia Zhuang, and Xiaoru Wang. 2017. "Determination of Trace Metals and Analysis of Arsenic Species in Tropical Marine Fishes from Spratly Islands." *Marine Pollution Bulletin* 122 (1): 464–69. <https://doi.org/https://doi.org/10.1016/j.marpolbul.2017.06.017>.

Li, Peng, Xiao-qin Zhang, Yi-jun Chen, Hong-zhen Lian, and Xin Hu. 2014. "A Sequential Solid Phase Microextraction System Coupled with Inductively Coupled Plasma Mass Spectrometry for Speciation of Inorganic Arsenic." *Analytical Methods* 6 (12): 4205–11.

<https://doi.org/10.1039/C4AY00438H>.

Li, Yingzhan, Nathan Grishkewich, Lingli Liu, Chang Wang, Kam C Tam, Shanqiu Liu, Zhiping Mao, and Xiaofeng Sui. 2019. "Construction of Functional Cellulose Aerogels via Atmospheric Drying Chemically Cross-Linked and Solvent Exchanged Cellulose Nanofibrils." *Chemical Engineering Journal* 366: 531–38.

<https://doi.org/https://doi.org/10.1016/j.cej.2019.02.111>.

Li, Yingzhan, Lei Xu, Bo Xu, Zhiping Mao, Hong Xu, Yi Zhong, Linping Zhang, Bijia Wang, and Xiaofeng Sui. 2017. "Cellulose Sponge Supported Palladium Nanoparticles as Recyclable Cross-Coupling Catalysts." *ACS Applied Materials & Interfaces* 9 (20): 17155–62.

<https://doi.org/10.1021/acsami.7b03600>.

Li, Yingzhan, Liqian Zhu, Bijia Wang, Zhiping Mao, Hong Xu, Yi Zhong, Linping Zhang, and Xiaofeng Sui. 2018. "Fabrication of Thermoresponsive Polymer-Functionalized Cellulose Sponges: Flexible Porous Materials for Stimuli-Responsive Catalytic Systems." *ACS Applied Materials & Interfaces* 10 (33): 27831–39. <https://doi.org/10.1021/acsami.8b12060>.

Li, Yuqi, Canfeng Guo, Ronghui Shi, Hui Zhang, Lingzhu Gong, and Libo Dai. 2019. "Chitosan/Nanofibrillated Cellulose Aerogel with Highly Oriented Microchannel Structure for Rapid Removal of Pb (II) Ions from Aqueous Solution." *Carbohydrate Polymers* 223 (November): 115048. <https://doi.org/10.1016/j.carbpol.2019.115048>.

Liu, Yan. 2021. *Eluent Regeneration and Ion Reflux Devices and Their Applications in Ion Chromatography. Separation Science and Technology (New York)*. Vol. 13. Academic Press. <https://doi.org/10.1016/B978-0-12-813075-9.00010-8>.

Llompart, Maria, Maria Celeiro, Carmen García-Jares, and Thierry Dagnac. 2019. "Environmental Applications of Solid-Phase Microextraction." *TrAC Trends in Analytical Chemistry* 112 (March): 1–12. <https://doi.org/10.1016/j.trac.2018.12.020>.

- Lu, Peng, and Chen Zhu. 2011. "Arsenic Eh-PH Diagrams at 25°C and 1 Bar." *Environmental Earth Sciences* 62 (8): 1673–83. <https://doi.org/10.1007/S12665-010-0652-X/FIGURES/5>.
- Luo, Xiaogang, Xiaojuan Lei, Xiuping Xie, Bo Yu, Ning Cai, and Faquan Yu. 2016. "Adsorptive Removal of Lead from Water by the Effective and Reusable Magnetic Cellulose Nanocomposite Beads Entrapping Activated Bentonite." *Carbohydrate Polymers* 151 (October): 640–48. <https://doi.org/https://doi.org/10.1016/j.carbpol.2016.06.003>.
- Machate, David Johane. 2023. "Anthropogenic Hyperactivity for Natural Resources Increases Heavy Metals Concentrations in the Environment: Toxicity of Healthy Food and Cancer Risks Estimated." *Journal of Trace Elements and Minerals* 4 (June): 100057. <https://doi.org/10.1016/j.jtemin.2023.100057>.
- Maia, Luisa Cardoso, Liliane Catone Soares, and Leandro Vinícius Alves Gurgel. 2021. "A Review on the Use of Lignocellulosic Materials for Arsenic Adsorption." *Journal of Environmental Management* 288 (June): 112397. <https://doi.org/10.1016/j.jenvman.2021.112397>.
- Malik, D. S., C. K. Jain, and Anuj K. Yadav. 2017. "Removal of Heavy Metals from Emerging Cellulosic Low-Cost Adsorbents: A Review." *Applied Water Science*. Springer. <https://doi.org/10.1007/s13201-016-0401-8>.
- Matos, Wladiana O., Francisco L.F. da Silva, Savarin Sinaviwat, Emma J. Menzies, Andrea Raab, Eva M. Krupp, and Joerg Feldmann. 2022. "Wild Shrimp Have an Order of Magnitude Higher Arsenic Concentrations than Farmed Shrimp from Brazil Illustrating the Need for a Regulation Based on Inorganic Arsenic." *Journal of Trace Elements in Medicine and Biology* 71 (May): 126968. <https://doi.org/10.1016/j.jtemb.2022.126968>.
- Mc Naught, a. D., and A Wilkinson. 2019. *The IUPAC Compendium of Chemical Terminology*. *The IUPAC Compendium of Chemical Terminology*. International Union of Pure and

- Applied Chemistry (IUPAC). <https://doi.org/10.1351/goldbook>.
- Minami F., Alexandre. 2017. "Evaluation of As, Cd, Cr and Pb Mobility and Bioaccessibility in Mineral Fertilizers."
- Mischnick, Petra, and Dane Momcilovic. 2010. "Chemical Structure Analysis of Starch and Cellulose Derivatives." *Advances in Carbohydrate Chemistry and Biochemistry* 64 (C): 117–210. [https://doi.org/10.1016/S0065-2318\(10\)64004-8](https://doi.org/10.1016/S0065-2318(10)64004-8).
- Mohammadabadi, Siroos Iravani, and Vahid Javanbakht. 2020. "Development of Hybrid Gel Beads of Lignocellulosic Compounds Derived from Agricultural Waste: Efficient Lead Adsorbents for a Comparative Biosorption." *Journal of Molecular Liquids* 315 (October): 113715. <https://doi.org/https://doi.org/10.1016/j.molliq.2020.113715>.
- Momzyakova, K. S., Z. T. Valishina, T. R. Deberdeev, A. A. Aleksandrov, A. A. Berlin, and R. Ya Deberdeev. 2021. "Structural Analysis of Powder Celluloses by FTIR Spectroscopy." *Polymer Science - Series D* 14 (2): 288–92. <https://doi.org/10.1134/S1995421221020222/TABLES/2>.
- Montoro Leal, P., E. Vereda Alonso, M. M. López Guerrero, M. T. Siles Siles Cordero, J. M. Cano Pavón, and A. García de Torres. 2018. "Speciation Analysis of Inorganic Arsenic by Magnetic Solid Phase Extraction On-Line with Inductively Coupled Mass Spectrometry Determination." *Talanta* 184 (July): 251–59. <https://doi.org/https://doi.org/10.1016/j.talanta.2018.03.019>.
- Morales-Simfors, Nury, and Jochen Bundschuh. 2022. "Arsenic-Rich Geothermal Fluids as Environmentally Hazardous Materials – A Global Assessment." *Science of The Total Environment* 817: 152669. <https://doi.org/https://doi.org/10.1016/j.scitotenv.2021.152669>.
- Mota Santos, Leandro. 2021. "Avaliação de Elementos Terras Raras Em Ecossistema Aquático



- Da Represa de Guarapiranga, São Paulo,” April. <https://doi.org/10.11606/T.46.2021.TDE-11112021-114451>.
- Nag, Soma, and Swarup Biswas. 2021. “Cellulose-Based Adsorbents for Heavy Metal Removal,” 113–42. [https://doi.org/10.1007/978-3-030-47400-3\\_5](https://doi.org/10.1007/978-3-030-47400-3_5).
- Najib, Nadira, and Christos Christodoulatos. 2019. “Removal of Arsenic Using Functionalized Cellulose Nanofibrils from Aqueous Solutions.” *Journal of Hazardous Materials* 367: 256–66. <https://doi.org/https://doi.org/10.1016/j.jhazmat.2018.12.067>.
- Nie, Guangjun, Yipeng Zang, Wenjin Yue, Mengmeng Wang, Aravind Baride, Aliza Sigdel, and Srinivas Janaswamy. 2021. “Cellulose-Based Hydrogel Beads: Preparation and Characterization.” *Carbohydrate Polymer Technologies and Applications* 2 (December): 100074. <https://doi.org/10.1016/j.carpta.2021.100074>.
- O’Connell, David W, Colin Birkinshaw, and Thomas F O’Dwyer. 2006. “Removal of Lead(II) Ions from Aqueous Solutions Using a Modified Cellulose Adsorbent.” *Adsorption Science & Technology* 24 (4): 337–48. <https://doi.org/10.1260/026361706779319670>.
- Ogeda, Thais Lucy. 2011. “Enzymatic Hydrolysis of Pretreated Cellulose.” University of São Paulo.
- Oliveira, Rita de Cássia, Márcia Aparecida Ribeiro de Carvalho, Helena Ramirez Domingos Mainenti, Ely Caetano Xavier Junior, Paula de Novaes Sacinelli, Leandro Barreto Vargas dde Carvalho, Renato Marçullo Borges, et al. 2009. “Avaliação Dos Fatores de Risco Relacionados à Exposição Ao Chumbo Em Crianças e Adolescentes Do Rio de Janeiro.” *Ciência & Saúde Coletiva* 14 (6): 2039–48. <https://doi.org/10.1590/S1413-81232009000600011>.
- Olympio, Kelly P.K., Pedro V. Oliveira, Juliana Naozuka, Maria R.A. Cardoso, Antonio F.

- Marques, Wanda M.R. Günther, and Etelvino J.H. Bechara. 2010. "Surface Dental Enamel Lead Levels and Antisocial Behavior in Brazilian Adolescents." *Neurotoxicology and Teratology* 32 (2): 273–79. <https://doi.org/10.1016/J.NTT.2009.12.003>.
- Oyewo, Opeyemi A., Bongani Mutesse, Taile Y. Leswifi, and Maurice S. Onyango. 2019. "Highly Efficient Removal of Nickel and Cadmium from Water Using Sawdust-Derived Cellulose Nanocrystals." *Journal of Environmental Chemical Engineering* 7 (4). <https://doi.org/10.1016/J.JECE.2019.103251>.
- Ozdemir, Sadin, Ersin Kılınc, Ömer Acer, and Mustafa Soylak. 2021. "Simultaneous Preconcentrations of Cu(II), Ni(II), and Pb(II) by SPE Using E. Profundum Loaded onto Amberlite XAD-4." *Microchemical Journal* 171 (December): 106758. <https://doi.org/10.1016/J.MICROC.2021.106758>.
- Pandey, Lalit M. 2021. "Surface Engineering of Nano-Sorbents for the Removal of Heavy Metals: Interfacial Aspects." *Journal of Environmental Chemical Engineering* 9 (1): 104586. <https://doi.org/10.1016/j.jece.2020.104586>.
- Pei, Xiaopeng, Lan Gan, Zhaohui Tong, Haiping Gao, Shanyu Meng, Wenlong Zhang, Pixin Wang, and Yongsheng Chen. 2021. "Robust Cellulose-Based Composite Adsorption Membrane for Heavy Metal Removal." *Journal of Hazardous Materials* 406: 124746. <https://doi.org/https://doi.org/10.1016/j.jhazmat.2020.124746>.
- Pereira, Amanda Raimundi, Liliane Catone Soares, Filipe Simões Teodoro, Megg Madonyk Cota Elias, Gabriel Max Dias Ferreira, Ranylson Marcello Leal Savedra, Melissa Fabíola Siqueira, et al. 2020. "Aminated Cellulose as a Versatile Adsorbent for Batch Removal of As(V) and Cu(II) from Mono- and Multicomponent Aqueous Solutions." *Journal of Colloid and Interface Science* 576 (September): 158–75. <https://doi.org/10.1016/J.JCIS.2020.04.129>.

- Perendija, Jovana, Zlate S Veličković, Ilija Cvijetić, Steva Lević, Aleksandar D Marinković, Milena Milošević, and Antonije Onjia. 2021. "Bio-Membrane Based on Modified Cellulose, Lignin, and Tannic Acid for Cation and Oxyanion Removal: Experimental and Theoretical Study." *Process Safety and Environmental Protection* 147: 609–25.  
<https://doi.org/https://doi.org/10.1016/j.psep.2020.12.027>.
- Podgorski, Joel, and Michael Berg. 2020. "Global Threat of Arsenic in Groundwater." *Science* 368 (6493): 845–50. <https://doi.org/10.1126/science.aba1510>.
- Popowich, Aleksandra, Qi Zhang, and X. Chris Le. 2016. "Arsenobetaine: The Ongoing Mystery." *National Science Review* 3 (4): 451–58. <https://doi.org/10.1093/NSR/NWW061>.
- Puziy, A. M., O. I. Poddubnaya, V. N. Zaitsev, and O. P. Konoplitska. 2004. "Modeling of Heavy Metal Ion Binding by Phosphoric Acid Activated Carbon." *Applied Surface Science* 221 (1–4): 421–29. [https://doi.org/10.1016/S0169-4332\(03\)00956-5](https://doi.org/10.1016/S0169-4332(03)00956-5).
- Qiu, Xiaoyun, and Shuwen Hu. 2013. "'Smart' Materials Based on Cellulose: A Review of the Preparations, Properties, and Applications." *Materials* 6 (3): 738–81.  
<http://www.mdpi.com/1996-1944/6/3/738>.
- Qu, Jianhua, Xue Tian, Zhao Jiang, Bo Cao, Modupe Sarah Akindolie, Qi Hu, Chengcheng Feng, Yan Feng, Xianlin Meng, and Ying Zhang. 2020. "Multi-Component Adsorption of Pb(II), Cd(II) and Ni(II) onto Microwave-Functionalized Cellulose: Kinetics, Isotherms, Thermodynamics, Mechanisms and Application for Electroplating Wastewater Purification." *Journal of Hazardous Materials* 387: 121718.  
<https://doi.org/https://doi.org/10.1016/j.jhazmat.2019.121718>.
- Qu, Jianhua, Yihang Yuan, Qingjuan Meng, Guangshan Zhang, Fengxia Deng, Lei Wang, Yue Tao, Zhao Jiang, and Ying Zhang. 2020. "Simultaneously Enhanced Removal and Stepwise Recovery of Atrazine and Pb(II) from Water Using  $\beta$ -Cyclodextrin Functionalized

Cellulose: Characterization, Adsorptive Performance and Mechanism Exploration.” *Journal of Hazardous Materials* 400: 123142.

<https://doi.org/https://doi.org/10.1016/j.jhazmat.2020.123142>.

Rajakovic, Ljubinka, and Vladana Rajakovic-Ognjanovic. 2018. “Arsenic in Water: Determination and Removal.” In *Arsenic - Analytical and Toxicological Studies*. InTech.

<https://doi.org/10.5772/intechopen.75531>.

Reid, Michael S., Karen S. Hoy, Jordan R.M. M Schofield, Jagdeesh S. Uppal, Yanwen Lin, Xiufen Lu, Hanyong Peng, and X. Chris Le. 2020. “Arsenic Speciation Analysis: A Review with an Emphasis on Chromatographic Separations.” *TrAC Trends in Analytical Chemistry* 123 (February): 115770. <https://doi.org/10.1016/J.TRAC.2019.115770>.

Reid, Monica L, Marc B Brown, Gary P Moss, and Stuart A Jones. 2008. “An Investigation into Solvent-Membrane Interactions When Assessing Drug Release from Organic Vehicles Using Regenerated Cellulose Membranes.” *Journal of Pharmacy and Pharmacology* 60 (9): 1139–47. <https://doi.org/10.1211/jpp.60.9.0004>.

Ren, Yi, Yulong Ma, Guangyu Min, Wenbin Zhang, Lu Lv, and Weiming Zhang. 2021. “A Mini Review of Multifunctional Ultrafiltration Membranes for Wastewater Decontamination: Additional Functions of Adsorption and Catalytic Oxidation.” *Science of The Total Environment* 762 (March): 143083. <https://doi.org/10.1016/J.SCITOTENV.2020.143083>.

“Resolução ANP N° 5 DE 03/02/2009 - Federal - LegisWeb.” 2009. 2009.

<https://www.legisweb.com.br/legislacao/?id=112030>.

Santra, Dhiman, and Mitali Sarkar. 2016. “Optimization of Process Variables and Mechanism of Arsenic (V) Adsorption onto Cellulose Nanocomposite.” *Journal of Molecular Liquids* 224 (December): 290–302. <https://doi.org/10.1016/J.MOLLIQ.2016.09.104>.

- Shaji, E., M. Santosh, K.V. Sarath, Pranav Prakash, V. Deepchand, and B.V. Divya. 2021. "Arsenic Contamination of Groundwater: A Global Synopsis with Focus on the Indian Peninsula." *Geoscience Frontiers* 12 (3): 101079. <https://doi.org/10.1016/j.gsf.2020.08.015>.
- Shakoor, Muhammad Bilal, Nabeel Khan Niazi, Irshad Bibi, Ghulam Murtaza, Anitha Kunhikrishnan, Balaji Seshadri, Muhammad Shahid, et al. 2016. "Remediation of Arsenic-Contaminated Water Using Agricultural Wastes as Biosorbents." *https://doi.org/10.1080/10643389.2015.1109910* 46 (5): 467–99. <https://doi.org/10.1080/10643389.2015.1109910>.
- Shan, Bing, Ruixia Hao, Hui Xu, Jiani Li, Yinhuang Li, Xiyang Xu, and Junman Zhang. 2021. "A Review on Mechanism of Biomineralization Using Microbial-Induced Precipitation for Immobilizing Lead Ions." *Environmental Science and Pollution Research* 2021 28:24 28 (24): 30486–98. <https://doi.org/10.1007/S11356-021-14045-8>.
- Sharma, Priyanka R., Aurnov Chattopadhyay, Chengbo Zhan, Sunil K. Sharma, Lihong Geng, and Benjamin S. Hsiao. 2018. "Lead Removal from Water Using Carboxycellulose Nanofibers Prepared by Nitro-Oxidation Method." *Cellulose* 25 (3): 1961–73. <https://doi.org/10.1007/s10570-018-1659-9>.
- Shehata, Ahmed M., and Hisham A. Nasr-El-Din. 2015. "Zeta Potential Measurements: Impact of Salinity on Sandstone Minerals." *Proceedings - SPE International Symposium on Oilfield Chemistry* 2: 789–805. <https://doi.org/10.2118/173763-MS>.
- Sheng, Ping Xin, Yen Peng Ting, J. Paul Chen, and Liang Hong. 2004. "Sorption of Lead, Copper, Cadmium, Zinc, and Nickel by Marine Algal Biomass: Characterization of Biosorptive Capacity and Investigation of Mechanisms." *Journal of Colloid and Interface Science* 275 (1): 131–41. <https://doi.org/10.1016/J.JCIS.2004.01.036>.
- Shrestha, Rakesh, Sagar Ban, Sijan Devkota, Sudip Sharma, Rajendra Joshi, Arjun Prasad

- Tiwari, Hak Yong Kim, and Mahesh Kumar Joshi. 2021. "Technological Trends in Heavy Metals Removal from Industrial Wastewater: A Review." *Journal of Environmental Chemical Engineering* 9 (4): 105688. <https://doi.org/10.1016/j.jece.2021.105688>.
- Singh, Kiran, T.J.M. Sinha, and Shalini Srivastava. 2015. "Functionalized Nanocrystalline Cellulose: Smart Biosorbent for Decontamination of Arsenic." *International Journal of Mineral Processing* 139 (June): 51–63. <https://doi.org/10.1016/j.minpro.2015.04.014>.
- Siqueira Petri, Denise F, Soowhan Choi, Harald Beyer, Thomas Schimmel, Michael Bruns, and Gerhard Wenz. 1999. "Synthesis of a Cellulose Thiosulfate and Its Immobilization on Gold Surfaces." *Polymer* 40 (6): 1593–1601. [https://doi.org/10.1016/S0032-3861\(98\)00381-4](https://doi.org/10.1016/S0032-3861(98)00381-4).
- Sorlini, Sabrina, and Francesca Gialdini. 2010. "Conventional Oxidation Treatments for the Removal of Arsenic with Chlorine Dioxide, Hypochlorite, Potassium Permanganate and Monochloramine." *Water Research* 44 (19): 5653–59. <https://doi.org/10.1016/j.watres.2010.06.032>.
- Spano, Giuseppina, Vincenzo Giannico, Mario Elia, Andrea Bosco, Raffaele Laforteza, and Giovanni Sanesi. 2020. "Human Health–Environment Interaction Science: An Emerging Research Paradigm." *Science of The Total Environment* 704 (February): 135358. <https://doi.org/10.1016/J.SCITOTENV.2019.135358>.
- Sun, Chang, Jiadong Ni, Chunyan Zhao, Jinmei Du, Change Zhou, Shugen Wang, and Changhai Xu. 2017. "Preparation of a Cellulosic Adsorbent by Functionalization with Pyridone Diacid for Removal of Pb(II) and Co(II) from Aqueous Solutions." *Cellulose* 24 (12): 5615–24. <https://doi.org/10.1007/s10570-017-1519-z>.
- Suopajarvi, Terhi, Henrikki Liimatainen, Mikko Karjalainen, Heikki Upola, and Jouko Niinimäki. 2015. "Lead Adsorption with Sulfonated Wheat Pulp Nanocelluloses." *Journal of Water Process Engineering* 5: 136–42. <https://doi.org/https://doi.org/10.1016/j.jwpe.2014.06.003>.

- Syeda, Hina Iqbal, and Pow-Seng Seng Yap. 2022. "A Review on Three-Dimensional Cellulose-Based Aerogels for the Removal of Heavy Metals from Water." *Science of The Total Environment* 807 (February): 150606.  
<https://linkinghub.elsevier.com/retrieve/pii/S0048969721056849>.
- Tan, K.L., and B.H. Hameed. 2017. "Insight into the Adsorption Kinetics Models for the Removal of Contaminants from Aqueous Solutions." *Journal of the Taiwan Institute of Chemical Engineers* 74 (May): 25–48. <https://doi.org/10.1016/j.jtice.2017.01.024>.
- Tao, Danyang, Changzhi Shi, Wei Guo, Yamin Deng, Yue'e Peng, Yuanyuan Yuhe He, Paul K.S. Lam, Yuanyuan Yuhe He, and Kai Zhang. 2022. "Determination of As Species Distribution and Variation with Time in Extracted Groundwater Samples by On-Site Species Separation Method." *Science of the Total Environment* 808 (February): 151913.  
<https://doi.org/10.1016/j.scitotenv.2021.151913>.
- Tarragó, Oscar, and Mary Jean Brown. 2017. "Agency for Toxic Substances and Disease Registry : Case Studies in Environmental Medicine (CSEM)."  
<http://www.atsdr.cdc.gov/csem/csem.html>.
- Templeton, Douglas M., Freek Ariese, Rita Cornelis, Lars-Göran Göran Danielsson, Herbert Muntau, Herman P. van Leeuwen, Ryszard Lobinski, et al. 2000. *Guidelines for Terms Related to Chemical Speciation and Fractionation of Elements. Definitions, Structural Aspects, and Methodological Approaches (IUPAC Recommendations 2000)*. *Pure and Applied Chemistry*. Vol. 72. Walter de Gruyter GmbH.  
<https://doi.org/10.1351/pac200072081453>.
- Templeton, Douglas M., and Hitomi Fujishiro. 2017. "Terminology of Elemental Speciation – An IUPAC Perspective." *Coordination Chemistry Reviews* 352 (December): 424–31.  
<https://doi.org/10.1016/J.CCR.2017.02.002>.

- Tran, Hai Nguyen, Sheng-Jie You, Ahmad Hosseini-Bandegharaei, and Huan-Ping Chao. 2017. "Mistakes and Inconsistencies Regarding Adsorption of Contaminants from Aqueous Solutions: A Critical Review." *Water Research* 120: 88–116.  
<https://doi.org/https://doi.org/10.1016/j.watres.2017.04.014>.
- Vadakkekara, Georgi J, Sabu Thomas, and C P R Nair. 2019. "Maleic Acid Modified Cellulose for Scavenging Lead from Water." *International Journal of Biological Macromolecules* 129: 293–304. <https://doi.org/https://doi.org/10.1016/j.ijbiomac.2019.02.037>.
- Viana, José Lucas Martins, Adriana Felix de Souza, Amauris Hechavarría Hernández, Lucas Pellegrini Elias, Carlos Eduardo Eismann, Ary Tavares Rezende-Filho, Laurent Barbiero, Amauri Antonio Menegario, and Anne Hélène Fostier. 2022. "In Situ Arsenic Speciation at the Soil/Water Interface of Saline-Alkaline Lakes of the Pantanal, Brazil: A DGT-Based Approach." *Science of The Total Environment* 804: 150113.  
<https://doi.org/https://doi.org/10.1016/j.scitotenv.2021.150113>.
- Vijayalakshmi, K., B. Mahalakshmi Devi, Srinivasan Latha, Thandapani Gomathi, P. N. Sudha, Jayachandran Venkatesan, and Sukumaran Anil. 2017. "Batch Adsorption and Desorption Studies on the Removal of Lead (II) from Aqueous Solution Using Nanochitosan/Sodium Alginate/Microcrystalline Cellulose Beads." *International Journal of Biological Macromolecules* 104 (November): 1483–94.  
<https://doi.org/https://doi.org/10.1016/j.ijbiomac.2017.04.120>.
- Virk, Rajbinder K., Roobee Garla, Naveen Kaushal, Mohinder P. Bansal, Mohan L. Garg, and Biraja P. Mohanty. 2023. "The Relevance of Arsenic Speciation Analysis in Health & Medicine." *Chemosphere* 316 (March): 137735.  
<https://doi.org/10.1016/J.CHEMOSPHERE.2023.137735>.
- Wang, Fudong, Jin Li, Yuan Su, Qian Li, Baoyu Gao, Qinyan Yue, and Weizhi Zhou. 2019.



“Adsorption and Recycling of Cd(II) from Wastewater Using Straw Cellulose Hydrogel Beads.” *Journal of Industrial and Engineering Chemistry* 80: 361–69.

<https://doi.org/https://doi.org/10.1016/j.jiec.2019.08.015>.

Wang, Futao, Yuanfeng Pan, Pingxiong Cai, Tianxiang Guo, and Huining Xiao. 2017. “Single and Binary Adsorption of Heavy Metal Ions from Aqueous Solutions Using Sugarcane Cellulose-Based Adsorbent.” *Bioresource Technology* 241 (October): 482–90.

<https://doi.org/10.1016/j.biortech.2017.05.162>.

Wang, Min, Lin Yue, Sobia Niazi, Imran Mahmood Khan, Yin Zhang, and Zhouping Wang. 2022. “Synthesis and Characterization of Cinnamic Acid Conjugated N-(2-Hydroxy)-Propyl-3-Trimethylammonium Chitosan Chloride Derivatives: A Hybrid Flocculant with Antibacterial Activity.” *International Journal of Biological Macromolecules* 206 (May): 886–95.

<https://doi.org/10.1016/J.IJBIOMAC.2022.03.075>.

Wang, Nan, Ru-Na Jin, A M Omer, and Xiao-kun Ouyang. 2017. “Adsorption of Pb(II) from Fish Sauce Using Carboxylated Cellulose Nanocrystal: Isotherm, Kinetics, and Thermodynamic Studies.” *International Journal of Biological Macromolecules* 102: 232–40.

<https://doi.org/https://doi.org/10.1016/j.ijbiomac.2017.03.150>.

WHO. 2017. “Guidelines for Drinking-Water Quality: Fourth Edition Incorporating the First Addendum.” *World Health Organization*. World Health Organization.

<https://www.ncbi.nlm.nih.gov/books/NBK442376/>.

———. 2022. “Lead Poisoning.” 2022. <https://www.who.int/news-room/fact-sheets/detail/lead-poisoning-and-health>.

Wu, Hsien Ming, Dan Tzu Lin-Tan, Mei Li Wang, Hong Yuan Huang, Chyi Long Lee, Hsin Shih Wang, Yung Kuei Soong, and Ja Liang Lin. 2012. “Lead Level in Seminal Plasma May Affect Semen Quality for Men without Occupational Exposure to Lead.” *Reproductive*

*Biology and Endocrinology : RB&E* 10 (1): 1–5. <https://doi.org/10.1186/1477-7827-10-91/FIGURES/1>.

Wu, Qi, Hui He, Hang Zhou, Fei Xue, Hongxiang Zhu, Shile Zhou, Lei Wang, and Shuangfei Wang. 2020. "Multiple Active Sites Cellulose-Based Adsorbent for the Removal of Low-Level Cu(II), Pb(II) and Cr(VI) via Multiple Cooperative Mechanisms." *Carbohydrate Polymers* 233: 115860. <https://doi.org/https://doi.org/10.1016/j.carbpol.2020.115860>.

Wu, R P. 2019. "Removal of Heavy Metal Ions from Industrial Wastewater Based on Chemical Precipitation Method." *EKOLOJI* 28 (107): 2443–52.

Xu, Xinyi, Xiao-kun kun Ouyang, and Li-Ye Ye Yang. 2021. "Adsorption of Pb(II) from Aqueous Solutions Using Crosslinked Carboxylated Chitosan/Carboxylated Nanocellulose Hydrogel Beads." *Journal of Molecular Liquids* 322 (January): 114523. <https://doi.org/https://doi.org/10.1016/j.molliq.2020.114523>.

Yang, Wenchao, Zhaowei Wang, Shuang Song, Jianbo Han, Hong Chen, Xiaomeng Wang, Ruijun Sun, and Jiayi Cheng. 2019. "Adsorption of Copper(II) and Lead(II) from Seawater Using Hydrothermal Biochar Derived from Enteromorpha." *Marine Pollution Bulletin* 149 (December): 110586. <https://doi.org/10.1016/J.MARPOLBUL.2019.110586>.

Yang, Xuan, Kaiyuan Shi, Igor Zhitomirsky, and Emily D Cranston. 2015. "Cellulose Nanocrystal Aerogels as Universal 3D Lightweight Substrates for Supercapacitor Materials." *Advanced Materials* 27 (40): 6104–9. <https://doi.org/10.1002/adma.201502284>.

Yousif, Ahmed M., Osama F. Zaid, and I. A. Ibrahim. 2016. "Fast and Selective Adsorption of As(V) on Prepared Modified Cellulose Containing Cu(II) Moieties." *Arabian Journal of Chemistry* 9 (5): 607–15. <https://doi.org/10.1016/J.ARABJC.2015.02.004>.

Yu, Hang, Jing Wang, Jun-xia xia Yu, Yi Wang, and Ru-an an Chi. 2020. "Adsorption

Performance and Stability of the Modified Straws and Their Extracts of Cellulose, Lignin, and Hemicellulose for Pb<sup>2+</sup>: PH Effect.” *Arabian Journal of Chemistry* 13 (12): 9019–33.  
<https://doi.org/10.1016/j.arabjc.2020.10.024>.

Yu, Xiaolin, Shengrui Tong, Maofa Ge, Lingyan Wu, Junchao Zuo, Changyan Cao, and Weiguo Song. 2013. “Synthesis and Characterization of Multi-Amino-Functionalized Cellulose for Arsenic Adsorption.” *Carbohydrate Polymers* 92 (1): 380–87.  
<https://doi.org/10.1016/J.CARBPOL.2012.09.050>.

Yuan, Chaolei, Qi Li, Zhaoyang Sun, Wenjun Zhang, Jiangrong Chen, Zheng Chen, Shuo Na, and Hongwen Sun. 2022. “Chemical Oxidation of Arsenic in the Environment and Applications: A Mini Review.” *Pedosphere* 32 (June).

Zhang, Jinju, Lei Li, Yanxiang Li, and Chuanfang Yang. 2017. “Microwave-Assisted Synthesis of Hierarchical Mesoporous Nano-TiO<sub>2</sub>/Cellulose Composites for Rapid Adsorption of Pb<sup>2+</sup>.” *Chemical Engineering Journal* 313: 1132–41.  
<https://doi.org/https://doi.org/10.1016/j.cej.2016.11.007>.

Zhang, Ziwei, Yinhu Wu, Liwei Luo, Guoliang Li, Yuebiao Li, and Hongying Hu. 2021. “Application of Disk Tube Reverse Osmosis in Wastewater Treatment: A Review.” *Science of The Total Environment* 792 (October): 148291.  
<https://doi.org/10.1016/J.SCITOTENV.2021.148291>.

Zhao, Han, Xiao-Kun Ouyang, and Li-Ye Yang. 2021. “Adsorption of Lead Ions from Aqueous Solutions by Porous Cellulose Nanofiber–Sodium Alginate Hydrogel Beads.” *Journal of Molecular Liquids* 324: 115122. <https://doi.org/https://doi.org/10.1016/j.molliq.2020.115122>.

Zhou, Yiming, Shiyu Fu, Liangliang Zhang, Huaiyu Zhan, and Mikhail V. Levit. 2014. “Use of Carboxylated Cellulose Nanofibrils-Filled Magnetic Chitosan Hydrogel Beads as Adsorbents for Pb(II).” *Carbohydrate Polymers* 101 (1): 75–82.

<https://doi.org/https://doi.org/10.1016/j.carbpol.2013.08.055>.

Zou, Haimin, Chen Zhou, Yongxin Li, Xiaosong Yang, Jun Wen, Xiaoke Hu, and Chengjun Sun.

2019. "Occurrence, Toxicity, and Speciation Analysis of Arsenic in Edible Mushrooms."

*Food Chemistry* 281: 269–84.

<https://doi.org/https://doi.org/10.1016/j.foodchem.2018.12.103>.

## CURRICULUM SUMMARY

### PERSONAL DATA

**Nome:** Dairon Pérez Fuentes

**Place and date of birth:** Güines, December 26, 1993

### EDUACTION

Havana University, Havana, Cuba, 2017.

Bachelor degree, Chemistry.

### COMPLEMENTARY TRAINING

- Short course in Conversation and Writing in Portuguese for Foreigners (level C1). (Charge time: 16h). University of São Paulo, USP, Sao Paulo, Brazil, 2021
- Short-term course in Writing Techniques. (Charge time: 3h). Institute of Chemistry, University of São Paulo, IQ-USP, Brazil, 2021.
- Short-term course in Communication and Scientific Writing. (Charge time: 12h). American Chemical Society, Washington, United States, 2021.
- Head of Geological Projects. (Charge time: 60h). School of Energy and Mines, EEM, Cuba, 2018
- Experimental Methods of Materials Science and Technology II. (Charge time: 60h).
- Institute of Science and Technology of Materials, IMRE, Cuba, 2018.
- Short course on Advances and perspectives of photoemission techniques.
- Institute of Science and Technology of Materials, IMRE, Cuba. 2018

- Short course on MEV Applications in the Characterization of materials and nanomaterials. (Charge time: 20h). Institute of Science and Technology of Materials, IMRE, Cuba, 2018
- Short course in Atomic Spectroscopy and X-ray Fluorescence. Characterization of matter. (Course: 20h). Institute of Science and Technology of Materials, IMRE, Cuba, 2018.
- Inductively Coupled Plasma Mass Spectrometry (ICP-MS). (Charge time: 64h). University of Havana, UH, Havana, Cuba, 2017
- Introduction to X-ray Diffraction (DRX). (Charge time: 64h). Institute of Science and Technology of Materials, IMRE, Cuba, 2017.
- Short course in Applied Statistics and Design of Experiments. (Charge time: 64h). Institute of Science and Technology of Materials, IMRE, Cuba, 2017.
- Scientific research methodology. (Charge time: 60h). Institute of Science and Technology of Materials, IMRE, Cuba, 2017.

## **PUBLICATIONS**

### **FULL ARTICLES PUBLISHED**

- FURTADO, LAÍSE MOURA; FUENTES, DAIRON PÉREZ; ANDO, RÔMULO AUGUSTO; OLIVEIRA, PEDRO VITORIANO; SIQUEIRA PETRI, DENISE FREITAS. Carboxymethyl cellulose/sugarcane bagasse/polydopamine adsorbents for efficient removal of Pb<sup>2+</sup> ions from synthetic and undergraduate laboratory wastes. **JOURNAL OF CLEANER PRODUCTION**. v.380, p.134969, 2022.

- DE SOUZA, DIENE FRANCE; DA SILVA, MARLIANE DE CÁSSIA SOARES; DE PAULA ALVES, MAIANE; FUENTES, DAIRON PÉREZ; PORTO, LUCAS EDUARDO OLIVEIRA; DE OLIVEIRA, PEDRO VITORIANO; KASUYA, MARIA CATARINA MEGUMI; ELLER, MONIQUE RENON. By-Products as Substrates for Production of Selenium-Enriched *Pleurotus ostreatus* Mushrooms. **Waste and Biomass Valorization**. v.13, p.989 - 1001, 2021.
- SCULL, Idania Rodríguez; ELIAS-IGLESIAS, A.; FUENTES, DAIRON PÉREZ; SAVON-VALDES, L. L.; HERRERA-VILLAFRANCO, M.; POMPA-CASTILLO, N. Effect of season on the nutritional components of *Spathodea campanulata* Beauv. **Pastos y Forrajes**. v.44, p.109, 2021.

#### **ABSTRACTS PUBLISHED IN CONGRESS PROCEEDINGS**

- FUENTES, D. P.; PORTO, L. E. O.; Pedro V. Oliveira; PETRI, D. F. S. Microcrystalline cellulose beads for removal and recovery of Pb (II) from different waters: batch and column adsorption studies, **20° ENQA, Bento Gonçalves, RS, Brazil 2022.**
- PORTO, LUCAS EDUARDO OLIVEIRA; FUENTES, D. P.; OLIVEIRA, PEDRO VITORIANO. Speciation of Gd (III) from GD-chelate using microcrystalline cellulose beads for separation and preconcentration from waters, **20° ENQA, Bento Gonçalves, RS, Brazil 2022.**
- FUGIWARA, J. J. A.; FUENTES, D. P.; PORTO, L. E. O.; OLIVEIRA, PEDRO VITORIANO. Sugarcane bagasse as adsorbent for metal ions removal from

wastewater from teaching laboratories, **20° ENQA, Bento Gonçalves, RS, Brazil 2022.**

- FURTADO, LAÍSE MOURA; FUENTES, D. P.; PETRI, D. F. S. Sugarcane bagasse/polydopamine/carboxymethyl cellulose adsorbents for the removal of bisphenol A and Pb(II) from wastewater, **GRUN II – Groundwater Remediation using Nano/biotechnology with focus on the Contaminated Resources in Brazil. 2021.**

#### **ACADEMIC ACTIVITIES**

- Monitoring in the Teaching Improvement Program (PAE): discipline of Instrumental Analytical Chemistry (QFL0238), Institute of Chemistry of the University of São Paulo (IQ USP) with supervision of Prof(a). Claudimir Lucio do Lago, 2021.